# A STUDY OF THE IGNITION DELAY CHARACTERISTICS OF COMBUSTION IN A COMPRESSION IGNITION ENGINE OPERATING ON BLENDED MIXTURES OF DIESEL AND GASOLINE

THOO WEI JET

BE (HONS) MECHANICAL

2016

# ABSTRACT

The interest to study diesel-gasoline fuel mix for CI engine combustion had been motivated by the higher thermal efficiency of CI engine compared to SI engine which gasoline normally runs in and the report of having lower $NO_x$ and PM emissions for gasoline combustion in CI engine. The experimental CI engine was unable to run on 100% gasoline but able to run on gasoline blend as high as G80 with default SOI timing setting. 100% gasoline would not run despite it contains only 20% more gasoline than G80 due to its extremely longer ignition delay caused by the exponential increase of gasoline blend's ID. Engine brake thermal efficiencies of all gasoline blends tested up to G80 were comparable and averaged at 24.2%, 33.8% and 39.8% for engine speed-load conditions of 2000rev/min 2.5bar BMEP, 2000rev/min 5bar BMEP and 2000rev/min 8.5bar BMEP, accordingly. This finding confirmed that gasoline blend could be a new alternative fuel that offers comparable performance to the liquid fuel market for CI engine. In Europe, diesel blended with a small percentage of biodiesel or ethanol has been common to liquid fuel market.

The study focused on ID that was closely correlated to $NO_x$ and soot formations in engine cylinder instead of $NO_x$ and PM emissions at tailpipe. The longer ID of 100% gasoline in relative to diesel could go up to 14CAD resulted in increased proportion of premixed combustion to mixing-controlled combustion at the rate of 40 Joule per CAD increase in ID. This incremental premixed combustion proportion was ideal for low $NO_x$ and soot formations in CI engine. ID was able to be discriminated into physical delay, a period dictated by engine speed-load conditions and controlled fuel breakup, fuel vaporisation and fuel-air mixing; and chemical delay, a period dictated by fuel chemical kinetic mechanism and controlled the amount of heat released. This finding gave valuable insight to the fact that proportion of premixed combustion and mixing-controlled combustion were controlled by chemical delay. Zero-dimensional theoretical combustion study with chemical kinetic mechanism confirmed that the exponential increased ID trend of

gasoline blends was attributed to chemical delay. Hence a gasoline blend close to 100% gasoline would have very lean premixed combustion and small mixing-combustion which correlated to very low $NO_x$ and soot formations in cylinder. In order to understand the $NO_x$ and soot formations in cylinder in detail, a 73species reduced chemical kinetic mechanism that could represent gasoline blend combustion in CFD was developed. This reduced chemical kinetic mechanism could be used for future CFD work to understand effect of interactions between physical processes (fuel breakup, fuel vaporisation and fuel-air mixing) and chemical processes (activation of fuel combustion chemistry) on $NO_x$ and soot formations in cylinder.

This work founded an effective semi-automatic reduction methodology with MATLAB algorithms for developing the 73species CFD-compatible reduced chemical kinetic mechanism of gasoline blends. This platform made building a surrogate fuel's reduced chemical kinetic mechanism from multiple detailed chemical kinetic mechanisms of single component fuels fast, accessible and friendly to users of all background. DRG reduction technique had been enhanced by the multiple-stage ROP and multiple-step DRG approaches. The multiple-stage ROP and multiple-step approaches increased the species size reduction of chemical kinetic mechanisms by additional 8% and 13.5%, accordingly. The additional species size reduction capability of both approaches would be beneficial for the reduction of chemical kinetic mechanism for CFD use which is practically limited to size of 100species for feasible computational errors and speed. Apart from the limitation for the percentage of gasoline blend that could be used in the experimental CI engine, the lower compressibility of gasoline blends in relative to diesel had caused the SOI timing to be retarded up to 3CAD in this pump-triggered type of injection system. This shift of combustion phase had no significant effect on the ID and heat-release characteristics. The combustion phase shift can be easily compensated by advancing the SOI accordingly.

# LIST OF PUBLICATIONS

1) WJ. Thoo, A. Kevric, HK. Ng, S. Gan, P. Shayler, A. La Rocca, "Characteristic of ignition delay period for a compression ignition engine operating on blended mixtures of diesel and gasoline," Applied Thermal Engineering, vol. 66, pp. 55-64, 2014.
2) WJ. Thoo, A. Kevric, HK. Ng, S. Gan, P. Shayler, "Semi-Empirical Correlations of Physical and Chemical Delay Period of Diesel-Gasoline Combustion," in Proceedings of the FISITA 2012 World Automotive Congress, pp.493-502, 2013.

# ACKNOWLEDGEMENT

I would like to give thanks to God for His wisdom and strength for me to persevere through the hardship of completing this thesis. I would also like to thank my family for their endless support and best of hope for me. Next, I want to express my gratitude to my supervisor Professor Ng Hoon Kiat for giving me this opportunity to pursue this PhD, his continuous support and believing in me, and guided me through the entire course of study. Special thanks to Professor Paul Shayler for his guidance during the study period I spent in the UK and also Arman for helping me to get adjusted to the UK campus and the engine laboratory.

# TABLE OF CONTENTS

# LIST OF ABBREVIATION

| | |
|---|---|
| ATDC | after top dead centre |
| APP | accelerated pedal position |
| BMEP | brake mean effective pressure |
| BSFC | brake specific fuel consumption |
| BTDC | before top dead centre |
| CA | crank angle |
| CAD | crank angle degree |
| cc/cycle | cubic centimetre per millisecond cycle |
| CCD | charged-couple device |
| CFD | computational fluid dynamics |
| CI | compression ignition |
| CO | carbon monoxide |
| CSP | computational singular perturbation |
| CTC | characteristic time |
| DAQ | data acquisition |
| DN | density |
| DRG | directed relation graph |
| ECU | engine control unit |
| EDC | Eddy dissipation concept |
| EGR | exhaust gas recirculation |
| EOI | end of injection |
| EP | error propagation |
| ETBE | ethyl tert-butyl ether |
| exp | experiment |
| FMEP | friction mean effective pressure |
| FP | flash point |
| HC | hydrocarbon |
| HCCI | homogeneous charge compression ignition |
| HHV | higher heating value |

| | |
|---|---|
| $HO_2$ | hydroperoxyl radical |
| $H_2O$ | hydrogen dioxide radical |
| $H_2O_2$ | hydrogen peroxide radical |
| ID | ignition delay |
| ILDM | intrinsic low-dimensional manifolds |
| IMEP | indicated mean effective pressure |
| ISFC | indicated specific fuel consumption |
| J | Joule |
| J/degree | Joules per degree |
| KH-RT | Kelvin-Helmholtz and Rayleigh-Taylor |
| LLNL | Lawrence Livermore National Laboratory |
| MEP | mean effective pressure |
| MCC | mixing-controlled combustion |
| MON | Motor Octane number |
| ms | millisecond |
| n.a | not available |
| $NO_x$ | nitrogen oxides |
| NTC | negative temperature coefficient |
| O | oxide radical |
| OH | hydroxyl radical |
| PDPA | phase Doppler particle analyse |
| PIV | particle imaging velocimetry |
| PM | particulate matter |
| PMC | premixed combustion |
| ppm | parts per million |
| RCM | rapid compression machine |
| RDFS | revised depth first search |
| rev/min | revolutions per minute |
| RIF | Representative Interactive Flamelet |
| RON | research octane number |
| ROP | rate of production |

| | |
|---|---|
| SI | spark ignition |
| sim | simulation |
| SOC | start of combustion |
| SOI | start of injection |
| T | temperature |
| TDC | top dead centre |
| U.S. | United States |
| vol. | volume |
| VS | viscosity |
| 0-D | zero-dimensional |

# NOMENCLATURE

| | |
|---|---|
| $\phi$ | equivalence ratio |
| $\rho$ | density |
| c | speed of sound |
| $\beta$ | insentropic bulk modulus |
| $\Delta P_{loss}$ | Pressure loss in pipe |
| $f$ | friction coefficient |
| $L$ | Length of pipe |
| $D$ | Pipe diameter |
| $p$ | Fluid density |
| $u$ | fluid velocity |
| $\mu$ | Kinematic viscosity |
| Re | Reynold's number |
| $W$ | Work per cycle (Joule) |
| $V_d$ | Displacement volume of cylinder (cubic metre) |
| $P$ | Engine's power (Watt) |
| $N$ | Engine speed (rev/s) |
| $n_R$ | Number of crank revolution per engine power stroke |
| $T$ | Torque of crankshaft ( $Nm$ ) |
| $W_{c,i}$ | Indicated work done by in-cylinder content on piston per engine cycle (Joule) |
| o | degree |
| $\tau_{ig}$ | ignition delay |

| | |
|---|---|
| $r_{AB}$ | normalised contribution for DRG |
| $V_{A,i}$ | stoichiometric coefficient |
| $\delta_{Bi}$ | Delta |
| $\omega_i$ | net rate of production |
| $\omega_{fi}$ | rate of production of forward reaction |
| $\omega_{ri}$ | rate of production of backward reaction |

# LIST OF FIGURE

# LIST OF TABLE

# CHAPTER 1

# Introduction

## 1.1 Alternative fuel for engine

Currently, the liquid fuels market is dominated by the use of diesel for CI engines and gasoline for spark ignition (SI) engines. In both cases, the fuels are blended with a few percent of biodiesel or ethanol, respectively in Europe. In the future and across the developed and emerging markets of the world, the range of fuels used will increase as biofuels, new fossil fuel feedstock and processing methods, as well as variations in fuel standards continue to influence the choice of fuel mix composition. The uncertainty presents a challenge requiring better understanding of how fuel properties influence engine behaviour and using blends of diesel and gasoline allows extremes to be covered in a simple and progressive way.

## 1.2 Advantages of diesel-gasoline blends for compression ignition engine.

The fuel mix of diesel and gasoline runs in a CI engine also allows the potential of gasoline blend to be studied. Compression-ignited engine is well known for its superior thermal efficiency over spark-ignited engine as it consists of lower pumping losses and higher volumetric efficiency achieved by the absence of throttle valve, higher piston compression ratio, less heating of inducted charge in intake manifold and less dilution of fresh charge [1]. Beside the higher thermal efficiency of gasoline combustion in CI engine in relative to SI engine, combustion of gasoline in CI engine was reported to have lower $NO_x$ and PM emissions than conventional CI engine which operates with diesel [1].

## 1.3 Review on gasoline combustion in CI engine

Two approaches are commonly adopted to deliver the mix of diesel and gasoline fuels into CI engines. One strategy uses port fuel injection for gasoline and direct

injection for diesel, which is known as the gasoline homogeneous charge induced ignition [2, 3]. The other strategy blends diesel and gasoline fuels together before directly injecting the fuel blend into the combustion chamber [2, 4, 5, 6]. Both employ common rail system for direct injection which eliminates the effect of the fuel's physical properties changes such as density and bulk modulus on injection timing. Although both fuelling strategies can achieve the reported benefits, gasoline homogenous charge induced ignition involves complicated control of two different injectors which requires the careful control of mixture reactivity and stratification [3]. The simplicity in the second approach allows combination of multiple injections, boost pressure, exhaust gas recirculation (EGR) and gasoline as the fuel blend component to be used for simultaneous reduction of $NO_x$ and PM emissions while maintaining or even lowering the indicated specific fuel consumption (ISFC) in a CI engine [2, 4, 5, 6, 7].

The increase of gasoline proportion in the fuel mix was found to prolong the ID period [2, 5, 7, 8, 9], which was reported to be the attribute to simultaneous reduction in $NO_x$-soot emissions and defying the conventional $NO_x$-soot trade-off [2, 7, 8]. These works were either conducted in single-cylinder engines at low engine speed (<1500rev/min), low engine load (<6bar IMEP) and advanced SOI timings (up to -9CAD ATDC) [5, 8] or in actual 4 cylinder engines but with low percentage gasoline blends (G40 or less) [7, 9]. These engine conditions, engine SOI timing settings and fuel blends are hardly practical in actual CI engine application. Therefore it would be useful to extend the ranges of all these parameters in an actual CI engine due to gasoline combustion characteristics could be compensated by the diesel portion in low percentage gasoline blends. This provides novelty for this work to study the ID characteristics and limitation of higher gasoline blends at higher range of engine speed-load conditions.

From the discussion above, the choice of fuelling strategy using gasoline-diesel blends may provide the necessary cost-effective solutions to lowering the tailpipe emissions of $NO_x$ and soot while at the same time maintaining a superior fuel economy and power output. Set against this background, there is a need to better

understand how gasoline addition into diesel fuel changes the in-cylinder ignition behaviour of a typical compression ignition engine. In the work reported here, the influence of fuel type has been the focus and the experimental work has been conducted on an engine with fuel injected in a single injection event. Fuel composition has been varied by blending diesel and gasoline in various proportions up to 80% gasoline by volume. The engine was a light duty, turbocharged, direct injection compression ignition engine with a mechanical pump injection system.

### 1.4 Surrogate fuels suitable for diesel and gasoline

In order to better understand the effect of gasoline on ID behaviour and the resulting benefits with diesel-gasoline fuel mix, chemical kinetic modelling can be utilised to complement engine test bed studies [10]. However, accurately predicting the chemical kinetics contribution to ID for diesel-gasoline blends is difficult since both diesel and gasoline are multi-component fuels. These components are commonly grouped into five main categories, namely n-alkanes, iso-alkanes, napthenes, aromatics and olefins [11, 12, 13]. Ideally, fuel surrogates with similar carbon numbers as the components found in diesel and gasoline should be chosen for kinetic modelling to produce better representation of the heat-release characteristics. The size of the fuel surrogate mechanisms is another important factor to be considered. Pitz et al. [11] evaluated the existing single-component fuels in terms of relevance to practical systems, understanding of mechanism and properties information. Based on this work, the single-component fuels which are rated the highest in terms of mechanism understanding and being the most relevant to the fuel components in diesel and gasoline are n-heptane, iso-octane, 1-pentene, methylcyclohexane and toluene. Hernandez et al. [14] proposed a combined kinetic mechanism of n-heptane (50%) and toluene (50%) as a diesel fuel surrogate for auto-ignition simulations under homogeneous charge compression ignition (HCCI) engine conditions. In another work, the combined kinetic mechanisms of n-heptane/toluene and n-heptane/toluene/1-hexene were used as diesel fuel surrogates [15]. As for kinetic modelling of gasoline combustion, Mehl et al. [13] discussed the use of n-heptane, iso-octane, toluene and 1-hexene as well as their mixtures as gasoline fuel surrogates under the conditions of a rapid compression machine and a

jet stirred reactor. Recently, Lee et al. [16] developed a gasoline fuel surrogate model comprising iso-octane, n-heptane and toluene which was validated against data from a shock tube and a rapid compression machine. These studies demonstrated that the chosen surrogate fuels are capable of predicting the ID period of diesel and gasoline combustions. The novelty of the theoretical study lies in determining the contribution of chemical delay to ID which is closely correlated to $NO_x$ and soot emissions, through the development of a binary kinetic model, which is a low cost, high fidelity approach to examining the ignition process. Here, the effects of gasoline blend proportions on injection timing and the trends of ID variations are appropriately elucidated. The results will advance both knowledge and understanding of gasoline-diesel combustion, and in the long run may transform fuelling and operating strategies for more efficient and cleaner engines.

### 1.5 Review on CFD Modelling with chemical kinetic mechanism

Combustion in CI engine comprised of physical mixing, heat transfer, evaporation and chemical reactions. Multidimensional CFD modelling with chemical kinetic mechanism is able to give insight to these processes better than the quick predictions provided by the CHEMKIN chemical kinetic modelling. Based on the numerous CFD modelling works which have been done, size of chemical kinetic mechanism used for CFD modelling has to be within a reasonable size limit (below 100species) to give a feasible simulation time scale [17, 18, 19]. Therefore the reduction of the sizes of detailed mechanisms and skeletal mechanisms are crucial. The most challenging part of mechanism reduction is to maintain the accuracy of the predicted results. Chemical mechanism is developed for predicting ignition delay, heat release and rate of production of every species in the whole combustion chemical process. For this work, the focus would be on prediction of ignition delay and heat release only hence the accuracy of species production was not considered. The work on CFD modelling of CI combustion with chemical kinetic mechanism is extremely scarce. The available one is a work on biodiesel mechanism [17, 18, 20]. This gives the novelty of developing a reduced mechanism that could represent ID characteristics of diesel and gasoline blends, for studying ID characteristics of diesel-gasoline blends and ultimately $NO_x$ and soot formations in cylinder. CFD

study also able to simulate physical-chemical interaction of diesel-gasoline blends combustion in CI engine that could enhance the zero-dimensional theoretical study of diesel-gasoline blends.

This thesis consists of six chapters. The first or the current chapter introduces the objectives, challenges and novelties involved in this work as well as acts as a guide for readers to all other chapters of the thesis. The second chapter reviewed the literatures available that are relevant to this work. The relevant topics to be reviewed are such as gasoline combustion in CI engine, effect of engine parameters and fuel properties on combustion characteristics in CI engine, discrimination of physical and chemical effects of fuel properties on combustion, chemical kinetic mechanisms of surrogate fuels relevant to gasoline and diesel, and chemical kinetic mechanisms reduction techniques. The main work is divided into three parts and presented in the next three chapters of this thesis. The first part explains in detailed about the engine setup and the experimental studies conducted followed by the experimental findings in Chapter 3. The second part covers the development of the ternary chemical kinetic mechanism which could represents diesel-gasoline blends and theoretical study on physical delay and chemical delay with the ternary chemical kinetic mechanism as per explained in Chapter 4. Although the theoretical study has not been extended to CFD modelling, but the ternary chemical kinetic mechanism for diesel-gasoline blend has been reduced in size to the level suitable for CFD modelling. The detailed reduction process is covered in Chapter 5. The final chapter which is chapter 6 concludes the main findings of the work. The breakdown of the chapters is as summarised in Table 1.1.

*Table 1.1: Chapters breakdown.*

| Chapter | Title |
|---|---|
| 1 | Introduction |
| 2 | Literature review |
| 3 | Experimental study of the diesel-gasoline combustion in CI engine |
| 4 | Numerical study with chemical kinetic mechanisms for diesel and gasoline |
| 5 | Binary chemical kinetic mechanism for CFD application |
| 6 | Conclusion |

# CHAPTER 2

## Literature review

This chapter reviewed the work of other researchers that were relevant to this study. Section 2.1 highlighted the work of gasoline combustion in CI engine. This section helped to discover the main objective and novelty of this study. Section 2.2 looked into effect of engine parameters and fuel properties of gasoline on combustion characteristics in CI engine. Section 2.3 focused how physical and chemical processes in cylinder be discriminated. The rest of the review included information of how a reduced chemical kinetic mechanism can be developed for CFD modelling purpose.

### 2.1: Gasoline combustion in CI engine

In recent years, the use of gasoline in CI engines had attracted interest because of its benefits such as the thermal efficiency was higher than gasoline spark-ignited combustion or even conventional diesel compression-ignited combustion [2, 4], and lower $NO_x$ and PM emission [2, 4, 5]. There were two approaches commonly used to inject diesel and gasoline into CI engine. One used port fuel injection for gasoline and direct injection for diesel which was known as the gasoline homogeneous charge induced ignition [2, 3]. The other blended diesel and gasoline together before directly injected the fuel blend [2, 4, 5, 6]. Both used common rail injectors for direct injection which eliminated the effect of the change of physical properties such as density and bulk modulus on the injection timing suffered by the older pump type injection system. Although both approaches exhibited the above benefits, but the gasoline homogenous charge induced ignition involved complicated control of two different injectors which required the consideration of mixture reactivity and mixture stratification [3]. The simplicity of the second approach allowed $NO_x$ and PM reduction strategies such as multiple injections,

intake boost and exhaust gas recirculation (EGR) to be used along with the study of diesel and gasoline blends [2, 4, 5, 6, 7, 8]. The combination of these $NO_x$ and PM reduction strategies and diesel-gasoline blends was found able to simultaneously reduce $NO_x$ and PM emissions while maintaining or even increasing the thermal efficiency of a CI engine [4, 8]. The increase of gasoline proportion prolonged the ID [2, 5, 7, 8, 9] which was claimed to be the reason for able to defy the conventional $NO_x$-soot trade-off as mentioned [2, 7, 8]. These works were either conducted in single-cylinder engines at low engine speed (<1500rev/min), low engine load (<6bar IMEP) and advanced SOI timings (up to -9CAD ATDC) [5, 8] or in actual 4 cylinder engines but with low percentage gasoline blends (G40 or less) [7, 9]. Under these engine conditions, engine SOI timing settings and fuel blends are hardly practical in actual CI engine application. Apart from $NO_x$ and PM emissions which had been the major interest in diesel combustion, HC and CO emissions of diesel-gasoline blends were studied [6]. The increase of gasoline proportion in fuel blends was found to alter the ignition delay and global equivalence ratio which were correlated to HC and CO emissions instead of altering these emissions directly.

### 2.2: Effect of engine parameters and fuel properties on combustion characteristics in CI engine.

The objective of this review section was to provide understanding towards effect of engine parameters and fuel properties towards combustion characteristics hence they could be discriminated in future work. Figure 2.2-1 showed the important parameters that could quantify combustion characteristics in diesel engine. The factors of these parameters were the engine parameters (engine load, engine speed, boost pressure, start of injection timing and EGR) and fuel properties (properties were explained in latter paragraph) as depicted in Figure 2.2-2. Effect of engine parameters on combustion characteristics was reviewed first followed by effect of fuel properties on combustion characteristics. Engine parameters such as boost pressure, injection timing and EGR (exhaust gas recirculation) were active parameters that can be used to optimise a diesel engine but engine speed and load were passive parameters which depend on application. Engine load had no direct

effect on engine performance except brake power. However, engine speed-load condition was controlled by injection pressure and injection duration which would affect engine performance. Thus, injection pressure and injection duration were the studied engine parameters instead of engine load. Higher injection pressure or longer injection duration was required to maintain an engine at same speed but higher load. Studies of effects of engine parameters on engine performance and emissions performed by various researchers were illustrated in Figure 2.2-3. Montgomery et al. [19] reported combustion with EGR (exhaust gas recirculation) had significantly reduction in $NO_x$ emission. The reasons for the $NO_x$ reduction were decrease in radical species present during combustion and inert exhaust gas decreased combustion temperature. Uludogan et al. [20] observed that combustion at higher engine speed has higher maximum generated work output; lower $NO_x$ and soot productions. At higher engine speed, stronger fluid turbulence inside engine cylinder enhanced air-fuel mixing. Better air-fuel mixing was claimed to inhibit CO (carbon monoxide) production. CO gas had high internal energy that reduced average engine in-cylinder temperature and pressure hence high engine speed enhanced combustion efficiency. Combustion efficiency was inversely proportional BSFC (brake specific fuel consumption). As for emissions, soot and $NO_x$ formation were claimed to be controlled by in-cylinder gas temperature which was governed by effects of air-fuel mixing, unburnt fuel, and CO production [20]. $NO_x$ production was directly proportional to peak in-cylinder temperature. Soot production was a function of temperature and local fuel equivalence ratio. Lower $NO_x$ production at higher engine speed could be explained by the lower peak in-cylinder temperature due to better air-fuel mixing followed by smaller portion of premixed combustion. Combustion at higher speed had leaner mixtures leading to lower soot formation rates. Although high speed combustion would have lower soot formation, lower $NO_x$ formation, higher combustion efficiency and higher work output but there were limitations to employ high speed for engine optimisation. One of the limitations was fuel delivery. Higher engine speed also meant less time for fuel to be delivered into cylinder. Thus, same amount of fuel had to be delivered in longer CAD duration and perhaps earlier before piston

reached TDC if same set of injection hardware were to be used. Second limitation was practicability of high engine speed. Most of the engine applications required variable speeds especially for vehicles. Uludogan et al. [20] also studied the effect of start of injection timing on combustion characteristics. Advanced injection timing was found to cause injected fuel to ignite earlier before piston reached TDC (top-dead-centre). Thus part of the work from power stroke would be lost to counter compression stroke. Retarded fuel injection timings increased the amount of unburnt fuel and CO. Jayashankara et al. [21] studied the effect of fuel injection timing and intake pressure on diesel engine performance. He found that advanced injection timing caused the peak in-cylinder pressure and temperature to be higher but retarded injection timing showed otherwise. These observations were consistent with Uludogan's findings which stated that CO emission was higher with retarded fuel injection timing and CO gas had high internal energy but Jayashankara had different explanation. As injection timing was advanced, fuel portion of premixed combustion was increased due to low temperature and pressure which was insufficient to ignite fuel vapour; ignition delay time and combustion duration were longer. Larger premixed air-fuel mixture portion led to more rapid burning rate and hence higher peak in-cylinder pressure and temperature. Therefore, retarded injection timing was effective on $NO_x$ reduction as high temperature was the main criterion of $NO_x$ production. Figure 2.2-4 illustrated the importance of soot oxidation rate. Retarded injection timing condition was shown to have lower soot oxidation rate by higher soot concentration at the end of expansion stroke. For the effect of boost pressure on engine performance, higher intake air pressure reduced peak heat release rate for premixed phase and increased heat release rate for mixing-controlled phase; higher intake air pressure increased $NO_x$ emission but reduced soot emission. Wang et al. [22] claimed that higher injection pressure would promote longer liquid fuel spray penetration length. Kim et al. [23] found that liquid fuel spray penetration length to be shorter at higher ambient pressure.

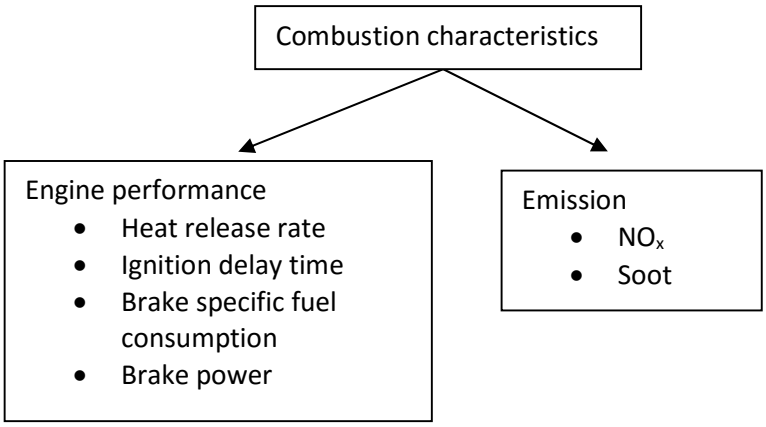


*Figure 2.2-1: List of important parameters which measure combustion characteristics in diesel engine.*

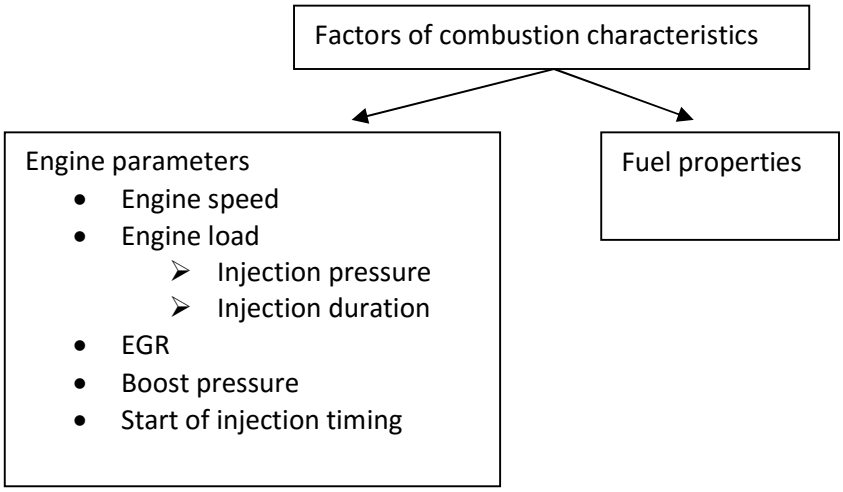


*Figure 2.2-2: Factors of combustion characteristics.*

Tat et al. [24] suggested that fuel physical properties such as density (ρ), speed of sound (c) and isentropic bulk modulus (β) had significant effect on fuel injection timing. There was a correlation that governs these properties, $\beta=c^2 \rho$, being used to calculate the isentropic bulk modulus. The results indicated that the speed of sound and bulk modulus of the monoesters of soybean oil are higher than those for diesel fuel and these can cause advancement in the fuel injection timing of diesel engines [24]. Bulk modulus represented the resistance against volumetric deformation, higher magnitude indicates higher resistivity.

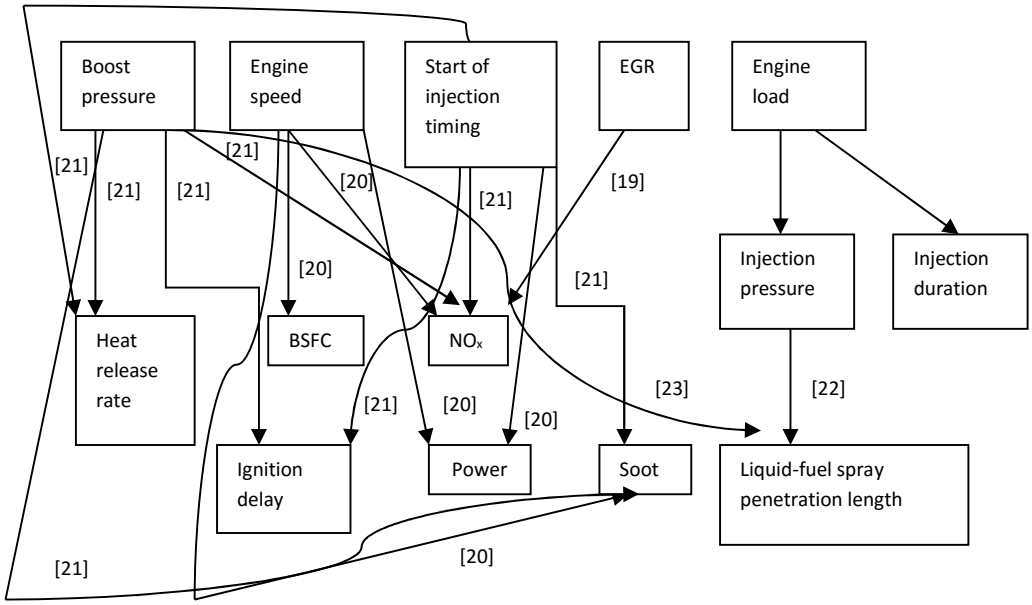


*Figure 2.2-3: Effects of various engine parameters on engine performance and emissions studied by numerous researchers.*

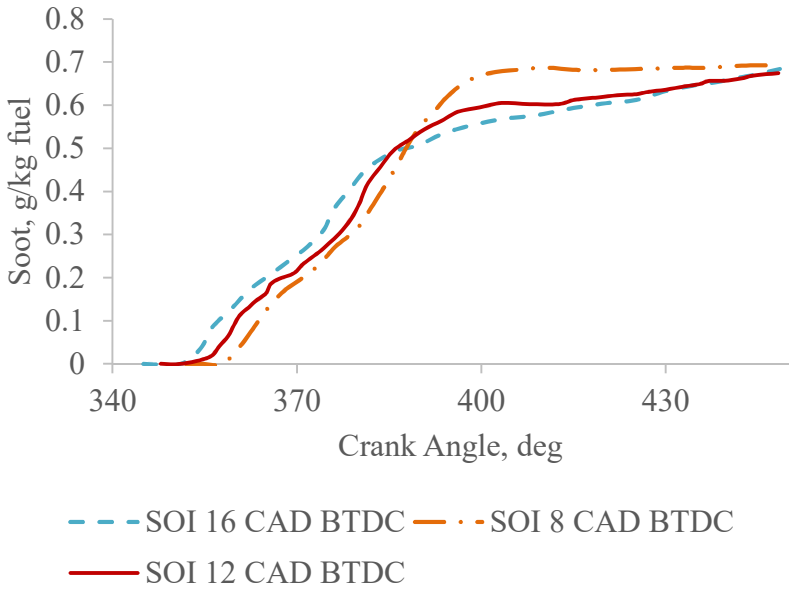


*Figure 2.2-4: Average cumulative soot emission **[21]**.*

A fuel with higher bulk modulus would yield more rapid pressure increase once being compressed. This explained the advanced injection timing event for the monoesters of soybean oil. Frederic et al. [25] studied the impact of fuel physical properties such as specific heat, thermal conductivity, viscosity, density and bulk modulus on fuel mass flow and injection timing in a common-rail direct injection system. Specific heat and thermal conductivity were found to have negligible effect towards injection process. The fuel mass flow rate and injection timing were dictated by the pressure difference between pressure at injector feed pipe and pressure at injector hole. Due to pressure at injector feed pipe fluctuated according to pressure-wave induced by opening and closing actions of injector holes [25], synchronisation of the pressure-wave and injection activation controlled the fuel mass injected into combustion chamber. Because of this fact, the pressure-wave was the main factor to changes in injected fuel mass and injection timing. The pressure-wave's amplitude and phase were governed by pressure loss at injector feed pipe and bulk modulus of fuel. Fuel with higher bulk modulus would have better damping characteristics hence amplitude of pressure-wave at injector feed pipe would be lower. Pressure loss at injector feed pipe was correlated with formulas for predicting pressure loss in pipe. The formulas are in equation 2.2-1.

$$\Delta P_{\text{loss}} = f\left(\frac{L}{D}\right)\left(\frac{pu^2}{2}\right) \tag{2.2-1}$$

$$\text{Re} = \frac{puD}{\mu} \tag{2.2-2}$$

According to the Equation 2.2-1, pressure loss was proportional to fuel variables such as friction coefficient and fluid density. Friction coefficient values were determined by referring to Moody chart with Reynold's number as the reference. In Equation 2.2-2, fluid density and viscosity were the determinant variables for Reynold's number. Fuel mass flow rate and injection timing were concluded to be governed by fuel properties such as density, viscosity and bulk modulus [25]. In complement with Frederic's study which was looking into the injection characteristics of fuel before it leaves the injector, Joaquin et al. [26] focused on

injection characteristics after fuel leaves the injector. In this paper, five indicative parameters were established to show fuel-air mixing efficiency. The indicative parameters were denoted as A, B, C, D and E. They were all calculated from fuel properties such as surface tension, kinematic viscosity and density. Parameter A represented the turbulence of fuel injected into combustion chamber. Parameters B and C expressed the time necessary for liquid fuel jet to disintegrate into micro-drops. Parameter D indicated the diameter of fuel drops after atomisation. Before the fuel atomisation occurred, micro-drop's diameter was not constant and it fluctuated in oscillatory pattern. Parameter E was the dimensionless property for wave length of the oscillation. Values of these indicative parameters for typical diesel were included in this paper. Prediction of fuel-air mixing efficiency for biodiesel as relative to diesel could be made by comparing these indicative parameters of both types of fuels. Ayhan et al. [27] established correlations among fuel physical properties such as higher heating value (HHV), viscosity (VS), density (DN) and flash point (FP) through studies of 14 different types of transesterified biodiesels. The correlations were shown below (labelled as Equation 2.2-3 to Equation 2.2-7).

$$HHV = 0.4625\,VS + 39.45 \quad (2.2\text{-}3)$$

$$VS = -16.155DN + 930.78 \quad (2.2\text{-}4)$$

$$VS = 22.981FP + 346.79 \quad (2.2\text{-}5)$$

$$HHV = -0.0259DN + 63.776 \quad (2.2\text{-}6)$$

$$HHV = 0.021FP + 32.12 \quad (2.2\text{-}7)$$

## 2.3: Discrimination of physical and chemical effects of fuel properties on combustion

After reviewing the effect of fuel properties on compression ignition combustion, ignition delay was observed to be attributed to physical injection timing, mixing delay, and chemical reaction delay. Physical injection timing advancement of biodiesel [28, 29, 30] would cause fuel injection to occur at lower pressure and

temperature in-cylinder condition hence prolonging ignition delay. In spite of prolonged ignition delay due to advanced injection timing, ignition delay was affected by air-fuel physical mixing and combustion chemistry [31]. Ignition delay measurements of combustions in typical production direct-injection diesel engines were reviewed [32, 33, 34]. Gumus et al. [32] defined ignition delay as the crank-angle-degree interval from the maximum pressure of fuel line to the maximum rate of in-cylinder pressure rise. Zheng et al. [33] defined ignition delay as the crank angle degree interval between start of injection (SOI) and the point where net heat release rate turned positive after the initial dip coinciding with SOI. The SOI was not experimentally determined but taken as the point where net heat release rate showed a dip before the rapid rise which indicates the start of combustion. In this work [33], SOI for all fuels were considered to be same and at 17 CA BTDC. Radu et al. [34] defined ignition delay as the crank-angle-degree interval from fixed start of injection, 18 CA BTDC to start of combustion which was referred to the intersection of motored cycle and firing cycle pressure traces. All three definitions of ignition delay could not provide a distinctive evaluation on the effect by air-fuel physical mixing or combustion chemistry. Würmel et al. [35] studied the effect of diluent gases on ignition delay times in the shock tube and in the rapid compression machine. With shock tube and rapid compression machine, factors of ignition delay such as injection timing and fuel-air mixing were eliminated hence the effect of diluent gases on ignition delay governed by combustion chemistry could be studied. Diluent gases showed adverse effects on ignition delays for shock tube and rapid compression machine experiments. Argon decelerated ignition in rapid compression machine but otherwise in shock tube. The observation was claimed to be caused by the difference of ignition delay time scales of both experiments (1-200 ms for RCM and 10-1000 microsecond for shock tube). Pfahl et al. [36] and Mittal et al. [37] studied diesel combustion in shock tube and rapid compression machine. They observed two-stage combustion which consisted of negative temperature coefficient phenomenon at the early stage of combustion. The significance of performing homogeneous air-fuel mixture combustion experiment under diesel engine operating conditions had been shown. In order to study air-fuel

mixing effect on combustion, fuel spray atomisation and penetration were worth reviewing [29]. Espey et al. [38] studied the effect of temperature and density on liquid-phase fuel penetration in a direct injection diesel engine. An optical-access engine which had a piston-crown window and other windows located around the top of the cylinder wall, laser, CCD camera, intensifier gate, computer and digital delay generator were the main apparatus used in this experiment. Laser beams was calibrated to emit at the injected liquid-fuel sprays along their axes through the top windows. The liquid-phase fuel penetration was measured by analysing images of the elastically scattered laser light. Since the elastic-scatter signal from the liquid fuel droplets was several orders of magnitude greater than that of the fuel vapour or air, the images provided good measure of liquid-fuel location. Liquid penetration length was found to be inversely proportional to in-cylinder air temperature rise and increase of density. Fuel penetration length was also found to be reached before significant heat release. In general, for a given temperature, a shorter liquid-fuel penetration length was an indicator of a better air-fuel mixing [39]. Suh et al. [40] analysed the macroscopic and microscopic atomisation -characteristics of diesel fuel sprays by piezo-driven injection system and solenoid-driven injection system. Macroscopic characteristics such as spray penetration length and spray angle were analysed with fuel spray development images captured by laser imaging technique. Microscopic characteristics such as droplet velocity, droplet diameter, and droplet distributions were obtained using a phase Doppler particle analyse (PDPA) system. Piezo-driven injection system atomised fuel better than solenoid-driven injection system due to superior response time and injection rate. Whole experiment was conducted in high pressure chamber. Later, Moon et al. [41] employed different approach in tracking particle movement. Particle imaging velocimetry (PIV) and laser induced fluorescence technique were employed to investigate the air entrainment effect on liquid-fuel penetration length for single-hole nozzle and group-hole nozzle. PIV technique required some improvisations before it can be coupled with elastically scattered laser light imaging technique due to distraction of particle tracking induced by high intensity laser light. Particle tracer called Rhodamine B-water solution was added into combustion chamber to

mix well with air before fuel injection begins. This particle tracer emitted fluorescence light as laser light approaches. The fluorescence signal could be captured by camera when a proper long-pass filter (>560 nm) was used to eliminate laser signal. The fluorescence signal tracked air-particle velocity and laser light signal tracked liquid-fuel spray. By superimposing air-particle velocity contour to liquid-fuel spray contour, fuel evaporation ratio can be calculated. Fuel evaporation ratio was defined as the ratio of vapour mass inside the spray to the total mass of injected fuel. Fuel evaporation ratio was concluded to be proportional to enhanced air-entrainment velocity. Besides the researches dedicated to study macroscopic and microscopic characteristics of fuel sprays, there were researches meant for exploring numerical correlations and spray models that could predict these fuel spray characteristics. Martinez et al. [42] compared liquid-fuel penetration length of a direct injection diesel engine experiment with the one predicted by a numerical correlation. The results were in good agreement with a correlation coefficient of 93.3%. The correlation was used to predict liquid-fuel penetration length without performing resource-exhaustive experiments. In the experiment performed, instead of using laser as the light source for liquid-fuel spray imaging, Xe-polychromatic stroboscopic light source was used. This technique was also known as Ombroscopy. Effects of droplet evaporation, break-up and air entrainment on diesel fuel spray were studied theoretically by Sazhin et al. [43]. Results from three spray penetration models were compared with fuel spray penetration of experiment in this paper. The first one did not take break-up and air entrainment into account. The second model did not include air entrainment and the third model included all three factors. The third model was shown to predict the spray penetration better than the other two models hence fuel evaporation, break-up and air entrainment were equally important to fuel spray characteristics. Similar to study done by Suh et al. [40], macroscopic spray structure was measured by laser-imaging technique and microscopic fuel spray characteristics such as Sauter mean diameter and axial velocity were measured by phase Doppler particle analyser (PDPA) [44]. Lee et al. [44] compared the results from laser-imaging technique and PDPA were to numerical study which Kelvin-

Helmholtz and Rayleigh-Taylor (KH-RT) hybrid spray model was integrated. The KH-RT model's predictions were in good agreement with experimental results. Singh et al. [45] managed to measure soot volume and soot-cloud location through high-speed imaging technique. The experiment was performed in a modified optical-direct-injection diesel engine. Details of soot measurement by imaging technique were described in this paper. Images of soot from experiment were compared with contour generated from simulations. The simulations were performed using the KIVA-3v release-2 code implemented with three different combustion models: KIVA-CTC, KIVA-CHEMKIN, and KIVA-RIF. In consistent with research of Chang Sik Lee et al., KH-RT spray model was adopted in all three types of simulations.

Most of the reviewed fuel-spray imaging and particle tracking experiments were simplified and did not comply with combustion conditions of diesel engine. Some used constant-volume combustion chamber which had no compression/expansion effect and no air-turbulence effect but only fulfilled initial conditions upon start of injection. Even experiments with optical-direct-injection diesel engine [45] required some compromises relative to actual design of engine. The compromises were compression ratio reduction; flat piston-crown adaptation; oxygen dilution; fuel injection firing limitation of once every 10 engine cycles; and EGR prohibition. Lower compression ratio yielded lower top-dead-centre temperature and pressure condition hence elevated intake gas temperatures and pressures were required. Laser imaging technique captured images through the bottom piston-crown window, thus it must be flat. Frequency limitation of fuel injection firing, oxygen dilution and EGR prohibition were meant to solve engine over-heating issue. In spite of various compromises that experiments for fuel spray and combustion chemistry had, they provided valuable data to validate numerical spray models and combustion models. As illustrated, in term of experiment, effect of biodiesel properties on combustion chemistry can only be studied in homogeneous combustion which effect of air-fuel mixing was eliminated; effect of biodiesel properties on air-fuel mixing can only be studied in optical engine equipped with fuel spray imaging technology under compromised conditions. Thus, combustion chemistry and air-

fuel mixing behaviours can only be studied concurrently under uncompromised conditions in CFD-simulation integrated with well validated spray and combustion models. Zheng et al. [46] reported $HO_2$ as an important criterion that affected ignition delay in a computational study. Patel el al. [47] stated that intermediate species such as $H_2O$, $H_2O_2$, OH and O were important to initialisation of combustion chemistry. Combustion chemistry was inert before the presence of these important radicals hence delay of air-fuel mixing could be regarded as time from start of injection until these species concentrations began to increase rapidly. Modelling work with integrated chemical kinetic mechanism was the key to predicting formations of important intermediate species in combustion [48]. FLUENT-CHEMKIN was capable of performing CFD simulation involved complex fluid turbulence and detailed chemical kinetic mechanism [49, 50]. Fluent offered four options for turbulence-chemistry modelling work which were the Laminar Finite Rate, Finite rate/Eddy dissipation, Eddy dissipation, and Eddy dissipation concept (EDC) models [49]. Laminar Finite Rate model computed only the Arrhenius rate of chemical reactions and neglected turbulence-chemistry interaction. Finite rate/Eddy dissipation model computed both the Arrhenius rate of chemical reaction and air-fuel mixing rate but used smaller of the two. Eddy dissipation model computed only the air-fuel mixing rate. EDC model computed turbulence-chemistry interaction with detailed chemical mechanisms. Combustion in direct-injection diesel engine was governed by the interaction between turbulence-mixing and chemistry [31] hence EDC model seemed to be the most promising model. Hong et al. [31] reported that EDC model predicted methane combustion results well as compared to experimental results of direct-injection diesel engine. The chemistry-only combustion calculated reaction rate with formulas similar to Laminar Finite Rate model. A transition parameter was defined in this paper which accounts for the point of transition from chemistry-only model to EDC model. Effect of transition parameter was tested. Early stage of combustion (before rapid pressure rise) was found be insensitive to changes of transition parameters. Thus, this period of combustion depended solely on chemistry only. Late stage of combustion (after rate of pressure rise decreased

from peak) was found to be limited by rate of air-fuel mixing. Late stage of combustion coincided with mixing-controlled combustion. Later, Hong et al. performed similar study with diesel as fuel for experiment and n-heptane mechanism for simulation [51]. It was interesting to find that transition parameter affects premixed combustion portion in terms of peak pressure and phase. Smaller transition parameters were observed to yield results of lower peak pressure in premixed portion and retarded premixed portion. This was due to simulation with smaller transition parameter accounts for mixing-effect earlier hence the homogeneity of air-fuel mixture decreases. A less homogeneous mixture ignited later and with smaller premixed burned portion. This observation indicated mixing-effect play a major role in premixed combustion. Although Fluent did not have the feature of combustion model transition, but by running simulation with EDC model and simulation with Laminar Finite Rate model separately, the dependency of each phase of combustion on mixing-effect and chemical reactions could be compared.

## 2.4: Chemical kinetic mechanisms of surrogate fuels relevant to gasoline and diesel

Gasoline and diesel comprise similar sets of organic chemical constituents but have different chemical composition. Gasoline consists of hundreds of different species including n-paraffins, iso-paraffins, olefins, napthenes, cycloolefins, and aromatics in nature. Diesel consists of n-paraffins, iso-paraffins, napthenes and aromatics. The chemical compositions of diesel and gasoline were shown in Table 2.1 and Figure 2.4-1. According to Table 2.1 [12], Olefins comprised in diesel are less than three percent by volume hence it could be neglected in selection of diesel surrogate fuels; the abundant constituents groups of diesel fuel were aromatics, napthenes and paraffins (n- and iso-). Refer to Figure 2.4-1 [11], the abundant constituents groups of gasoline were aromatics, olefins and paraffins (n- and iso-).

*Table 2.1: Chemical compositions of ten diesel-fuel samples **[12]**.*

| Fuel constituent | Diesel fuel | | | | | | | | | |
|---|---|---|---|---|---|---|---|---|---|---|
| | D1 | D2 | D4 | D5 | D7 | D8 | D9 | D10 | D14 | D15 |
| Aromatics (vol. %) | 2.7 | 14.7 | 22.5 | 26 | 19.8 | 19.4 | 16 | 20.7 | 7.7 | 3.7 |
| Olefins (vol. %) | 1.4 | 2 | 2.2 | 1.6 | 0.9 | 0.2 | 0.7 | 1.8 | n.a | n.a |
| Saturates (vol. %) | 95.9 | 83.3 | 75.4 | 72.4 | 79.6 | 80.4 | 83.3 | 77.5 | n.a | n.a |
| Napthenes (wt %) | 53.6 | 38.8 | 29.6 | 27.2 | 32.9 | 32.9 | 25.5 | 32.5 | 50.7 | 48.8 |
| Paraffins (wt %) | 45.6 | 45.5 | 43.8 | 47.6 | 48.5 | 47.7 | 58.1 | 47.1 | 44.9 | 47.1 |

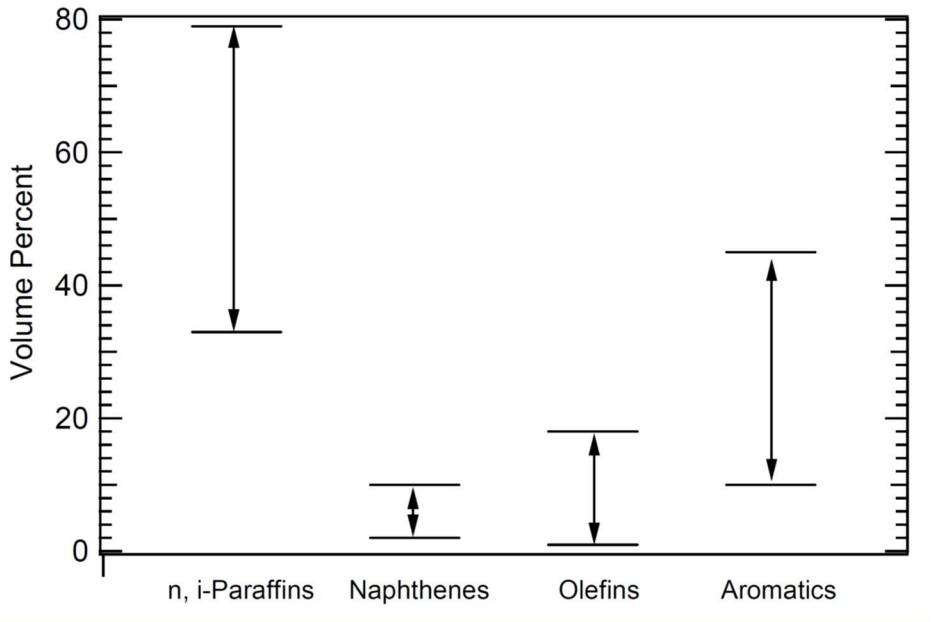


*Figure 2.4-1: Approximate ranges of paraffins, naphtenes, aromatics, and olefins in commercial U.S. gasoline **[11]**.*

*Table 2.2: Fuel surrogate component **[11]**.*

| Fuels | Relevance to Practical Systems | | | Understanding of Mechanism | | Property Information | |
|---|---|---|---|---|---|---|---|
| | Gasoline | Diesel | Jet | Low & Intermediate Temperatures | High Temperatures | Thermo-physical | Transport (thermal conductivity and transport) |
| | | | | | | | |
| **Straight-chain Alkanes** | | | | | | | |
| n-Heptane | A | B | B | A | A | A | A- |
| n-Decane | F | B | A | B | A- | A | A |
| n-Dodecane | F | B | A | B | B | A | A |
| n-Tetradecane | F | B | A | B | B | B+ | B |
| n-Cetane (n-hexadecane) | F | A | B | C | C | B+ | B |
| | | | | | | | |
| **Branched-chain Alkanes** | | | | | | | |
| iso-Octane (2,2,4-trimethylpentane) | A | C | B | A- | A | B+ | B |
| iso-Cetane (2,2,4,4,6,8,8-heptamethylnonane) | F | A | B | C | C | B- | C+ |
| iso-Dodecane (2-methylundecane) | F | C | A | D | D | D | D |
| | | | | | | | |
| **Cycloalkanes** | | | | | | | |
| Methylcyclohexane | C | C | B | C | C | B+ | B |
| Ethyl/propyl/butyl-cyclohexane | C | B | A | D | D | B | C |
| Decalin | F | B | B | D | D | B | B- |
| | | | | | | | |
| **Alkenes** | | | | | | | |
| 1-Pentene | B | F | C | B | B | B+ | C |
| Di-isobutylene | B | F | C | D | B | B | D |
| | | | | | | | |
| **Single-ring Aromatics** | | | | | | | |
| Toluene | A | A | C | C | C | A | B+ |
| Ethyl.propyl/butyl-benzene | C | B | A | C | C | B | B |

| | | | | | | | |
|---|---|---|---|---|---|---|---|
| Xylene | B | B | C+ | C | B | B | B |
| n-decyl-benzene | F | A | C | D | D | D | D |
| | | | | | | | |
| **Multi-ring Aromatics** | | | | | | | |
| Tetralin | C | C | C+ | D | C | B+ | B- |
| 1-Methyl-naphthalene | C | C | B | C | C | B | C |
| | | | | | | | |
| **Oxygenates** | | | | | | | |
| Ethanol | B | B | F | D | A | A | B+ |
| Dimethyl ether | F | F | F | A | A | B+ | B |

| Legend | | | | | |
|---|---|---|---|---|---|
| | A | B | C | D | F |
| Relevance to Practical Systems | Very important | Important | Possible surrogate, but not crucial | | No relevance |
| Understanding of Mechanism | Detailed mechanism(s) that has been validated over wide range | Mechanism(s) reported, but with modest discrepancies or limitations | Mechanism(s) reported, but with major discrepancies or limitations | No mechanism reported | |
| Thermo-physical Properties | EOS available (density to 0.3%) | Sufficient data for model (density to 3%) | Limited data only | Extremely limited/no experimental data, predictive model feasible | No data or predictive model available |
| Transport Properties | Correlations available for viscosity and thermal conductivity (5%) | Data available for models (5-10%) | Limited viscosity and/or thermal conductivity data | Extremely limited/no experimental data, predictive model feasible | No data or predictive model available |

Pitz et al. [11] took the effort to summarise all the existing studied surrogate fuels for gasoline, diesel and jet fuels with ratings as shown in Table 2.2 (nomenclature

of rating system was included). Determination of relevance of surrogate fuels to either diesel, gasoline or jet fuels were not explained. However, the relevance of surrogate fuels can be determined by study conducted by Yahyaoui et al. [52] In this study [52] oxidation of a ternary mixture of gasoline surrogate fuels such as iso-octane, toluene, 1-hexene, and ETBE (ethyl tert-butyl ether) were studied in jet-stirred reactor and shock tube experimentally and the results were compared to predictions of modelling work which employed kinetics of the same ternary mixture. This ternary mixture was proposed as gasoline surrogate fuel based on similarity of chemical composition between gasoline and ternary mixture. Three most abundant groups of constituents in gasoline such as paraffins, aromatics and olefins were represented by iso-octane, toluene and 1-hexene. ETBE was included as surrogate to oxygenated addictives in gasoline. This approach of choosing appropriate surrogate fuels still required more verification because Yahyaoui et al. did not compare the results of ternary mixture oxidation to gasoline combustion data. Naik et al. [53] performed modelling work for gasoline combustion in HCCI engine with kinetics of ternary mixture which consisted of iso-octane, n-heptane, toluene, methyl cyclohexane and 1-pentene. The ternary mixture used by Naik's work was similar to Yahyaoui's one except that Naik even considered the surrogate fuel (Methyl cyclohexane) which represented napthenes constituted in gasoline. Besides employing surrogate fuels to represent every group of species in gasoline, Naik compared surrogate mixtures with different composition of above species which yielded different RON and MON numbers. RON number was known to govern combustion in spark-ignition engine. In this work, a direct-injection compression ignition engine was used hence implication of RON number of surrogate fuels to combustion in this type of engine would be worth investigating. RON number of mixture was estimated by summing up RON values of every constituent which was calculated by multiplying its molar concentration with RON number of neat fuel [53]. Auto-ignition chemistry had been claimed to be governed by the concentration of OH radicals [54]. The start of combustion for a homogeneous combustion can be defined as the time when OH radical concentration reaches maximum. In order to understand the auto-ignition

chemistry of pure hydrocarbons that would be used as surrogate fuels for gasoline and diesel, review of initialisation chemistry of OH radical and propagation chemistry of OH radical till maximum concentration was studied. Co-oxidation of binary or ternary surrogate fuels mixture was shown to have common paths of oxidation as the hydrocarbons but also specific paths of oxidation which are only available for the mixtures [55, 56]. Therefore, interaction chemistry between different hydrocarbons was essential to be reviewed. Vanhove et al. [55] conducted experimental study of the oxidation and auto-ignition of five undiluted mixtures of hydrocarbons in a rapid compression machine below 900k. The mixture included heptanes/toluene, isooctane/toluene, isooctane/1-hexene, 1-hexene/toluene, and isooctane/1-hexene/toluene. The low-temperature oxidation of alkanes was dominated by peroxidation reactions of alkyl radicals and by a negative temperature coefficient (NTC) region of the rate [55]. Higher alkenes were oxidized through the same reactions, but have also specific pathways resulting from the presence of a double bond in the alkene molecule [55]. Aromatics were much less reactive in the same conditions unless they bear a long lateral alkyl chain [55]. The following sub-sections toluene, toluene/n-heptane, 1-hexene, 1-hexene/iso-octane, 1-hexene/toluene and isooctane/1-hexene/toluene were dedicated to explain combustion kinetics of various hydrocarbons and hydrocarbons mixtures.

**Toluene/air**

Vanhove reported a long ignition delay (exceeding 100ms) for combustion with mixture of toluene and air at temperature and pressure below 916K and 17bar. Combustion of toluene/air mixture at low temperature was claimed to be initiated by cleavage of weak O-O bond which forms reactive OH radical and end with a final auto-ignition.

At low temperature (below 1000k),

$$C_6H_5CH_3 + O_2 \rightarrow C_6H_5CH_2^* + HO_2^* \qquad (2.4\text{-}1)$$

$$C_6H_5CH_3 + OH^* \rightarrow C_6H_5CH_2^* + H_2O \quad (2.4\text{-}2)$$

$$C_6H_5CH_2^* + O_2 \rightarrow C_6H_5CHO + OH^* \quad (2.4\text{-}3)$$

$$C_6H_5CH_2^* + HO_2^* \rightarrow C_6H_5CH_2O^* + OH^* \quad (2.4\text{-}4)$$

$$C_6H_5CH_2O^* + O_2 \rightarrow C_6H_5CH_2O + HO_2^* \quad (2.4\text{-}5)$$

Intermediate reactions for Equation 2.4-3,

$$C_6H_5CH_2^* + O_2 \Leftrightarrow C_6H_5CH_2O - O^* \rightarrow C_6H_5CH^*O - OH \rightarrow C_6H_5CHO + OH^* \quad (2.4\text{-}6)$$

Intermediate reactions for Equation 2.4-4,

$$C_6H_5CH_2^* + HO_2 \Leftrightarrow C_6H_5CH_2O - OH^* \rightarrow C_6H_5CH_2O^* + OH \quad (2.4\text{-}7)$$

Reactions (equations 2.4-1 to equation 2.4-5) were the initialisation reactions of toluene oxidation at low temperature. Reactions (equation 2.4-6 and equation 2.4-7) were the intermediate reactions for reactions (equation 2.4-3 and equation 2.4-4). The final auto-ignition was provoked by reactions below (equation 2.4-8 and equation 2.4-9). Hydrogen peroxide decomposed as the temperature increased because of the exothermicity of the oxidation of toluene to benzaldehyde and water [55]. This step gave a sudden spike of OH-radical concentration which promoted auto-ignition. For auto-ignition of toluene/air at high temperature (above 1000k), reaction of equation 2.4-10 was responsible.

$$HO_2^* + HX \rightarrow H_2O_2 + X \quad (2.4\text{-}8)$$

$$H_2O_2 + M \rightarrow 2OH^* + M \quad (2.4\text{-}9)$$

At high temperature (above 1000k),

$$C_6H_5CH_3 + HO_2^* \rightarrow C_6H_5CH_2^* + H_2O_2 \qquad (2.4\text{-}10)$$

**Toluene/n-heptane**

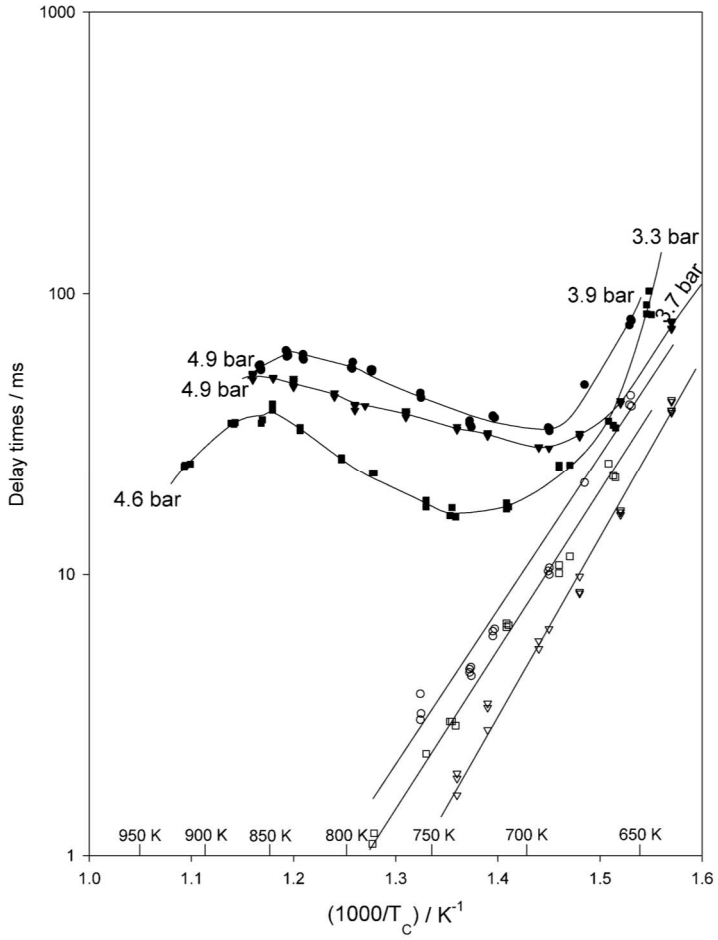


*Figure 2.4-2: Comparison of cool flame (white symbols) and auto-ignition delay times (black symbols) of stoichiometric pure n-heptane (squares), 1/1 n-heptane/benzene (triangles), and 1/1 stoichiometric n-heptane/toluene (circles). Pressures at top dead centre are added* ***[55]****.*

Vanhove et al. [55] performed experiments intended to study interactions between toluene and n-heptane and the cool flame and auto-ignition delay times were shown in Figure 2.4-2. According to this plot, addition of toluene or benzene would prolong the ignition delay time but not the cool flame delay; dependency of mixture reactivity to temperature was reduced as toluene and benzene were added. Toluene

was found to be effectively reacted because presence of benzaldehyde, benzene and ethylbenzene were found before auto ignition. Although addition of benzene to n-heptane had the same effect as toluene, but no trace of benzene oxidation was found. Hence, the changes observed for benzene additions were believed to be due to change of thermal properties of mixture.

**Toluene/iso-octane**

When toluene was added, ignition delay increased; temperature coefficient of cool flame delay increased (more rapid reduction of cool flame delay as temperature increased; temperature range for cool flame region became narrower; the oxidation scheme of iso-octane was not changed but rather it deactivated the pool of radicals by converting active radicals into stable benzyl radicals by reactions (Equation 2.4-2 and possibly equation 2.4-10).

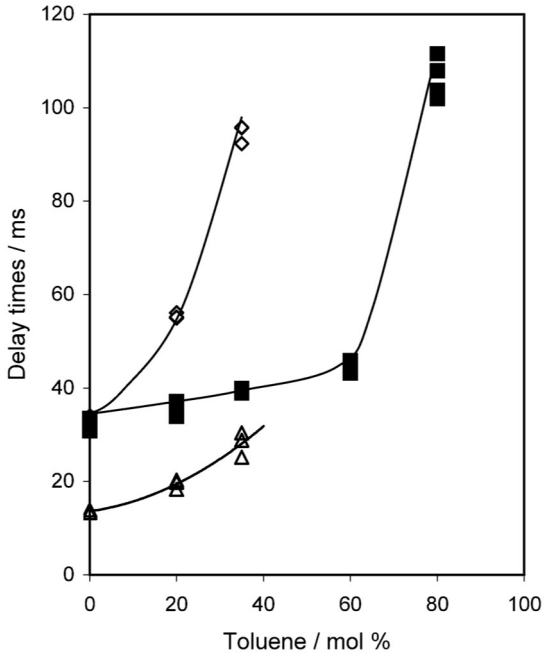


*Figure 2.4-3: Auto-ignition delay times of toluene/iso-octane mixtures for increasing amounts of toluene at temperature of 693K (white symbols, two stages of ignition) and at temperature of 856K (black squares, one stage of ignition). All initial mixtures were stoichiometric* ***[55]****.*

The increase of the delay times was much more sensitive to toluene composition at 693k than at 856k as shown in Figure 2.4-3. N-heptane/toluene mixture did not show this phenomenon because combustion occurred at lower pressure (lower octane number) hence either probability of an addition of $HO_2$ to benzyl radicals was reduced, competition for the pool of small radicals entirely in favour of n-heptane or both. For species that was formed by termination reactions of interactions between iso-octane and toluene were ethylbenzene and methylbutenylbenzene. They were stable products that played minor role in overall reactivity.

**1-hexene**

$$C=CH-CH_2^* + O_2 \Leftrightarrow C=CH-CH_2O_2^* \rightarrow C=CH-CH^*O_2H \rightarrow C=CH-CO^* + OH^* \quad (2.4\text{-}11)$$

$$C=CH-CH_2^* + HO_2 \rightarrow C=CH-CH_2O_2H \rightarrow C=CH-CH_2O^* + OH^* \quad (2.4\text{-}12)$$

$$C=CH-CH_2O^* + O_2 \rightarrow C=CH-CHO + HO_2^* \quad (2.4\text{-}13)$$

$$\text{alkene} + HO_2^* \rightarrow \text{oxirane} + OH^* \quad (2.4\text{-}14)$$

Reactions above (equation 2.4-11 to equation 2.4-14) were claimed to be responsible for initiation of auto-ignition for alkene. Hydrogen abstraction to activate pool of radicals mainly occurred at allylic hydrogen. The behaviour of long-chain alkenes varied according to the position of the double bond and the length of the alkyl chain. Double bond had a stabilising effect on the allylic-type radicals but a promoting effect on $HO_2$ radicals by reaction (equation 2.4-14).

**1-hexene/iso-octane**

Autoignition delay times of the isooctane/1-hexene 82/18 mixture were measured between 625K and 900K. Co-oxidation of iso-octane and hexene was found to be competition of main path oxidation only. No distinct species was formed by the co-oxidation.

**1-hexene/toluene**

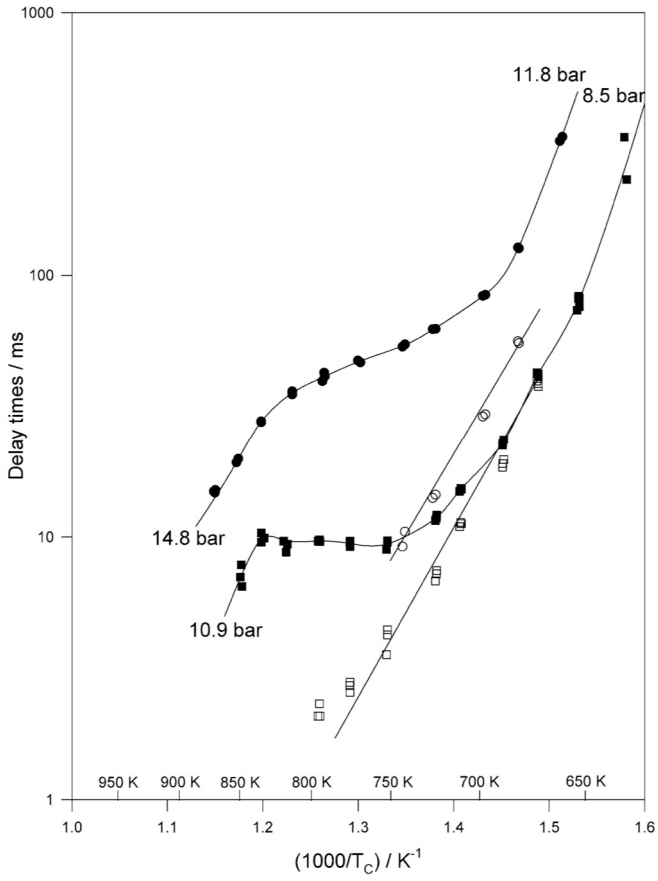


*Figure 2.4-4: Comparison of cool flame (white symbols) and auto-ignition delay times (black symbols) of the 30/70 1-hexene/toluene mixture (circles) with pure 1-*

*hexene (squares). Pressures at top dead centre were added. All initial mixtures were stoichiometric* ***[55]****.*

Addition of toluene to 1-hexene reduced the effect of cool flame as depicted in Figure 2.4-4. Heavier aromatics were formed: ethylbenzene, styrene, butenylbenzene, 3-heptenylbenzene and dibenzyl. These heavier termination products did no influence to the chemistry of auto-ignition.

**Iso-octane/1-hexene/toluene**

Auto-ignition of iso-octane/1-hexene/toluene mixture produced same sets of products as its pure hydrocarbons except that 1-hexene gave a relatively larger amount of hexadiene. Refer to Figure 2.4-5, above 800K, reactivity of pure hydrocarbons and surrogate mixture were almost identical. Crossed products of co-oxidation between hydrocarbons were said to have negligible effect on auto-ignition chemistry. Co-oxidation of mixture of different hydrocarbons was regarded as competition among reaction paths for active radicals such as OH and $HO_2$.

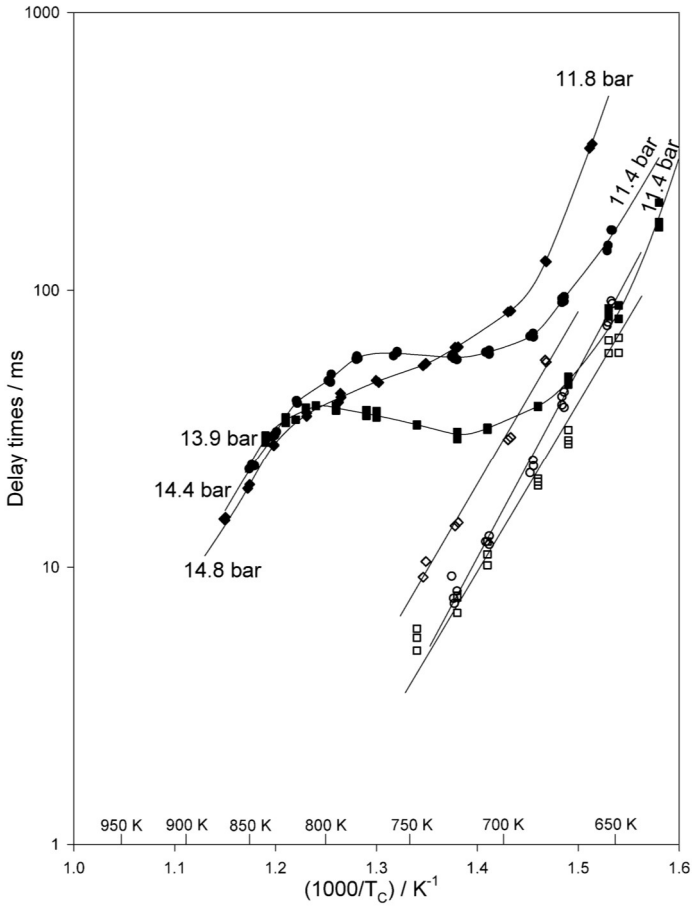


*Figure 2.4-5: Comparison of cool flame (white symbols) and auto-ignition delay times (black symbols) of the iso-octane/toluene/1-hexene 47/35/18 surrogate fuel (circles) with the 30/70 1-hexene/toluene mixture (diamonds) and the 82/18 iso-octane/1-hexene mixture (squares). Pressures at top dead centre were added. All initial mixtures were stoichiometric* ***[55]****.*

Andrae et al. [56] also did a kinetic study on co-oxidation of toluene and n-heptane by using modelling approach. The kinetic model employed in this study was validated against 35% n-heptane/65% toluene by liquid volume (28/72% by mole fraction) experimental data of high pressure shock tube [46] and toluene/air in shock tube [47]. Similar to Vanhove's work [44], Andrae argued unique crossed reactions of co-oxidation of toluene and n-heptane and the effects of these crossed reactions on auto-ignition characteristics and ignition delay times.

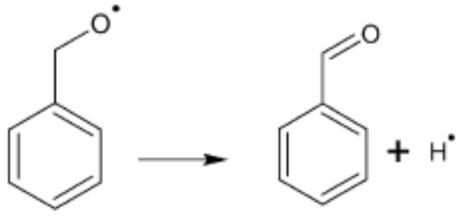

$$C_6H_5CH_2O^{\bullet} \rightarrow C_6H_5HC{=}O + H^{\bullet} \qquad (2.4\text{-}15)$$

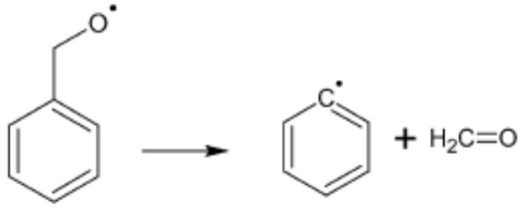

$$C_6H_5CH_2O^{\bullet} \rightarrow C_5H_5C^{\bullet} + H_2C{=}O \qquad (2.4\text{-}16)$$

Reactions (equation 2.4-15 and equation 2.4-16) were claimed to have higher reaction rate for toluene oxidation as compared to co-oxidation of toluene and n-heptane. Hence, the rate constants of these two reactions of toluene mechanism had to be adjusted after merging with n-heptane mechanism.

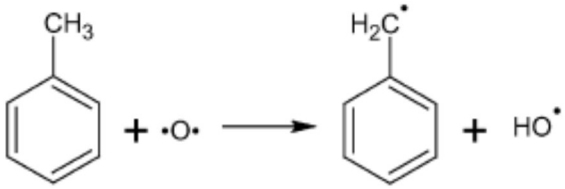

$$C_6H_5CH_3 + O^{\bullet\bullet} \rightarrow C_6H_5H_2C^{\bullet} + HO^{\bullet} \qquad (2.4\text{-}17)$$

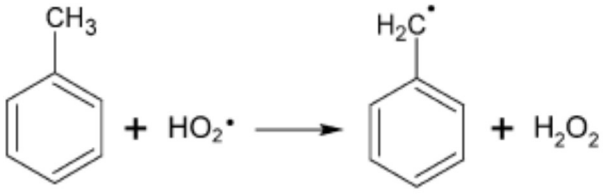

$$C_6H_5CH_3 + HO_2^{\bullet} \rightarrow C_6H_5H_2C^{\bullet} + H_2O_2 \qquad (2.4\text{-}18)$$

Reactions (equation 2.4-17 and equation 2.4-18) were claimed to be undergone by toluene molecules when they were reacted with larger pool of active radicals

introduced by mixture of n-heptane. Ethylbenzene was treated as terminate species in oxidation of toluene because no further oxidation was available for ethylbenzene molecule [56]. However, Andrae introduced further oxidation paths of ethylbenzene for co-oxidation of toluene and n-heptane.

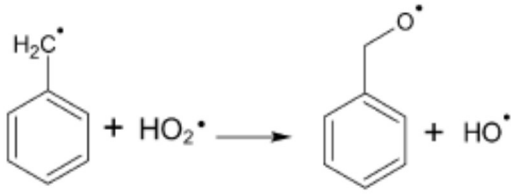


$$C_6H_5H_2C^{\bullet} + HO_2^{\bullet} \rightarrow C_6H_5CH_2O^{\bullet} + HO^{\bullet} \qquad (2.4\text{-}19)$$

Andrae et al. [56] reported enhanced oxidation rate of toluene when n-heptane was added and this effect was known as cross-acceleration. Quoted from Vanhove's work [55], rate of reaction (equation 2.4-19) was reduced as n-heptane was added to toluene. N-heptane (lower octane rating) mixture caused auto-ignited combustion to occur at lower pressure hence probability of this reaction to occur was lower. Rate of reaction (equation 2.4-19) needed to be reduced for co-oxidation of toluene/n-heptane mixture to decrease the over-predicted cross-acceleration effect. However, reduction of rate of reaction (2.4-19) would cause the prediction of ignition delay time to be unsatisfactory. Therefore, Andrae introduced a lumped reaction (equation 2.4-20) to overcome this issue. Crossed reactions of co-oxidation of toluene and n-heptane were only crucial for combustion at temperature below 1000k.

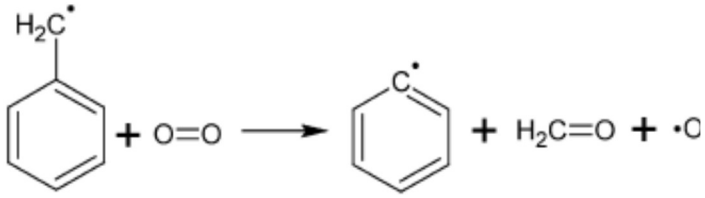


$$C_6H_5H_2C^{\bullet} + O{=}O \rightarrow C_6H_5C^{\bullet} + H_2C{=}O + O^{\bullet\bullet} \qquad (2.4\text{-}20)$$

All the works of chemical kinetic mechanism development involved validation against experimental data to justify the accuracy of the models' predictions. Experimental data from jet-stirred reactor, opposed-flow diffusion flame reactor, variable-pressure flow reactor, fixed-pressure flow reactor, shock tube, rapid compression machine, constant-volume combustion chamber and motored engine were used to validate the accuracy of mechanisms instead of data from internal combustion engines. Experiments of homogeneous combustions and flow reactors allowed combustion processes in an internal combustion engine to be isolated and studied separately. Especially CI combustion that occurred under wide range of temperature, pressure and equivalence ratio, many essential intermediate species and reactions could not be measured nor can they be understood with only the engine performance characteristics and emissions. Thus, homogeneous combustion and flow reactors experimental data were crucial for developing a chemical kinetic mechanism. Homogeneous combustion experiments modelled the transient phase of combustion or premixed combustion in diesel engine. Flow reactors modelled the steady-state phase of combustion or mixing–controlled combustion in diesel engine. Figure 2.4-6 illustrated the idea of choosing homogeneous combustion and flow reactors experimental data that were relevant to studied diesel engine. For this case, pressures and temperatures involved in transient-phase combustion were 54-60bar and 900-1000K; pressures and temperatures involved in steady-state combustion were 60-75bar and 1000-1620K. Combustion of fuel at different temperature range (low, medium or high) was governed by different sets of reactions. For methyl butanoate, Equation 2.4-21 to equation 2.4-26 were the paramount reactions at various temperature ranges [17].

For high temperatures (above 1200K),

$$H + O_2 \rightarrow O + OH \qquad (2.4\text{-}21)$$

For intermediate temperatures (850K-1200K),

$$H + O_2 + M \rightarrow HO_2 + M \qquad (2.4\text{-}22)$$

$$RH + HO_2 \rightarrow R + H_2O_2 \quad (2.4\text{-}23)$$

$$H_2O_2 + M \rightarrow OH + OH + M \quad (2.4\text{-}24)$$

For low temperatures (below 850K),

$$R + O_2 + M \rightarrow RO_2 + M \quad (2.4\text{-}25)$$

$$RO_2 \rightarrow QOOH \quad (2.4\text{-}26)$$

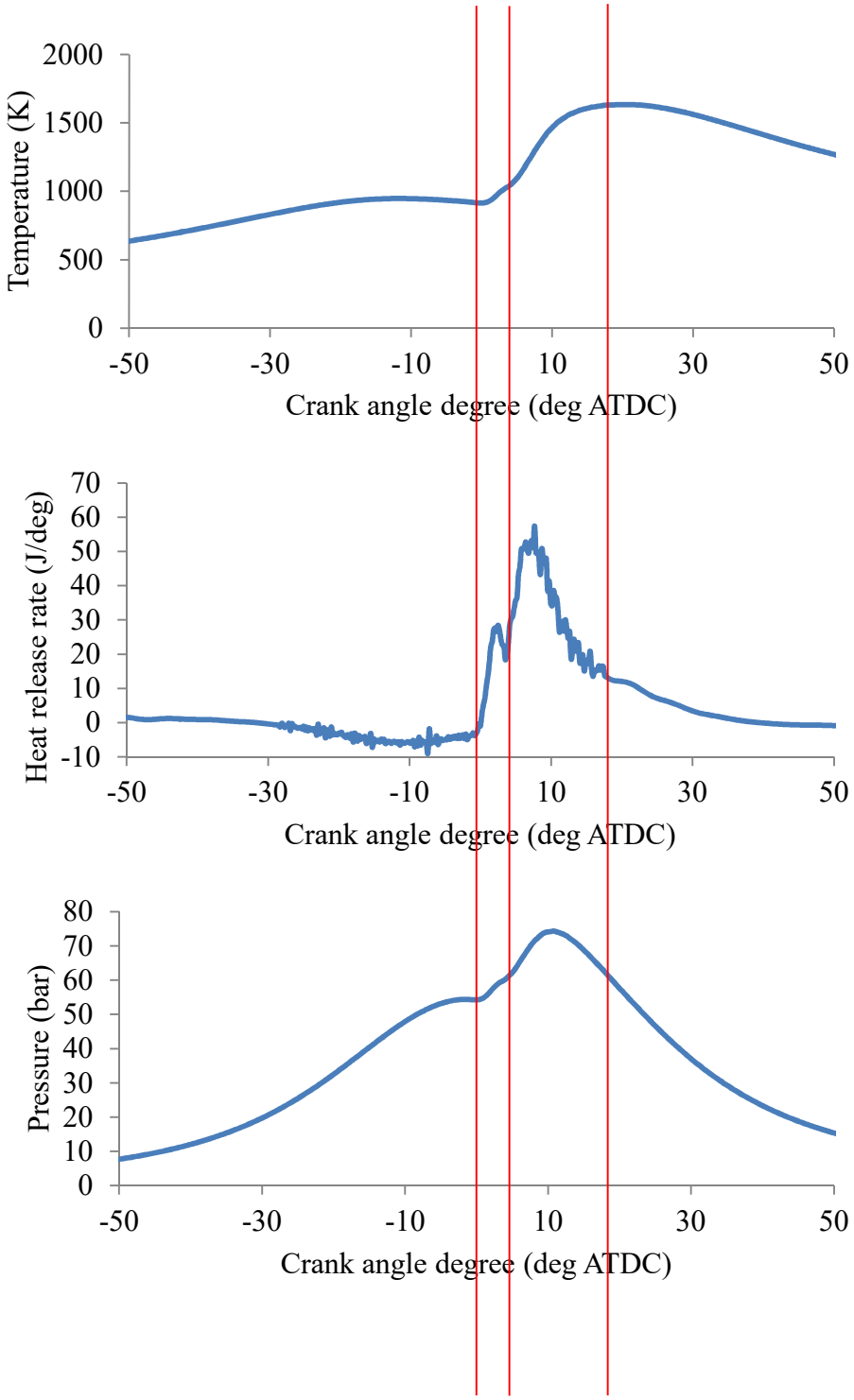


*Figure 2.4-6: Sample pressure, temperature and heat release rate traces of 2.4L engine.*

## 2.5: Chemical kinetic mechanisms reduction techniques

There had been numerous methods developed for chemical kinetic mechanism reduction over the year. The earlier and simpler methods revolved around absolute rate of production analysis, normalised sensitivity analysis, temperature sensitivity analysis, and mole fraction of species analysis. The absolute rate of production analysis measured the rate of production of all reactions that influence the composition of species that were being studied. The normalised sensitivity determined the sensitivity of a selected species in relation to the rates of reactions within a mechanism. The temperature sensitivity measured effect of temperature variation towards rates of reactions. The mole fraction of species analysis provided the details of species concentration through the entire chemical kinetic reaction period.

Brakora et al. [17] used a 3-step reduction strategy for reducing a methyl butanoate kinetic mechanism. The strategy began with a peak concentration analysis which fell in the category of the mole fraction of species analysis, followed by a reaction flux analysis which fell in the category of the absolute rate of production analysis, and finally the reaction rates of reactions were adjusted. In the first step, the concentration of every species was being analysed. Species with mole fractions smaller than the thresholds were taken as the insignificant species and eliminated. The thresholds of elimination such as $10^{-10}$, $10^{-9}$, $10^{-8}$, $10^{-7}$ were used to identify these insignificant species. After the reductions with these thresholds, ignition delays predicted by the skeletal mechanism were compared to the ignition delays predicted by the detailed mechanism at various engine operating conditions. The reduced mechanisms failed to predict ignition delay times at low temperature conditions. She then added back species with methyl ester structure and improved the accuracy of the reduced mechanisms.

For reaction flux analysis, flux was defined as the integral of reaction rate over time. By accessing pathways of relative flux among species, rate of destruction of reactant and rate of formation of product were mapped out. Species that had insignificant effect towards ignition delay time were eliminated. Reaction rate

adjustment was crucial after species were removed because slight change of ignition delay time was unavoidable. In this article [17], the differences of ignition delay times for low temperature combustion were more significant. Therefore, reactions known to be responsible for low temperature combustion were analysed and the reaction rates were tuned. Reaction rates of reactions such as mb2oo=mb2ooh4j and mb+o2=ho2+mb2j were altered. The final mechanism comprised of methyl butanoate and n-heptane combined to assimilate energy content and chemical structure to soy-based biodiesel as depicted in Table 2.3.

*Table 2.3: Comparison of soy-based biodiesel and methyl butanoate, a proposed surrogate for biodiesel fuel **[17]**.*

| | Soy-based Biodiesel | Methyl Butanoate | 1 mole MB + 2 moles n-heptane |
|---|---|---|---|
| Chemical Structure | $RC(=O)OCH_3$ | $R'C(=O)OCH_3$ | $R'C(=O)OCH_3 + 2\ C_7H_{16}$ |
| Chemical Formula | $\sim C_{19}H_{34}0_2$ | $C_5H_{10}O_2$ | $C_{19}H_{42}O_2$ |
| Lower H.V. (MJ/kg) | 36-38 | 27 | 39 |
| Molec. Mass (kg/kmol) | 292 | 102 | 302 |
| % Oxygen (by mass) | ~11% | ~30% | ~11% |

Patel et al. [47] used a more comprehensive technique to reduce a detailed n-heptane mechanism. This technique started with identifying the most essential species and reactions. Reaction and species flux analyses were performed (normalised sensitivity analysis). Threshold flux value was set at 1% of the largest flux of the reactions or species. Reactions and species with smaller flux than threshold were eliminated. Only fluxes of reactions within domain of interest were considered. Domain of interest was the time taken for global temperature rise of

400K. Later, rate of change of species concentration analysis was performed (mole fraction of species concentration analysis). Reactions and species that had insignificant influence of formation and destruction of active radicals such as $H_2O$, $H_2O_2$, OH, and O were eliminated. Next, two or more reactions with similar products or reactants were assimilated into single reactions to reduce number of reactions. Finally, Patel used a micro-genetic algorithm optimisation technique to optimise reaction rate constants of reduced mechanism to improve prediction of ignition delay time and temperature histories in relative to detailed mechanism.

Maroteaux et al. [57] employed sensitivity analysis (temperature sensitivity analysis and normalised sensitivity analysis) and rate of production analysis (mole fraction of analysis) for reducing an n-heptane mechanism. Sensitivity analysis gave the normalised sensitivity coefficient which measured the dependence of temperature (or concentration) on rate constants of considered reactions. Rate of production analysis measured the intermediate species concentration. Intermediate species with low concentration could be eliminated. The reduced mechanism had been validated against ignition delay time, IMEP and heat release rate data or the original mechanism after each step of reduction. There were 2 criteria being used to justify the accuracy of the reduced models. Ignition delay time variation must not exceed one crank-angle degree. IMEP and heat release rate variations were restricted to be lower than 6%.

Saylam et al. [54] used analysis of reaction rates and the analysis of sensitivity as mechanism reduction technique. Analysis of reaction rates by Saylam was similar to Patel's reaction flux analysis (normalised sensitivity analysis). It distinguished the fast and slow reactions contained in a mechanism. Sensitivity analysis approach of Saylam was similar to Patel's change of species concentration analysis which measured sensitivity of species concentration towards overall rates of reaction. Instead of eliminating slow reactions, sensitivity analysis identified rate-limiting reactions. Rate-limiting reactions were basically reactions that dictated the overall rate of reaction. Radical species OH was claimed to be a main chain carrier in the oxidation and auto-ignition of hydrocarbons hence it was chosen as the target

species for sensitivity analysis. The idea of removing slow reactions and non-rate-limiting reactions with thresholds were depicted in Figure 2.5-1.

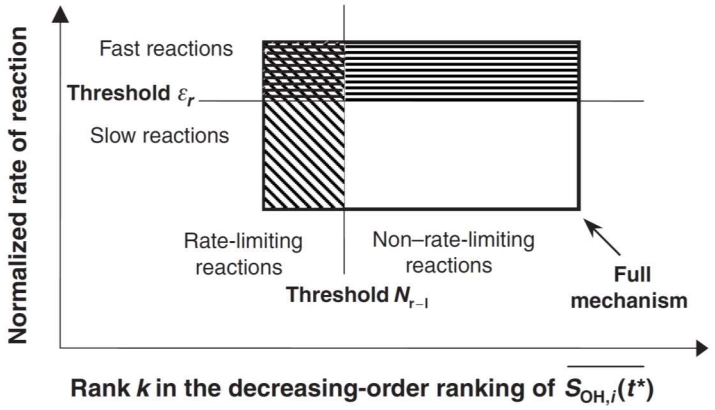


*Figure 2.5-1: Principle of redundant reaction selection and mechanism reduction **[54]**.*

Lu [58] first introduced the systematic mechanism reduction technique called direct relation graph. DRG was used to generate the 33species 205reactions skeletal mechanism with a specified accuracy requirement. The skeletal mechanism was then reduced to 20species and 16 reactions by using computational singular perturbation based on the assumption of quasi-steady-state species. A detailed ethylene oxidation mechanism consisted of 70species and 463reactions was used. Modelling of laminar flame speeds and non-premixed counter flow ignition with the skeletal or reduced mechanism showed very close agreement with those obtained by using the detailed mechanism over wide ranges of pressure, temperature and equivalence ratio. Lu [59] later demonstrated that DRG was applicable even when there was quasi-steady state species in chemical kinetic mechanism. When there were partial equilibrium reactions, Lu [59] took the reactions with fast forward and backward rates to be reversible. Reactions rates of slow reactions were computed through the equilibrium constant. The substantial cancellation of forward and backward reaction rates did significantly reduce the number of reactions present in mechanism but induce error for partial equilibrium reaction. Net rate of both forward and backward reactions could be used as the input for DRG to achieve the objective of reducing the number of reactions in

mechanism. This alternative approach could potential improve accuracy of mechanism with partial equilibrium reactions. DRG was compared to CSP (computational singular perturbation) and DRG-EP. CSP was able to reduce certain mechanisms with irreversible fast reactions but the size of the skeletal mechanism was larger than that reduced by DRG. However, as for DRG-EP, error propagation was found to be quite involved in the presence of fast processes, since the error induced for a species my directly affect other species through couplings by fast dynamics, in which case the geometric error damping assumption may be invalid [59]. Lu extended the DRG reduction with expert knowledge DRGX [60]. DRGX managed to produce smaller and more accurate skeletal mechanism than the conventional DRG.

This review provided vital motivations for this work. Previous works of gasoline combustion were conducted in very limited conditions which were hardly relevant to practical operating conditions of a CI engine. Single-cylinder engine has very simple cooling system which limits the gasoline combustion from running at engine speed and engine load relevant to a practical CI engine. The heat transfers would differ from an actual CI engine. Therefore the combustion can never reach a steady state of a CI engine when it is fully warmed-up and heat transfers stabilized. For this reason, it would be interesting to study gasoline combustion in steady state with a fully warmed-up CI engine. Besides the works that used single cylinder engine, there are other works that used a four cylinder CI engine but only with gasoline blends up to G40 and ran at low engine speed (< 1500rev/min) and low engine load (< 6bar BMEP). Increase the gasoline blends, engine speed and engine load would extend the knowledge of gasoline combustion in terms of ID characteristics which are correlated to $NO_x$ and soot formations and also limitation of fuel delivery of gasoline blends. The effect of engine parameters and fuel properties on combustion characteristics were reviewed. ID, $NO_x$ formation and soot formation were found to be controlled by engine boost pressure, engine speed, SOI timing and EGR. These information had helped to identify that engine speed, engine load and SOI timing as crucial parameters to study against ID. However the effect of combustion chemistry on ID remained unknown and hence the interest to

study the contribution of physical delay and chemical delay on ID was embarked. Discrimination of physical and chemical delay can be done via either experimental approach or CFD modelling. A zero-dimensional homogeneous combustion in combustion bomb, rapid compression machine or shock tube could be used to test chemical delay of gasoline blends. The drawback of the homogeneous combustion is that it is lack of interaction between physical mixing and chemical kinetic mechanism. An optical-engine experiment would provide the physicochemical interactions required to represent an actual CI engine, but with limitations such as unable to study gasoline blend combustion combustion at steady state due to overheating issues after a certain number of consecutive engine cycles and unable to attain compression ratio comparable to actual CI engine. A theoretical study via CFD modelling was found to be the most suitable approach to study ID characteristics and $NO_x$-soot formations of gasoline blend combustion in CI engine. There was no chemical kinetic mechanism available for diesel-gasoline blend from the literature. This highlighted the opportunity to develop a reduced chemical kinetic mechanism for diesel-gasoline blends, which could be used in CFD modelling. Based on the review for surrogate fuels, the detailed chemical kinetic mechanisms of n-heptane and iso-octane from LLNL were well validated and the most relevant to representing diesel and gasoline. A reduced chemical kinetic mechanism for diesel-gasoline blends can be built based on these two detailed mechanisms. Apart from the getting the appropriate mechanism for diesel-gasoline blends, reducing the size of the mechanism down to the level which is feasible for CFD modelling yet maintaining its accuracy in predicting ID remains a challenge. DRG reduction was shown to be very efficient and effective way to reduce detailed chemical kinetic mechanism down to a size useable for CFD modelling. DRG also has the potential to be written into programming algorithms and automate reduction process for chemical kinetic mechanisms. An automatic reduction algorithms would be very useful for building chemical kinetic mechanisms for CFD modelling because variables such as species to be retained and Arrhenius constants of reactions could easily be tweaked and the accuracy of the resulted reduced mechanism can quickly be validated against results of CFD modelling. Therefore

this work would cover the development of DRG-based automatic reduction algorithms and systematic reduction process for the species size reduction of diesel-gasoline blends' chemical kinetic mechanism. This development would provide a solid foundation for future CFD modelling work of gasoline blends combustion.

# CHAPTER 3

## Experimental study of the diesel-gasoline combustion in CI engine

Engine experiment was conducted to study the use of gasoline and diesel fuels in CI engine. The main objectives of this experiment study were to study the ID characteristics and fuel injection limitation of gasoline blends combustion in CI engine at extended conditions such as higher engine speed (> 1500rev/min), higher engine load (> 6bar BMEP) and higher gasoline blends (> G40) as compared to existing works that had been done. The two main category of engines available for this type of experiment included the modern common-rail direct-injection CI engine and the pump-triggered direct-injection CI engine. The conventional pump-triggered type of injection system was selected for this study due to its robustness against the changes of fuel blends which varied in fuel properties in relative to diesel. The engine setup and other devices were explained in the following.

### 3.1 Equipment and setup of engine rig

The experimental engine rig used for this study consisted of a 2.4litre pump-triggered direct-injection turbocharged diesel engine with piston jet, a modified cooling system, an electric motor/generator dynamometer, and a data acquisition equipment. This engine rig was used to study heat release characteristics of different fuels under steady-state and different speed-load operating conditions. Parameters that were used in this study were engine speed, engine load, SOI timing and fuel blend. Control of these parameters and acquisition of vital data for this study were explained in detailed in later section. Specifications of major sensors were shown in Table 3.1. Specifications of engine geometry were summarised in Table 3.2.

*Table 3.1: Specifications of major sensors.*

| Device | Measurement (units) | Resolution | Accuracy |
|---|---|---|---|
| Crankshaft encoder | Crank-angle position (º ATDC) and engine speed (rev/min) | ±0.05º ±0.00014rev/min | ±0.01º ±0.000028rev/min |
| Load cell | Engine load (N) | ±0.1N | |
| Pressure transducers | Fuel-line pressure and In-cylinder pressure | ±1e-6Pa | - |

*Table 3.2: Specifications of engine geometry.*

| Engine's geometric specifications | |
|---|---|
| Piston type | Piston with Mexican-hat bowl |
| Cylinder head type | Flat cylinder head |
| Engine capacity | 2.4 Litre |
| Displacement volume | 5.4951e-4 $m^3$ |
| Clearance volume | 3.136e-5 $m^3$ |
| Compression ratio | 18.5 |
| Stroke | 0.0946 m |
| Bore diameter | 0.0899 m |
| Connecting rod length | 0.1498 m |

The cooling system of this engine rig was designed to overcome the no-airflow condition of the stationary engine during operation. The original air-cooled heat exchangers of a car were substituted by liquid-cooled heat exchangers which run on either water or coolant. The charge air cooler (turbocharger's intercooler) was changed from air-to-air heat exchanger to tube-and-fin heat exchanger. The ordinary tube-and-fin radiator was replaced with shell-and-tube heat exchanger. The tube-and-fin oil cooler was changed to plate-heat exchanger. A schematic

diagram of the cooling system was depicted in Figure 3.1. The cooling system comprised of water and coolant cooling circuits. The heat exchanger emulated car radiator by removing heat from coolant with cool water supply from a cooling tower. Cool water from the cooling tower was used to chill compressed air which passed through the charge-air cooler. The coolant cooling circuit was used to remove heat from engine block, cool down exhaust gas with EGR cooler, and cool down engine oil with oil cooler. However the coolant was restricted by a thermostat when the temperature went below a threshold at approximately 70º Celsius for this rig. This was to ensure the engine warmed up to the optimum operating temperature as fast as possible, hence to reduce engine wear and shorten the time required for the engine to reach steady state condition. This rig also came with a chiller which could be used to provide additional cooling for oil sump and engine block. The features of this chiller were not used in this work. These modifications made the cooling capacity of the cooling system to be constant. The original cooling system from the car engine had cooling capacity that varied with rate of airflow which changed according to speed travelled by the car, temperature of the air, and the density of the air. This difference caused discrepancies of engine block temperatures and engine oil temperatures between the engine rig and the one from the car. However these discrepancies were taken to be negligible for this study. Engine block temperature with this cooling system was assumed to perform the same as the one from the car when the coolant temperatures before and after engine block were in the range of 85 to 95 degree Celsius. This simplification can be made for this study because the experiment was conducted under steady-state condition. Steady-state condition gave the cooling system amber of time to maintain the engine cylinder walls at a steady optimum temperature around 95 degree Celcius. If the engine were to perform below the optimum temperature, it would have too much of heat losses from the combustion through the cylinders. If the engine were to perform above the optimum temperature, it would be too hot to entrain dense air into the cylinders hence the volumetric efficiency would reduce. Hence the optimum engine wall temperature would give the extreme diesel-

gasoline fuel blends the best chance to combust successfully in this engine as compared to the actual engine temperatures.

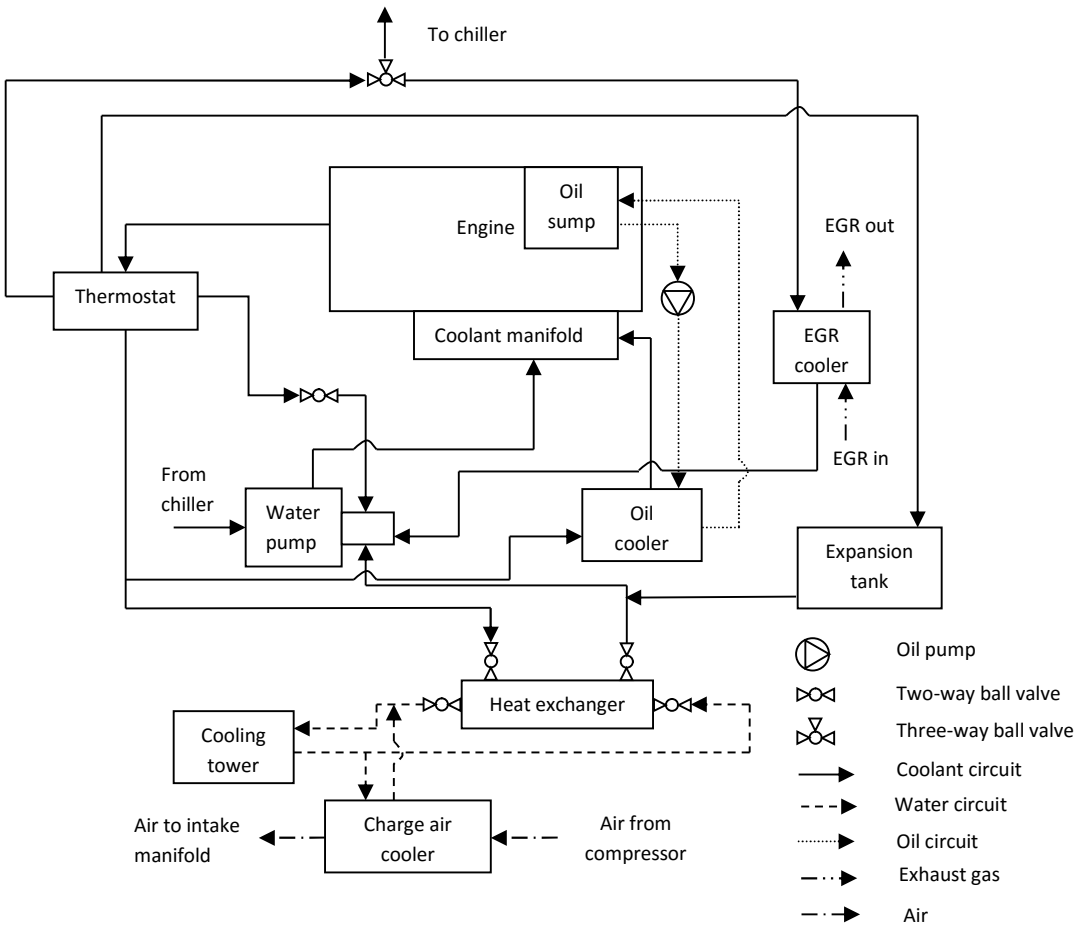


*Figure 3.1: Schematic diagram of cooling system of engine rig.*

The dynamometer of this engine rig was capable of generating driving torque and braking torque to the test engine. It emulated the transmission gearbox of a car and simulated speed-load conditions for the car engine. It also served as the starter motor of the engine and measured the engine speed and brake torque. Engine speed and brake torque were measured by the crankshaft encoder of the engine and the load cell of the dynamometer. Figure 3.2 illustrated the communication flow chart of the equipment of the engine rig. The dynamometer was controlled by a dynamometer controller which offered a constant-speed control. The controller

received a set point signal of speed from the voltage control device, computed an output signal to either motor or brake of the dynamometer (output signal to motor if engine produced negative torque or to brake if engine produced positive torque) , and then received a feedback signal of speed from the crankshaft encoder. This closed-loop control allowed the dynamometer to maintain the engine at the set-point speed regardless of the brake torque generated by the engine. The voltage control device provided another signal known as "accelerated pedal position" (APP) to be fed to the ECU. APP represented the physical pedal position of the car in percentage (0% represents idle position and 100% represents fully-accelerated position).

The APP signal produced by the voltage control device replaced the car's physical pedal and potentiometer setup. The ECU then read an engine map which consisted of the major variables received from the sensors such as APP, engine speed, start of injection time, EGR valve lift, and amount of fuel to be injected. The engine map interpolated a signal which represented the amount of fuel required to be injected for the distributor injection pump. The distributor injection pump was the equipment that ultimately controlled the amount of fuel injected by the injectors into the engine cylinders. The purpose of controlling the APP was to control the brake torque of the engine as brake torque produced by the engine was proportional to APP. Speed and brake torque of the engine were constantly displayed in data-acquisition software. Both needed to be verified manually and readjusted until required conditions were achieved. This constant-speed dynamometer setup came with a cautious step to be taken when the engine speed was reduced. As the engine speed was reduced, brake torque of the engine was automatically increased. Hence, the engine brake torque needed to be constantly monitored and reduced if necessary when the engine speed was reduced to avoid unintentionally spike of engine brake torque which may cause the engine to run at extreme load condition. By far, the fundamental of controlling the engine speed and brake torque with the equipment involved had been explained in detail.

For the start of injection time control, the main equipment involved were ECU and distributor injection pump. Distributor injection pump depicted in Figure 3.3 was responsible to distribute pressurised fuel to fuel injectors. The fuel distribution control was governed by signal received directly from the ECU. A data acquisition software named DAQ was used to send a digital signal of the required start of injection time to the ECU and later converted into the analogue signal by the ECU that controlled exactly when the distributor injection pump was activated.

The start of injection time signal from the DAQ software was pre-calibrated against the actual injector's start of injection time. Due to no live feedback of the start of injection time for this engine, the actual start of injection times were computed from outlet pressures of distributor injection pump (fuel-line pressure). Fuel injectors' nozzles opened at 200bar of fuel pressure hence this threshold was used for the measure of the start of injection time. Time when the fuel-line pressure reached 200bar was taken as the start of injection time.

The engine consisted of an EGR valve that could bypass exhaust gas to inlet manifold for exhaust gas recirculation purpose as depicted in Figure 3.4. The EGR valve lift was controlled by suction pressure created by a suction pump. Similar to the start-of-injection-time control, DAQ software fed the valve lift signal to the suction pump hence controlled the lift position of the EGR valve. The precise percentage of exhaust gas circulated to intake manifold was calculated based on carbon dioxide concentration measured by a gas analyser. This measurement setup was shown in Figure 3.4. A three-way valve was used to exchange between exhaust gas and intake gas. The gas analyser measured carbon monoxide, carbon dioxide and unburnt hydrocarbon. The volumetric ratio of carbon dioxide contained in intake gas to carbon dioxide contained in exhaust gas was taken as the measure of exhaust gas recirculation expressed in percentage. However the exhaust gas recirculation strategy was not included in the current study. It would be interesting to use EGR strategy to the gasoline combustion in CI engine as it was

shown to have the potential to simultaneously reduce both $NO_x$ and soot without the soot-$NO_x$ trade off experienced by conventional diesel combustion.

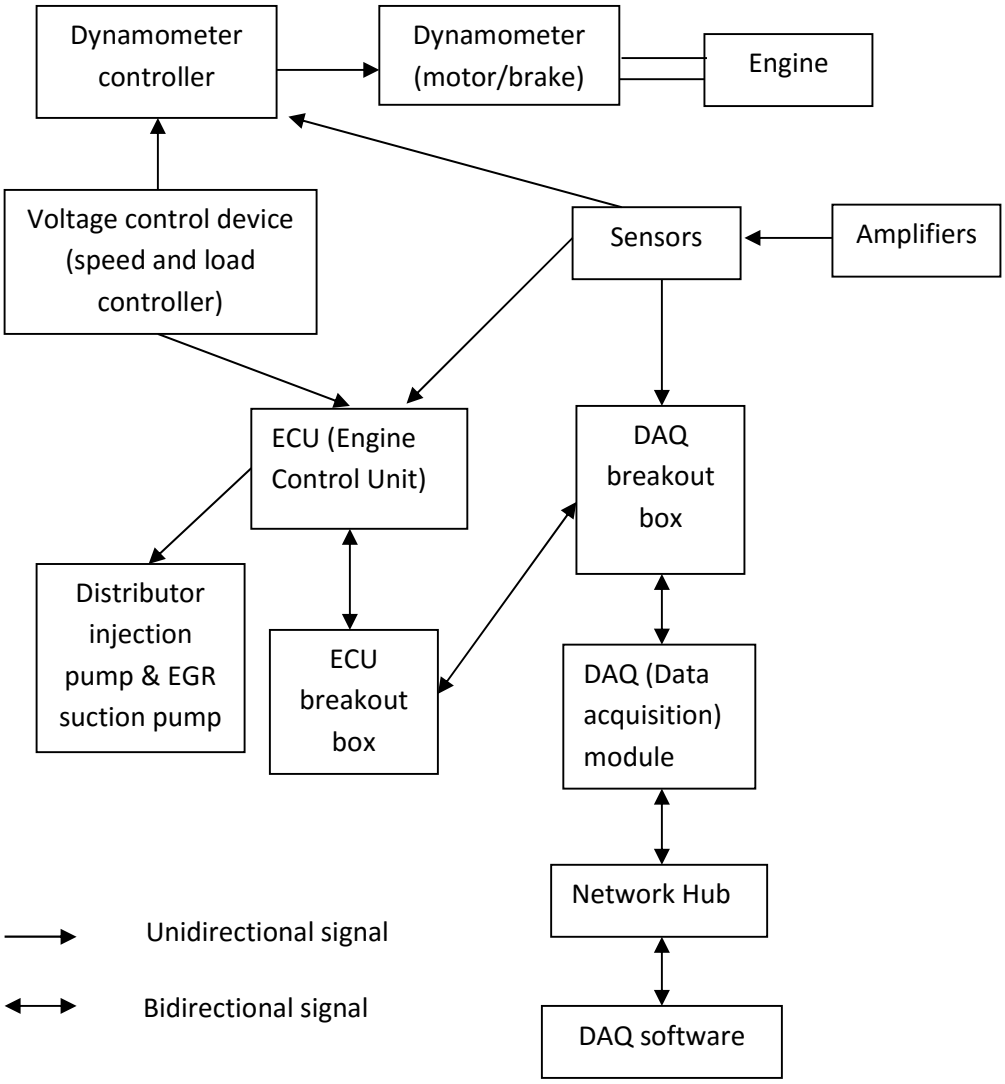


*Figure 3.2: Flow charts of communication among equipment via analogue and digital signals.*

The engine rig consisted of a diesel tank, a dumped tank and a mixed-fuel tank. The three fuel tanks served the purpose of running the engine on diesel-gasoline blends with precautionary steps to protect the engine. The diesel tank stored red diesel which had the same specifications as ordinary diesel from fuel station but with tax exemption. The dumped tank was used for disposal of unwanted fuel. The mixed-fuel tank was used to store diesel-gasoline blends. The setup of fuel

delivery from different fuel tanks was illustrated in Figure 3.3. This setup allowed the engine to warm up and cool down with diesel fuel only despite that diesel-gasoline blends were the test fuels. The fully warmed up engine gave the engine the best chance to burn the gasoline-diesel blends successfully because cold engine was expected to further prolong the ignition delay of the diesel-gasoline blends till the point of no combustion.

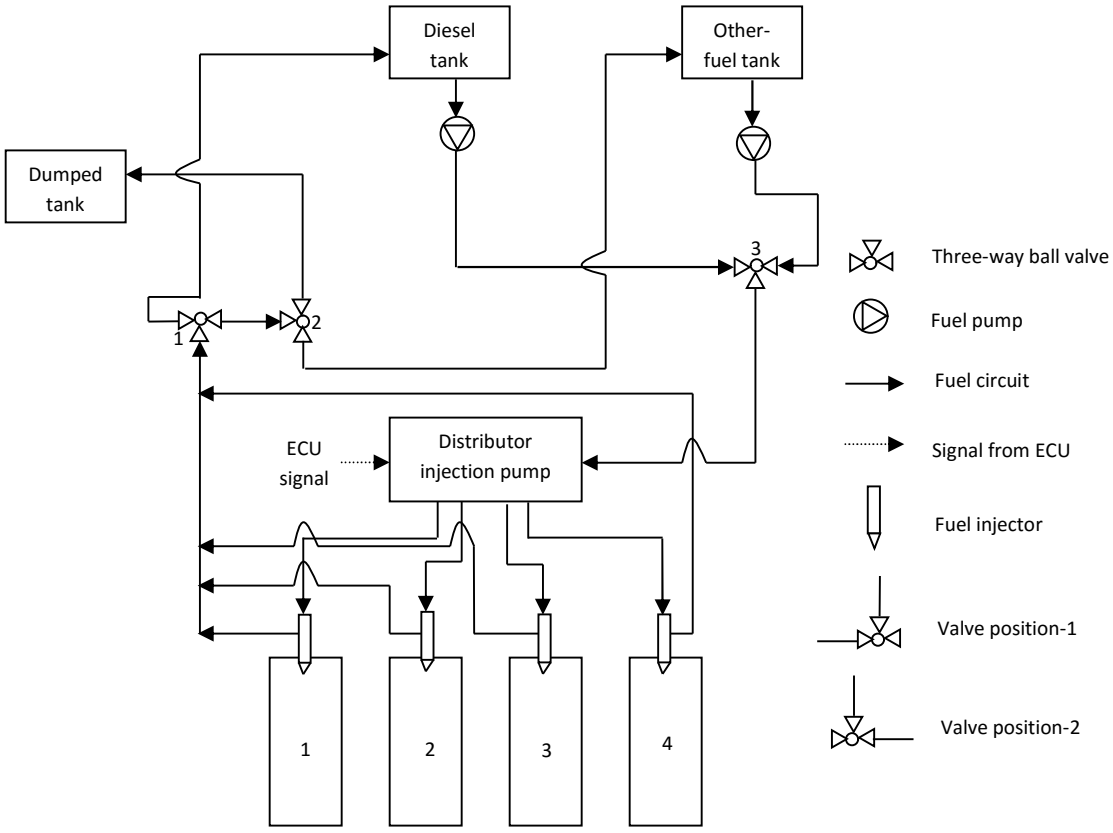


*Figure 3.3: Schematic diagram of fuel-injection equipment and fuel circuit of engine rig.*

All the three-way valves were in position-2 at the start and end of every test. Fuel from diesel tank was used when all the three-way valves were in position-2. The transition from diesel tank to mixed-fuel tank was done by switching all three valves to position-1. This three-tank setup required precautionary procedures to be taken to prevent fuels in both tanks to be contaminated by mixing with one another.

Valve-1 needed to be switched to position-1 first followed by valve-3 immediately. The transition of valve-1 directed the fuel returned from injectors to the dumped tank. The transition of valve-3 switched the fuel supply from diesel tank to mixed-fuel tank. Mixing of the new supply fuel with the remaining diesel in the fuel line was unavoidable during these transitions. Therefore, the contaminated fuel mixture had to be disposed to dumped tank. Valve-2 was to be remained at position-2 for approximately 10 seconds before it was switched to position-1 to ensure the fuel line was replaced entirely by the new supply fuel before the fuel in the fuel-line was returned back to the mixed-fuel tank. For switching fuel supply back to diesel tank from mixed-fuel tank, valve-2 was turned to position-2 first followed by valve-3 immediately right after it. Valve-1 was then turned to position-2 approximately 10 seconds after the switch of valve-3 to position-2. The three-tank setup allowed the engine to run on diesel-gasoline blends successfully even for the blend which contained as much as 70% of gasoline.

The main equipment of data acquisition were sensors, amplifiers, DAQ module, DAQ software, network hub, and computer. The sensors in this engine rig could be categorised into built-in sensors and external sensors. Built-in sensors were sensors that came with the engine. These sensors were connected to the ECU and provided feedbacks to ECU for engine-control purposes. External sensors were sensors installed to the rig to acquire additional data which were not measured by the built-in sensors but important for this study. The built-in sensors were crankshaft encoder which measured the engine speed and the crank-angle-degree position, ambient-air-temperature thermocouple, manifold air absolute pressure sensor, and thermistors which measured in-cylinder temperature. The external sensors in this work in were pressure transducers which measured in-cylinder pressures and fuel-line pressures of engine and dynamometer load cell which measured brake torque produced by the engine. The pressure transducers were installed in plug holes of cylinder-1 and cylinder-3 as depicted in Figure 3.3.

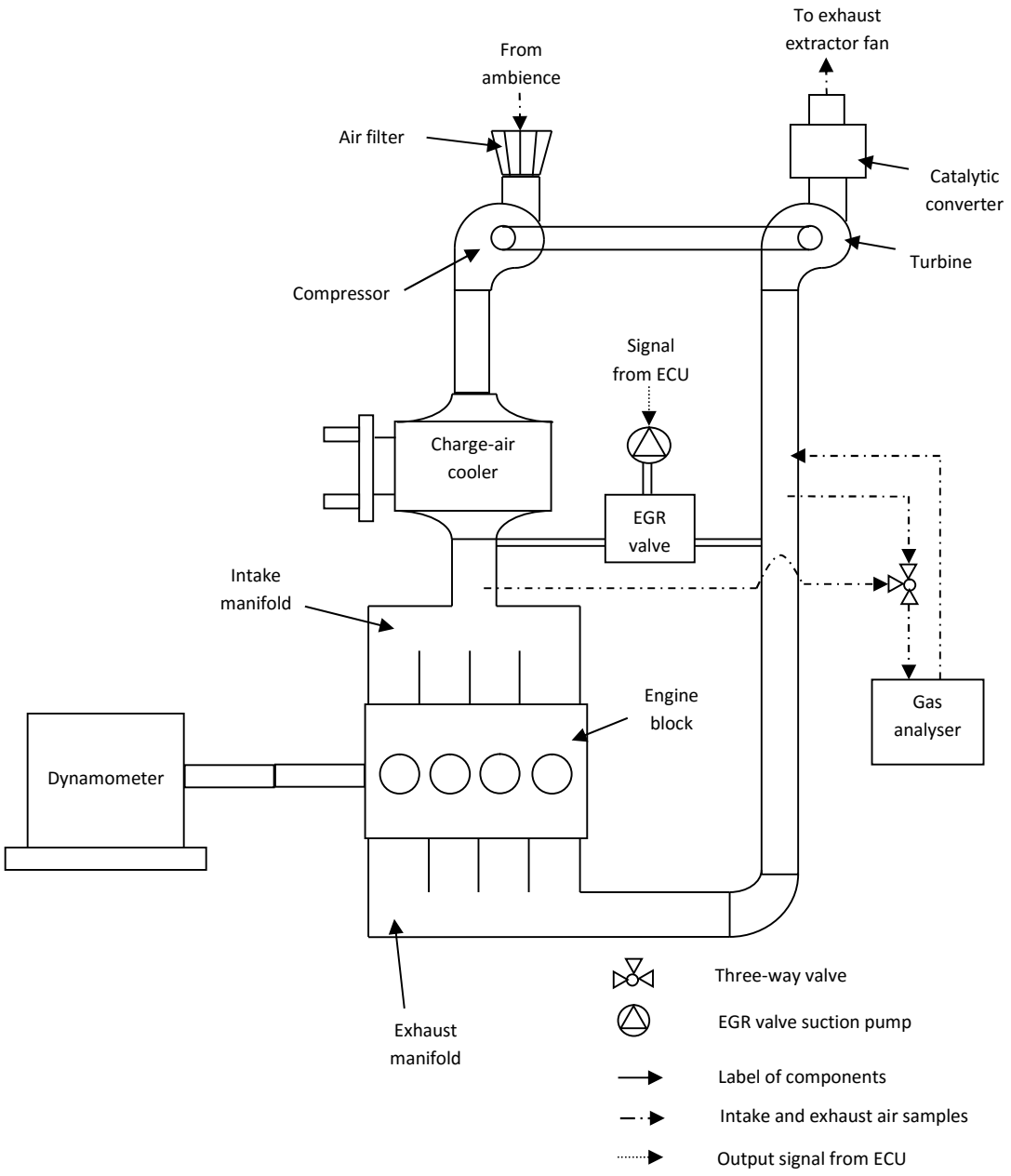


*Figure 3.4: Schematic diagram of main equipment and air-flow circuit of engine rig.*

### 3.2: Engine Tests and Data Processing

This engine rig setup was used to conduct engine tests for the study of heat release and ignition delay of different diesel-gasoline fuel mixtures under six different sets of part-load engine conditions more relevant to extra-urban driving. For engine speed of 1000rev/min and 2000rev/min, engine loads corresponded to brake mean

effective pressures (BMEP) of 2.5, 5, 7 bar and 2.5, 5, 8.5bar were tested, respectively under fully warmed up engine condition. The diesel-gasoline fuel blends were identified according to the blend proportions such that G10 was a blend of 10% gasoline and 90% diesel by volume. Diesel-gasoline blends varied from G10 up to G80 were used for this study. A lubricity additive, TOFA-S TK25 provided by Lubrizol, was added to all the fuel blends at concentration of 300 parts per million (ppm). The selected concentration had been shown to be effective in overcoming lubricity problems [61]. The added lubricity additive was verified to have no effect on injection timing, ignition delay and heat release rate. Hence the lubricity additive was added purely to protect the engine from potential additional wear introduced by diesel-gasoline combustion.

Two different DAQ software products, Labview and ATI Vision were used for data recording and engine monitoring in this work. Labview was responsible for high-frequency data recording and monitoring (up to 60,000 samples taken per second) such as in-cylinder pressures and fuel-line pressures. ATI Vision was used to monitor and record data from other sensors. For measurement of in-cylinder pressure and fuel-line pressure, synchronisation between pressure data and crank-angle-degree position of engine was crucial. The crankshaft encoder of this engine was capable of detecting top-dead-centre positions of pistons and rotation of crankshaft with crank-angle-degree resolution up to 0.5 CAD. Instead of synchronising pressure data with crank-angle-degree position which its resolution was limited at 0.5 CAD, pressure data were synchronised with time which had resolution limited by sampling frequency of the DAQ module. This time-based pressure data were then converted back to crank-angle-degree and resolution of 0.2 was reached. This conversion was made possible by employing top-dead-centre positions of pistons as a trigger to start of pressure recording. The compromise of this approach was either one set of pressure data of both cylinders cannot be used for any analyses. This was due to the crankshaft encoder had triggered either one set of the pressure data to be recorded first leaving crank-angle position of the other set of data unknown if difference of CAD position between cylinder-1 and

cylinder-3 were not accounted. Thus, for simplicity, only data recorded from TDC were further processed. The selected sets of in-cylinder pressure data were then corrected by adding the pressure difference between inlet manifold pressure and in-cylinder pressure at end of induction stroke to them. This pressure difference was supposed to be zero as the pressure at inlet manifold was equivalent to the in-cylinder pressure at the end of engine induction stroke. This correction was mandatory to compensate the setup error of pressure transducers. The setup error of fuel-line pressure transducers was corrected by deducting all recorded pressure values with respective fuel-line pressure at TDC positions, where fuel-line pressure was supposed to be zero. These setup errors were due to DAQ lag and can be recalibrated to save time needed for manual adjustments. Fuel-line pressures and in-cylinder pressures respected to crank-angle-degree were used to calculate useful engine performance measures such as heat-release rate, BMEP, ignition delay, start-of-injection time, and injection duration. The definitions of these measures will be elaborated.

$$\frac{dQ_n}{dt} = \frac{dQ_{ch}}{dt} - \frac{dQ_{ht}}{dt} = p\frac{dV}{dt} + \frac{dU_s}{dt} \tag{3.1}$$

$$\frac{dQ_n}{dt} = \frac{\gamma}{\gamma - 1} p\frac{dV}{dt} + \frac{1}{\gamma - 1} V\frac{dp}{dt} \tag{3.2}$$

$$\frac{dQ_n}{d\theta} = \frac{\gamma}{\gamma - 1} p\frac{dV}{d\theta} + \frac{1}{\gamma - 1} V\frac{dp}{d\theta} \tag{3.3}$$

Where,

$Q_n$ - Apparent net heat release (Joule)

$Q_{ch}$ -Apparent gross heat release (Joule)

$Q_{ht}$ - Heat transfer to walls (Joule)

$p$ - In-cylinder pressure (Pascal)

$V$ – In-cylinder volume at any crank-angle degree (cubic metre)

$U_s$ - Sensible internal energy of in-cylinder contents (Joule)

$\gamma$ - Ratio of specific heats (taken as 1.33 for this work)

$t$ - Time in reference of piston's position (second)

$\theta$ - Crank-angle-degree position (degree)

Equation 3.1, Equation 3.2, and Equation 3.3 were the mathematical formulas used to calculate net heat-release rate from in-cylinder pressure [5]. All the parameters were stated clearly as per above including units. Equation 3.1 stated that apparent net heat release rate was the difference between apparent gross heat-release rate and rate of heat transfer to walls. This difference was equal to the rate at which work is done on piston plus the rate of change of sensible internal energy of the in-cylinder contents. Equation 3.2 was a formula transformed from Equation 3.1 after adopted the ideal-gas law. Time based formula from Equation 3.2 was converted to crank-angle-degree based formula as per Equation 3.3 to give clearer description of piston position.

The ratio of specific heats varied according to the changes of global thermodynamic state in engine cylinder during combustion cycle. Assanis' work showed a reduction in magnitude with increasing temperature or richer air-fuel mixture [62]. The magnitudes typically varied from 1.25 to 1.4 [62]. For simplicity, an average value for the range of ratio of specific heats, 1.33, was used throughout a whole engine cycle for the calculation of apparent net heat release rate of this work. The induced errors in the magnitudes of heat release rates which were calculated via different ratios of specific heats were illustrated in Fig 3.5. Despite the error in magnitudes of heat release rates, the apparent premixed combustion phases and mixing-controlled combustion phases of the four sets of heat release rates remained unchanged. The error of heat release rate magnitude for the ratio of specific heats of 1.33 was less than 30% as compared to the other three sets. Hence this fixed value of ratio of specific heats was regarded to be able to provide an effective heat release rate calculation.

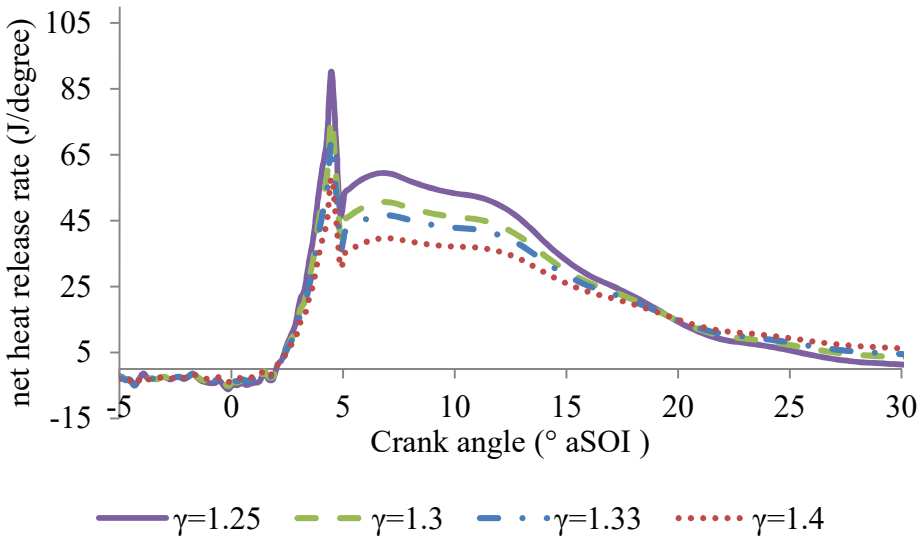


*Fig 3.5: Variation of heat release rates magnitudes according to different ratios of specific heats.*

Recorded in-cylinder pressure data were altered before they could be used to calculate net heat-release rate with Equation 3.3. The average of 40 consecutive sets of in-cylinder pressure data was to be used for every set of heat-release rate calculation. The noise of the averaged data was eliminated by data smoothing with cubic-spline-fitting technique. The cubic-spline-fitting did not affect the determination of ignition delay and heat release rate as the fitting was only applied for engine crank angle position before -40deg ATDC prior to the SOI and after PMC ended which varied according to different cases and was at approximately 10deg ATDC. The actually value for the end of PMC was determined by visual based on heat release rate plot.

Mean effective pressure (MEP) was an effective measure of the engine's ability to do work regardless of engine size. Equation 3.4 showed formulas to calculate MEP from engine's work per cycle and power. The types of power of the engine were divided into indicated power, brake power and friction power. Indicated power was the power delivered to piston by combustion of in-cylinder contents. Brake power was the output power of engine's crankshaft. The difference between the indicated power and the brake power were the friction power. The friction power

consisted of the power used to expel exhaust gas and induct fresh charge (pumping loss); to overcome friction of bearings, pistons, and other components; to drive engine accessories. The terminology of "brake", "friction", and "indicated" is applicable for MEP, work done on piston per cycle, and power. For instance, indicated work done on piston per cycle can be used to calculate indicated power and as well as IMEP (Indicated mean effective pressure) with Equation 3.4. Therefore, MEP could be calculated by either work done on piston per cycle or engine's power.

$$\text{MEP} = \frac{W}{V_d} = \frac{Pn_R}{V_d N} \tag{3.4}$$

$$P = 2\pi NT \tag{3.5}$$

$$W_{c,i} = \oint pdV \tag{3.6}$$

$W$ = Work per cycle (Joule)

$V_d$ =Displacement volume of cylinder (cubic metre)

$P$ = Engine's power (Watt)

$N$ = Engine speed (rev/s)

$n_R$ = Number of crank revolution per engine power stroke

$T$ = Torque of crankshaft ( $Nm$ )

$W_{c,i}$ = Indicated work done by in-cylinder content on piston per engine cycle (Joule)

BMEP (Brake mean effective pressure) was calculated by Equation 3.4 with input of brake power. Brake power was defined from engine speed and engine's output torque directly measured by sensors with Equation 3.5. IMEP was calculated from indicated work done on piston per cycle defined by Equation 3.6. The indicated work was divided into gross indicated work and net indicated work. The gross indicated work was the work done by in-cylinder content through compression and expansion strokes. The net indicated work was the work done by in-cylinder content through entire engine cycle including pumping loss. FMEP (Friction mean

effective pressure) was calculated from friction power. The friction power was the difference of gross indicated power and brake power.

Ignition delay time was defined as the time difference between start of injection and start of combustion. Start-of-combustion time was defined as the time when apparent net heat-release rate reached 2 joule per second. This figure was an estimated number to identify sudden peak of heat release rate for this engine. Start-of-injection time was taken as the time when fuel-line pressure reached 200bar which was the injector nozzle's opening pressure. Injection duration was the time interval between start of injection and end of injection. End-of-injection time was defined as the time when fuel-line pressure dropped below 200bar after the start of injection.

### 3.3: Gasoline combustion in CI engine

The study of gasoline combustion in CI engine mainly consisted of heat release, ignition delay, injection timings. These parameters helped to evaluate the practicality of running CI engine on gasoline. Tailpipe emission was not considered in this study. The development of net heat release from the start of injection to the end of combustion was illustrated in Figure 3.6 for a range of diesel/gasoline blend ratios at the three engine loads.

ID values clearly increased as the gasoline content increased, and in the majority of cases, the longer ID produced a higher premixed combustion spike associated with increased time for fuel vaporisation, mixing and ignition. The SOI, end of injection (EOI) and SOC timings were presented in Table 3.3 to demonstrate the positive ignition dwell periods for all the engine loads with gasoline blending levels from G0 to G80, except under low load condition.

*Table 3.3: Injection and SOC timings for three engine load conditions and gasoline blends from G0 to G80.*

| Load (BMEP) | 2.5bar | 5bar | 8.5bar |
|---|---|---|---|
| **SOI (CA ° ATDC)** | -4 to -1 | -4 to -1 | -4 to -1 |
| **EOI (CA ° ATDC)** | 3.2 to 6.2 | 8.7 to 11.7 | 11.7 to 14.7 |

| | | | |
|---|---|---|---|
| **SOC (CA ° ATDC)** | 2.9-8.5 | 2.2-8 | 0.9-6 |

The prolonged ID with increasing gasoline content reduced the positive ignition dwell period of the relevant cases. This limited the total heat release for the MCC phase but increased for the PMC phase, which was shown in Figure 3.6(c). The increase in the proportion of PMC over MCC was expected to trade $NO_x$ off for soot levels. The greatest cycle by cycle variations in peak heat release were observed for the G70 and G80 blends, which produced the longest ID periods. Unusual high frequency noise was noticeable for mid-load condition with G80 blend. The cycle-to-cycle variation of IMEP for G70 and G80 had a maximum difference of 10percent in magnitude as compared to 5percent in magnitude for other cases with lower gasoline blend. Both cyclic variation and high frequency noise could be due to unstable combustion promoted by the extended ignition delay, which were discussed later. The increase in ID produced by increasing the gasoline proportion in the blend was apparent as shown in Figure 3.7, for the results of all engine loads. The change of SOI was taken into account for all the ID periods presented here. The ID periods were the longest at the lightest load, and the rising sensitivity to gasoline content was the greatest, at the lightest engine load when cylinder pressures and temperatures are the lowest. At the higher load conditions, the effect of increasing gasoline fraction on ID was dampened due to shorten chemical delay period promoted by the higher in-cylinder pressure and temperature. The change in ID with an increasing proportion of gasoline in the fuel blend was insensitive to the engine cyclic variation of injection timing, but the lower bulk modulus of gasoline compared to diesel did affect the rate of pressure rise in the fuel line pressure, increase the time to reach the opening pressure of the injectors and delay the actual start of injection for a fixed demanded value. This effect was illustrated in Figure 3.8, for results taken at a fixed demanded SOI of -4° ATDC. The value of SOI for diesel fuel was as demanded by the engine control unit (ECU), in keeping with the injection control strategy being developed originally for diesel operation. As the proportion of gasoline in the blend was increased, the actual SOI occurred progressively later, and was retarded by approximately 3°CA relative to the demanded value for the G80 blend. The change in combustion phasing

produced a small reduction in indicated thermal efficiency and required an increase in the fuel delivery to achieve the target brake load. This and the lower heating value per unit volume of gasoline, which also required an increase in the volume of blended fuel needed, accounted for the increase in fuel volume injected with increasing proportion of gasoline as shown in Figure 3.9 (a). Around half the increase in the volume injected was accounted for by the lower density but similar heating value per unit mass of gasoline compared to diesel. The volumes of fuel injected had been converted to engine brake thermal efficiencies as show in Figure 3.9 (b). The brake thermal efficiencies averaged at 24.2%, 33.8% and 39.8% for engine speed-load conditions of 2000rev/min 2.5bar BMEP, 2000rev/min 5bar BMEP and 2000rev/min 8.5bar BMEP, accordingly. The variation of brake thermal efficiencies of gasoline blends were negligible and all were comparable to diesel. These data showed that gasoline blends were feasible alternative fuel for CI engine. Despite the actual SOI was retarded by gasoline blend, the small change in in-cylinder temperature and pressure did not have significant impact on ID. This was supported by the fact that the general engine cycle-to-cycle variation in SOI timing was always less than $2^0$CA for a set of fuel blend and operating condition, as well as the clear trend lines presented in Figure 3.7 which suggested that consistent ID was reproduced throughout.

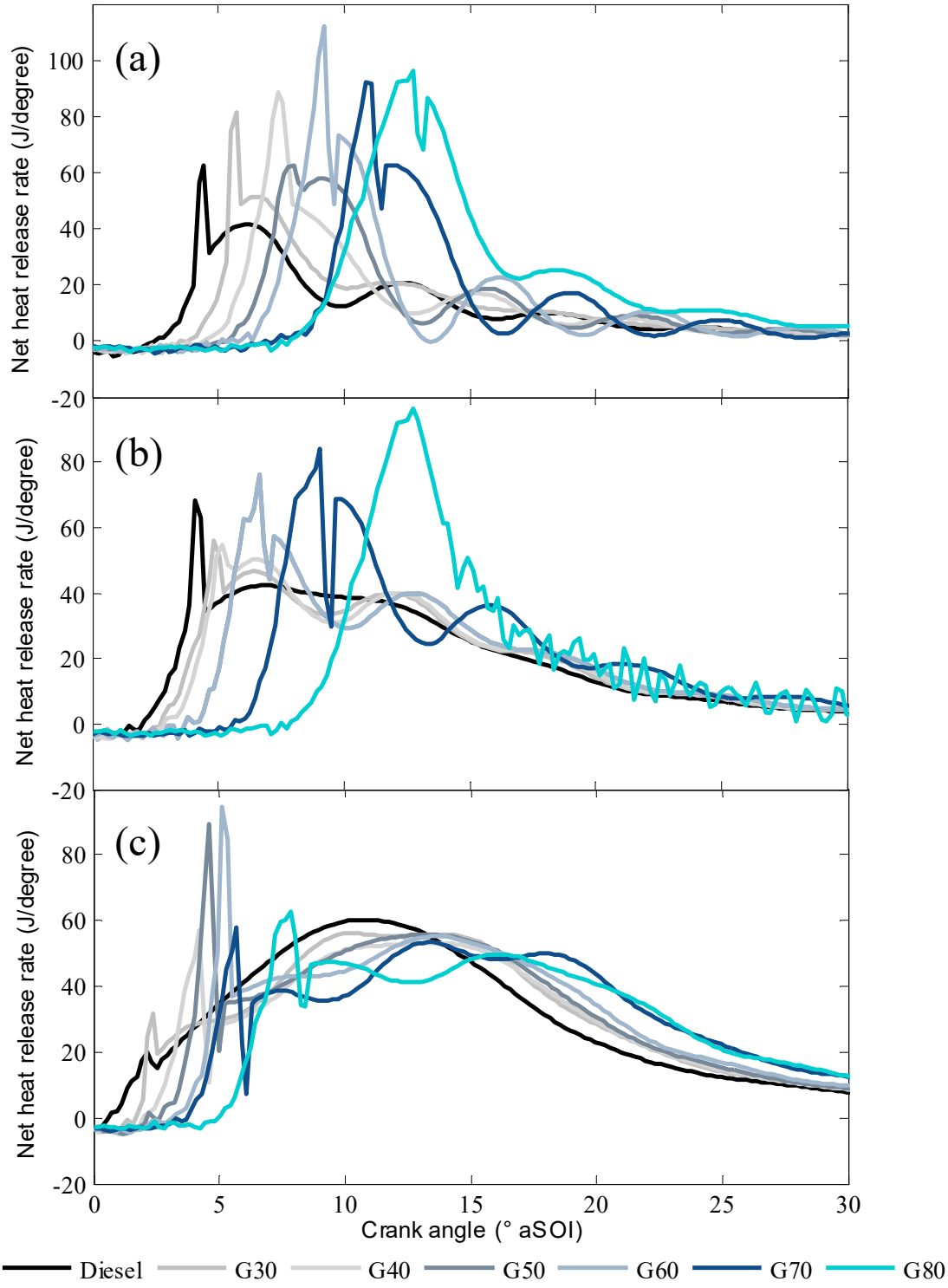


*Fig. 3.6: Net heat release rate profiles from engine test bed studies for diesel-gasoline blends at (a) low load (2.5 bar BMEP), (b) mid load (5 bar BMEP), and (c) high load (8.5 bar BMEP) conditions.*

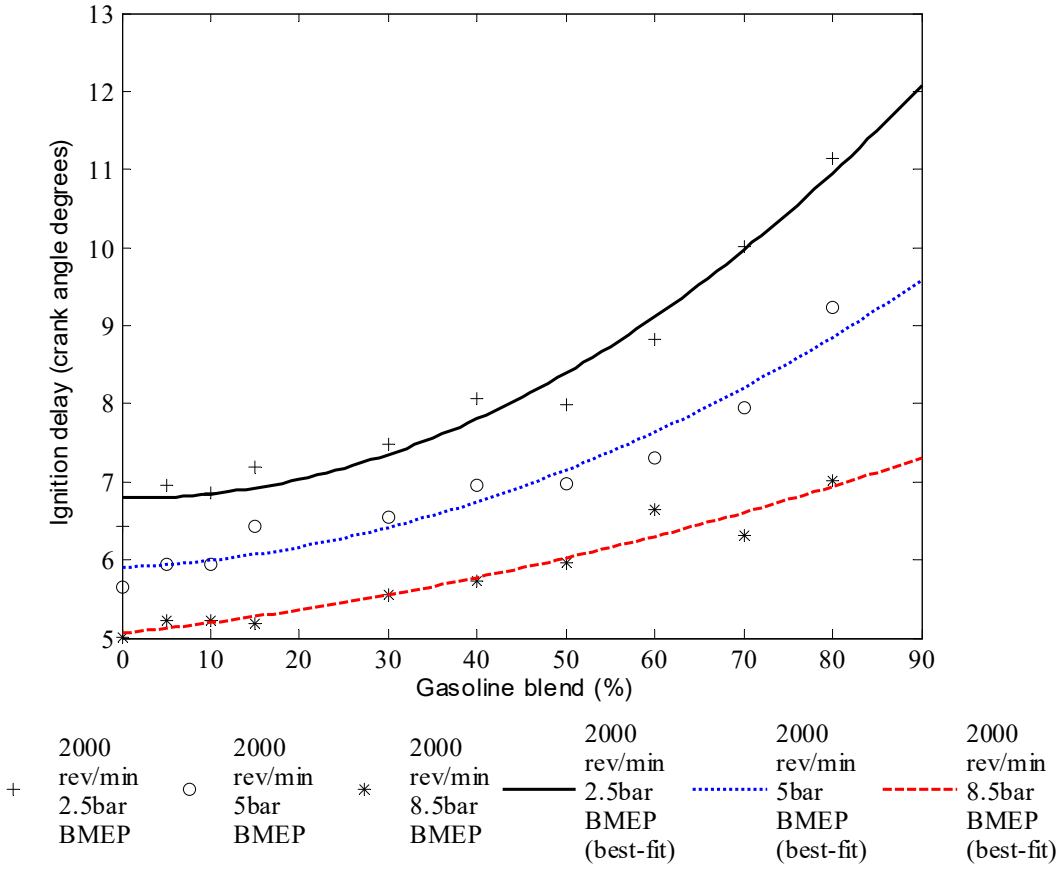


*Fig. 3.7: Measured ID periods from engine test bed studies for diesel-gasoline blends at low load (2.5 bar BMEP), mid load (5 bar BMEP) and high load (8.5 bar BMEP) conditions.*

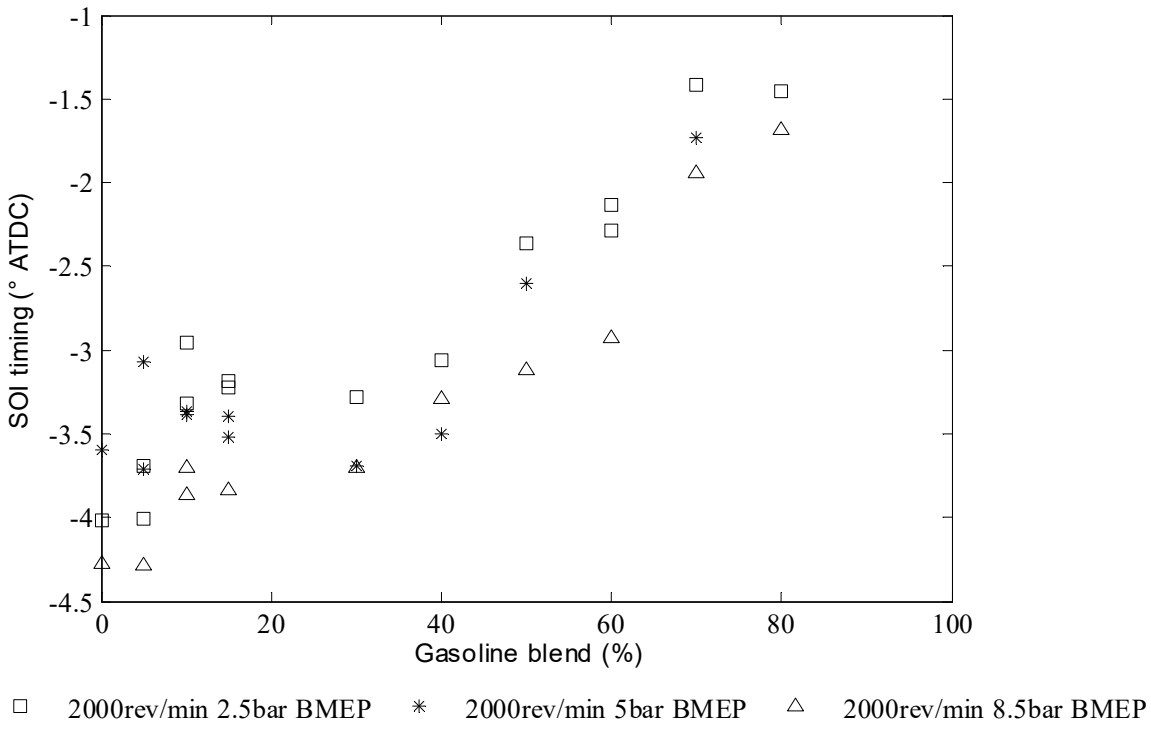


*Fig. 3.8: Variation of SOI timings with diesel-gasoline blends at low load (2.5 bar BMEP), mid load (5 bar BMEP) and high load (8.5 bar BMEP) conditions. All the conditions are run under the default engine map that demands SOI at -4º ATDC.*

The heat released in the premixed burn was shown in Figure 3.10 (a) to be linearly dependent on ID period. The inflection point of net heat release rate after the premixed burn was taken as the end of premixed burn. After a period which did not result in any significant contribution to the premixed charge (corresponding to the physical delay as described below), this was then produced at a constant rate, independent of the proportion of gasoline in the fuel blend. The main effect of increasing the gasoline content was to extend the ID period and allowed more time for the production of premixed charge.

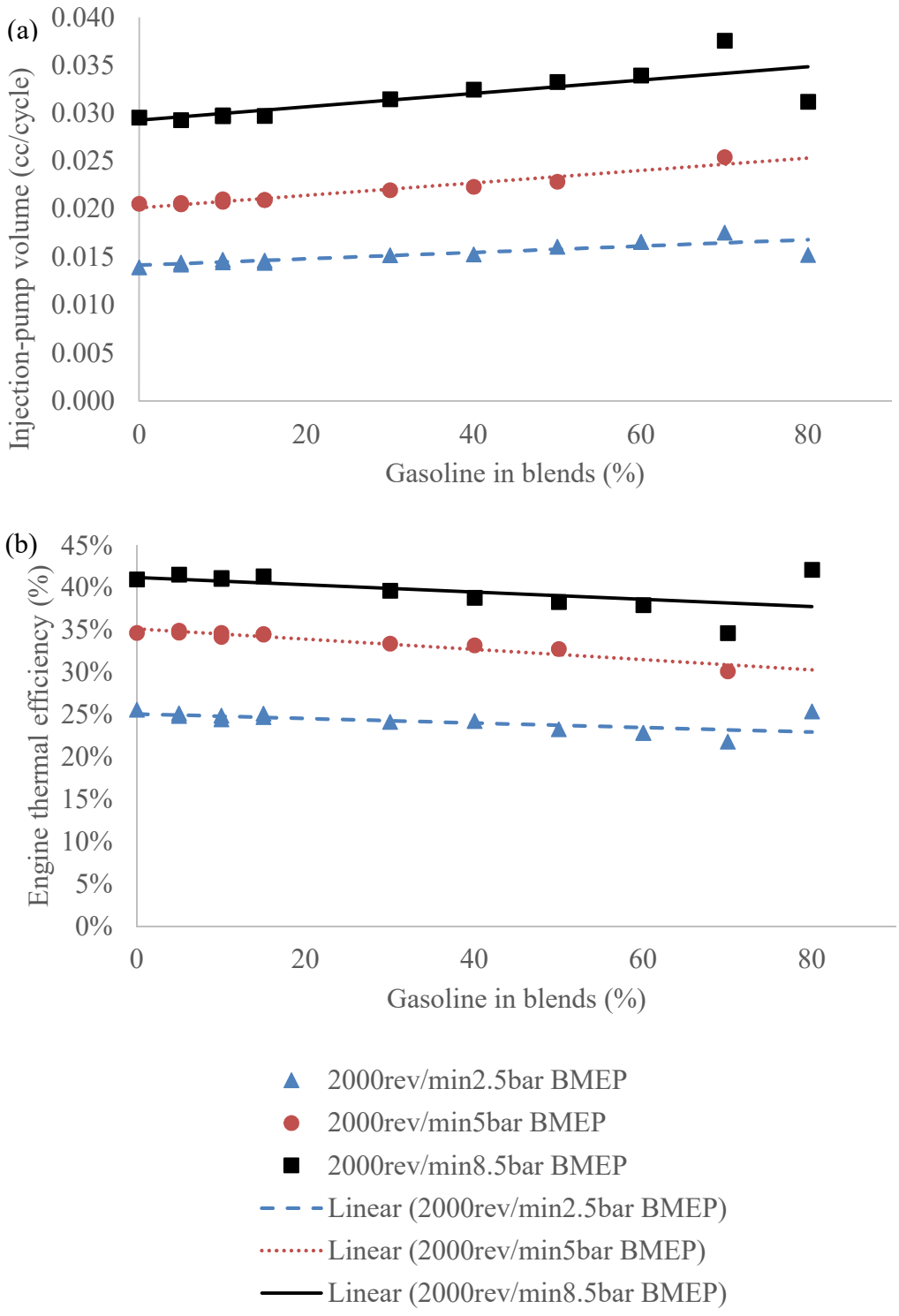


*Fig. 3.9: Variations of a) injection-pump plunger volumes and b) engine thermal efficiencies with diesel-gasoline blends at low load (2.5 bar BMEP), mid load (5 bar BMEP) and high load (8.5 bar BMEP) conditions.*

The low sensitivity to engine load shown by the best fit lines to the data was consistent with the premixed combustion being independent of the fuel volume injected, despite at least a threefold increase across the load range. Here, the dominance of chemical delay over physical delay in premixed charge preparation was demonstrated. The extrapolated trend lines in Figure 3.10(a) indicated that the minimum ID before any detectable premixed burn occurred was 3.5-4.0$^{o}$ CA at the engine speed of 2000 rev/min, corresponding to 0.29-0.33 millisecond (ms). The extrapolation was meant to demonstrate that there was always a minimum time (corresponding to the physical delay time) required for part of the injected fuel to mix, vaporise and produce measurable heat release. The production of vapour depended on the surface area of droplets generated in the spray formation processes and local mixing rates depended on spray penetration and momentum as well as charge turbulence. These spray processes depended on the properties of the fuel such as surface tension and physical processes which would vary with engine design and operating condition. The assumption here was that the physical processes dictate the minimum delay and that was independent of the proportion of gasoline in the fuel blend. Additionally, ignition process was also limited by the rate of air entrainment into the spray jet under typical diesel environment. Therefore, the physical delay could be independent of the change in fuel properties for different gasoline blends. For the data presented which was recorded for an engine at a fixed engine speed, if the physical delay was independent of the proportion of gasoline in the fuel blend then the extension observed with increasing gasoline content can only be associated with an increase in chemical delay.

The best fit lines to the data in Figure 3.10 (a) had a slope of approximately 35 Joule (J) per degree CA, indicated a period of 1.4$^{o}$ CA would be required to generate the premixed charge which burnt to release 50 J. The total ignition delay for this, comprised of the physical and chemical contributions, was approximately 5$^{o}$ CA. Consistent with this, if the first 3.6$^{o}$ CA was the physical delay period during which injection, droplet formation and spray penetration took place, the following 1.4$^{o}$ CA was the minimum chemical delay during which time vaporisation and mixing took place before the onset of premixed burning.

Implicitly, the physical delay and chemical delay periods were assumed to be completed in series as indicated in Figure 3.10 (b), produced a largely premixed charge state before chemical reactions started. This separation of the two contributions allowed zero-dimensional modelling of combustion chemistry to be done by CHEMKIN to predict the chemical delay contribution. More details on this modelling work were shown in Chapter 4.

There were a few limitations of running CI engine on gasoline discovered in this experimental study. When G80 fuel blend was tested at a lower engine speed of 1000rev/min, it produced unstable engine behaviour with cycle-by-cycle variation in cylinder work output approaching 50% lower than the demanded value. Advancing the SOI timing resolved the unstability problem. This may be due to the lower in-cylinder pressure and temperature that caused the G80 fuel blend to have an unsustainable combustion. Cases of 1000rev/min all had lower intake boost pressure than the 2000rev/min. Consistent finding and more elaborate explanation to why advancing the SOI timing would resolve the unstability issue was given in Chapter 4.

The problems of controlling injection timing were worsen by the effect of gasoline on the compressibility of the blends, which in the current study retarded the start of injection by up to 3$^{o}$ CA relative to results for diesel fuel and the same demanded value. If the blend ratio and compressibilty were unknown, this introduced uncertainty in the actual timing of injection delivered. The problem was largely associated with distributor pump line nozzle injection systems which had a significant volume of fuel in the line between the distributor pump and the injector nozzle. In light duty automotive applications, this type of system had been largely superceded by High Pressure Common Rail Fuel Injection Equipment which metered fuel delivery at the nozzle.

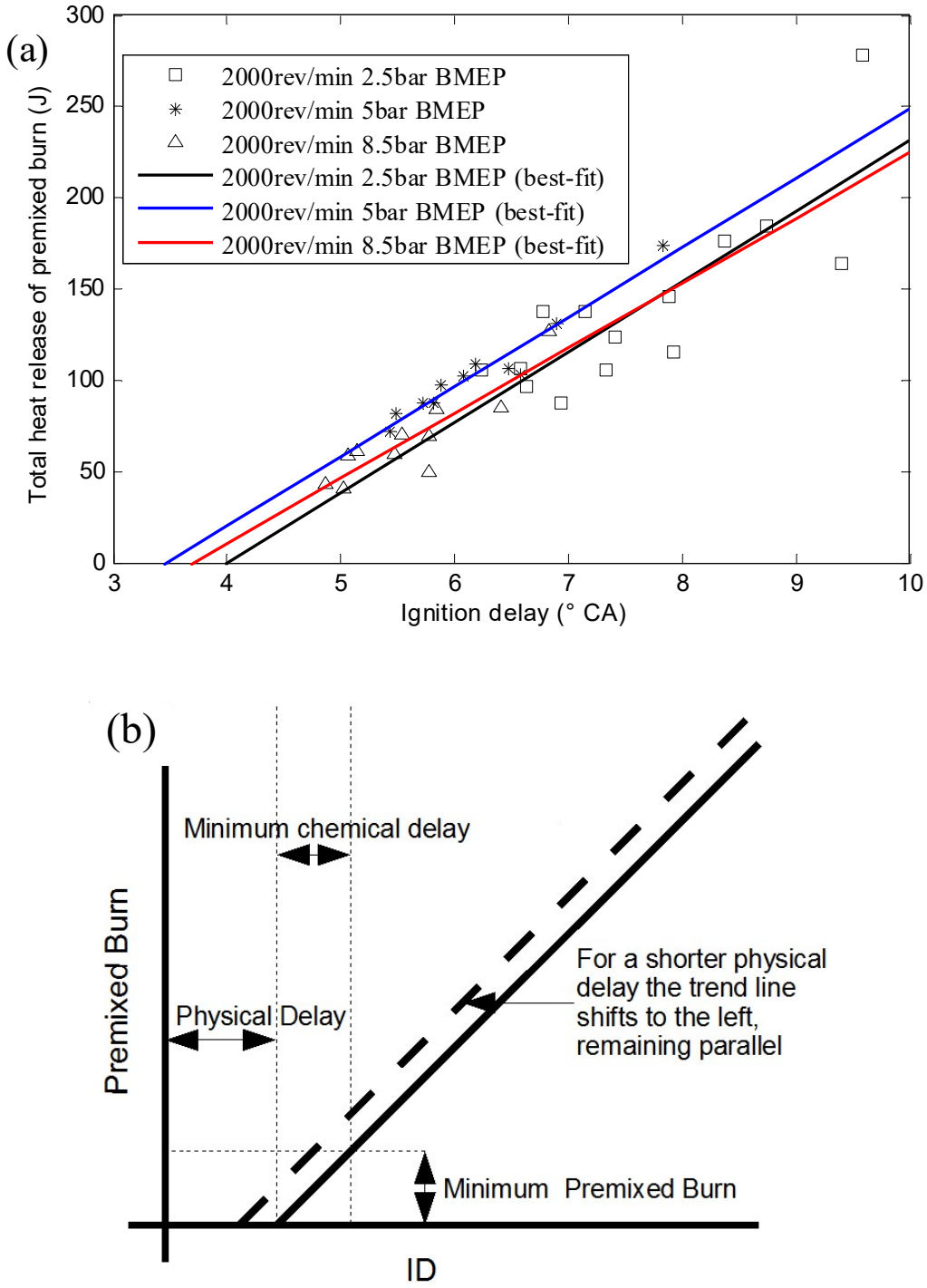


*Fig. 3.10: (a) Premixed burn versus ID period for diesel-gasoline blends at low load (2.5 bar BMEP), mid load (5 bar BMEP) and high load (8.5 bar BMEP) conditions, and (b) conceptual diagram of the physical delay, chemical delay and premixed burn.*

The engine rig performed really well throughout the entire experiment. The modified stationary water-cooled cooling system that replaced the original air-cooled one managed to maintain the temperature of the engine at the desired temperature. The additional pressure sensors installed at the fuel line and engine cylinders provided valuable insight to the heat release rate, injection timing and injection rate of the engine. Gasoline blends were shown to be able to perform perfectly in CI engine with performance such as power and BMEP comparable to diesel. The differences that set the gasoline blends apart from diesel were the retarded SOI timing and longer ignition delay. Physical delay and chemical delay were discriminated.

# CHAPTER 4

# NUMERICAL STUDY WITH CHEMICAL KINETIC MECHANISMS FOR DIESEL AND GASOLINE

This chapter covered the extension of the study of gasoline combustion heat release characteristics to numerical modelling with chemical kinetic mechanisms. The numerical modelling provided the additional insight to the contribution of chemical delay to the heat release characteristics. The development of the chemical kinetic mechanisms for diesel and gasoline used in the numerical modelling was included in this chapter.

## 4.1 Defining the criteria of surrogate fuels/development of diesel kinetics

In order to better understand the effect of gasoline on ID behaviour and the resulting benefits with diesel-gasoline fuel mix, chemical kinetic modelling can be utilised to complement engine test bed studies [10]. However, accurately predicting the chemical kinetics contribution to ID for diesel-gasoline blends was difficult since both diesel and gasoline were multi-component fuels. These components were grouped into five main categories, namely n-alkanes, iso-alkanes, napthenes, aromatics and olefins [11, 12, 13]. Ideally, fuel surrogates with similar chemical components found in diesel and gasoline should be chosen for chemical kinetic modelling as they would produce more accurate heat-release characteristics. The size of the fuel surrogate mechanisms was another important factor to be considered for effective and feasible modelling in terms of computational time and accuracy. Pitz et al. [11] evaluated the existing single-component fuels in terms of

relevance to practical systems, understanding of mechanism and properties information. Based on the work, the single-component fuels that were rated the highest in terms of mechanism understanding and being the most relevant to the fuel components in diesel and gasoline were n-heptane, iso-octane, 1-pentene, methylcyclohexane and toluene. The principles of choosing appropriate surrogate fuels for diesel and gasoline [11] inspired the study of the effect of surrogate fuel's Cetane number, Octane number and chemical properties on prediction of ignition delay time while searching for the right surrogate fuels for diesel and gasoline. The chosen surrogate fuels were combined to develop chemical kinetic mechanisms that could represent diesel and gasoline combustion. The developed ternary diesel-gasoline kinetic mechanism were shown able to simulate the ignition delay periods of diesel and gasoline combustion via a zero-dimensional numerical study conducted by CHEMKIN. The settings and model used in CHEMKIN were given in Table 4.1.

*Table 4.1. Selected models and corresponding settings for CHEMKIN simulations.*

| **CHEMKIN model and settings** | |
|---|---|
| Reactor Model | Closed Homogeneous Batch Reactor |
| **Reactor Physical Properties** | |
| Problem Type | Constrain Volume And Solve Energy Equation |
| **Solver** | |
| Absolute Tolerance | 1.00E-20 |
| Relative Tolerance | 1.00E-08 |
| Sensitivity Absolute Tolerance | 0.0001 |
| Sensitivity Relative Tolerance | 0.0001 |
| **Output Control** | |
| Use Solver Integration Steps | 20 |

N-heptane and toluene were first chosen as the surrogate fuels for diesel due to their relevance to diesel in term of chemical composition. The chemical kinetic mechanisms of n-heptane (version 3.0) from Lawrence Livermore National Laboratory (LLNL) [63] and chemical kinetic mechanism from the modelling work by Andrae et al. [56] were employed in this study. The n-heptane mechanism was

well validated under conditions of 3 to 40bar of pressure and 650K to 1350K of temperature at stoichiometric air fuel mixture as depicted in Figure 4.1. The toluene mechanism was validated against the available shock tube data [64, 65] under conditions of 12 to 50bar of pressures and 650K to 1350K of temperatures at air-fuel equivalence ratios of 0.25, 0.5 and 1 as shown in Figure 4.2.

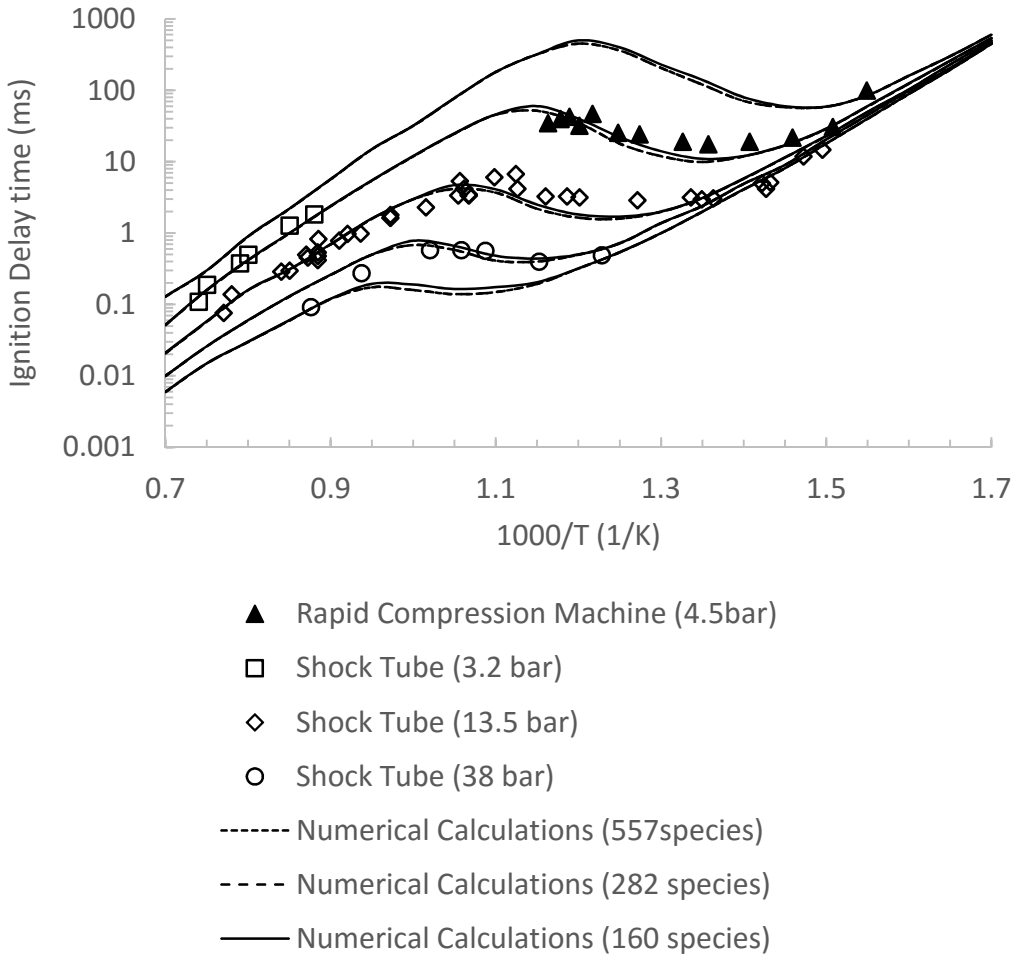


*Figure 4.1: Dashed lines represent ignition delay times predicted by detailed n-heptane mechanism **[38]**. Solid lines represent ignition delay times predicted by reduced n-heptane mechanisms **[66]**. Data plots are experimental data. This diagram was taken from paper by Seiser et al. **[66]** and replotted.*

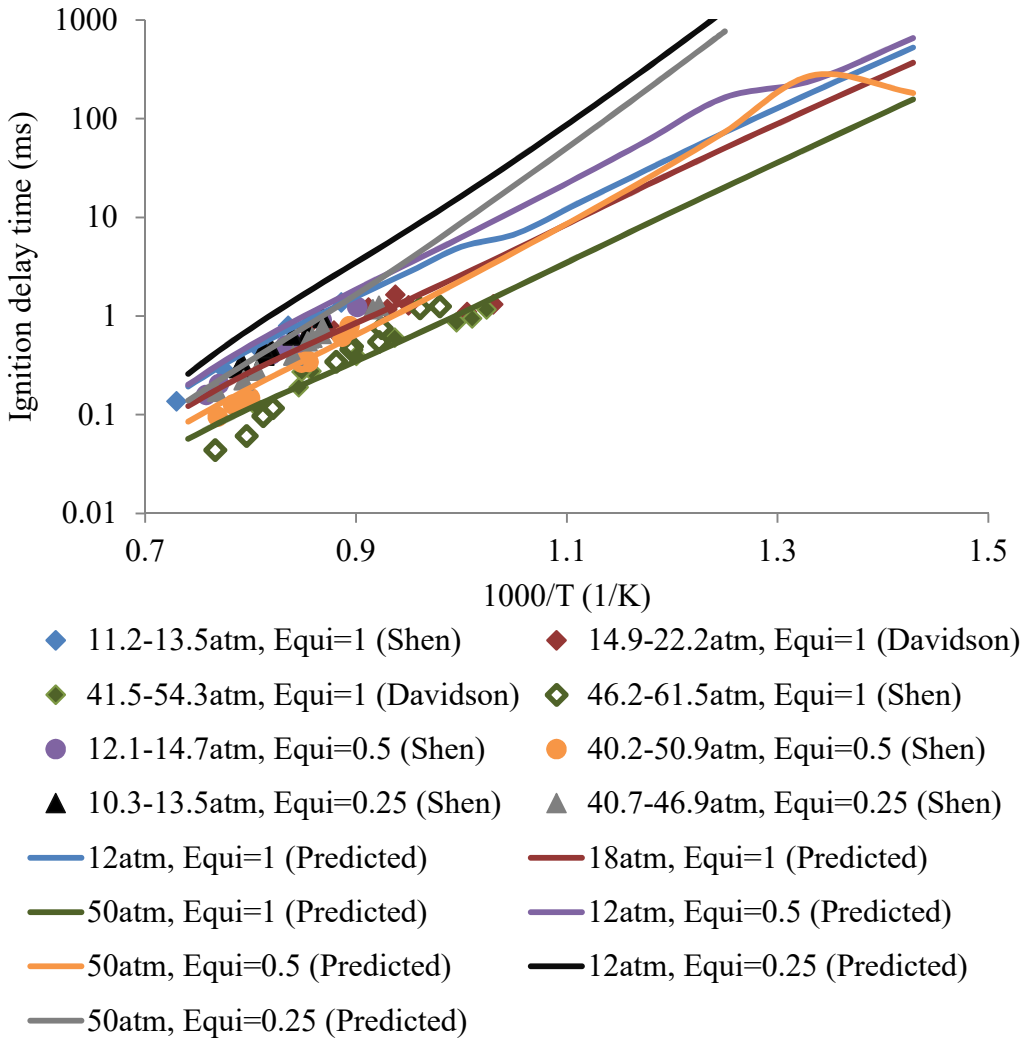


*Figure 4.2: Toluene shock tube experimental data (plots) of Hsi-Ping et al.* ***[64, 65, 67]****. CHEMKIN predictions (lines) of toluene chemical kinetic mechanism by Andrae et al.* ***[56]***

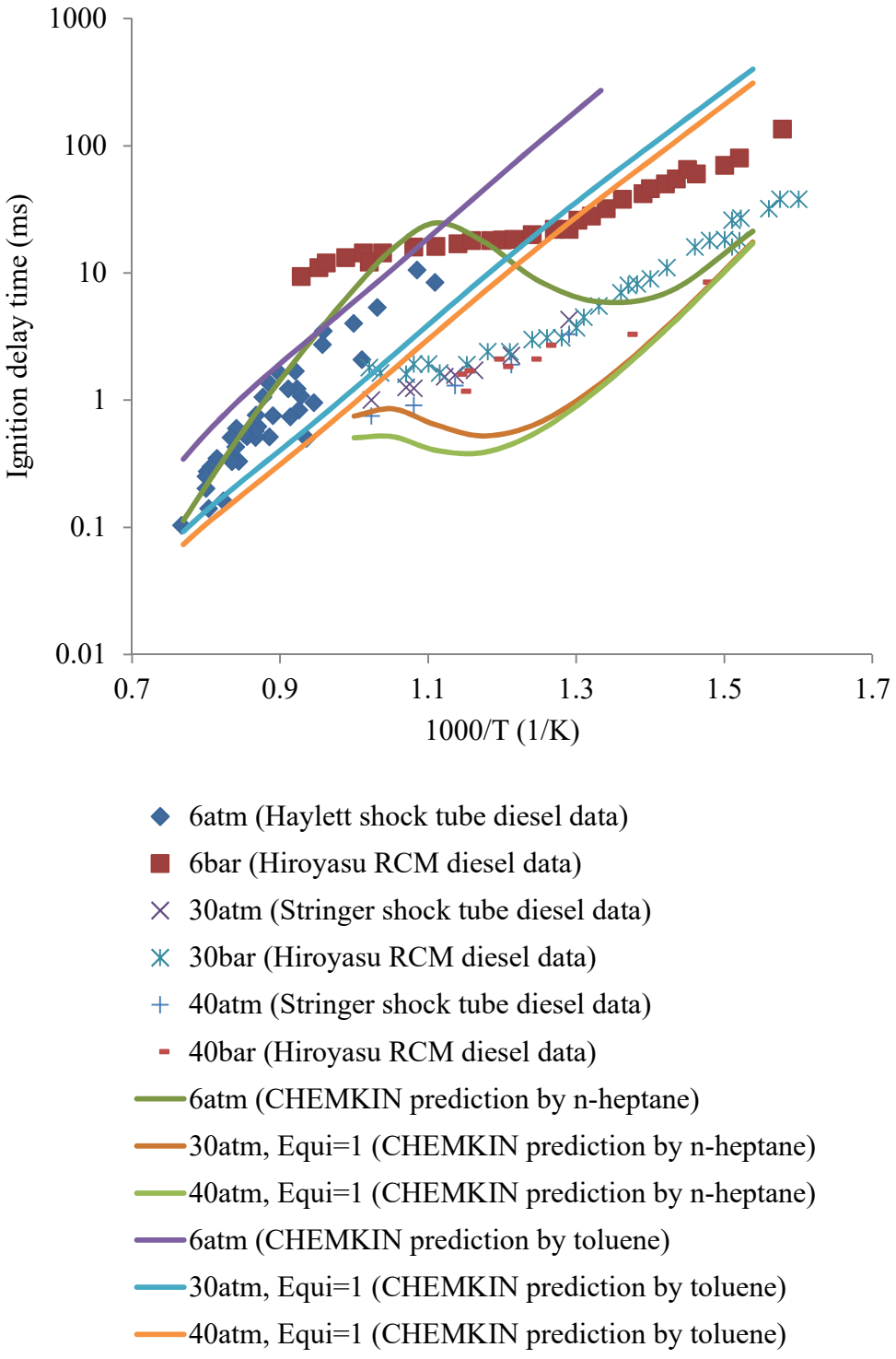


*Figure 4.3: Comparisons of n-heptane and toluene predictions by CHEMKIN to previous diesel combustion data of shock tube and rapid compression machine* ***[68, 69, 70]****.*

In order to test how suitable n-heptane and toluene were as surrogate fuels for diesel, both mechanisms were used to predict ignition delay periods which were compared to the available literature diesel combustion data of shock tube and rapid compression machine [68, 69, 70] at conditions of 6 to 40bar of pressures, 650K to 1350K of temperatures and stoichiometric air-fuel mixture as shown in Figure 4.3. Both mechanisms showed reasonable agreement at high temperatures which were above the cool flame temperatures. The major ID discrepancies between the mechanisms and the diesel combustion data were at the range of medium to low temperature combustion which occurred during and before the cool flame temperatures. This was attributed to the narrower range of cool flame and less intense cool flame of diesel as compared to n-heptane combustion. The narrower range of cool flame and less intense cool flame could be attributed to the higher composition of aromatics in diesel [55]. Cool flame characteristics was manifested by a period of combustion when the flame chemical reactions release very little heat. Chemical mechanisms that predicted these cool flame characteristics were essential for diesel-engine combustion as the in-cylinder pressure and temperature conditions overlapped the conditions that would manifest the cool flame characteristics. At this point, mixture of n-heptane and toluene seemed like a good binary blend which could match the ignition delays of diesel. However the compatibility of the binary blend could be due to the similar common fuel ratings such as the Cetane number, RON or simply similar chemical composition as diesel. In order to study these surrogate fuel's criteria, two potential diesel-surrogate mixtures comprised of any of the two components of n-heptane, toluene and ethanol were used to illustrate the compatibility of these criteria. First mixture comprised of 80% of n-heptane and 20% of toluene gave a close Cetane number, RON, and chemical composition in relative to diesel. Second mixture comprised of 85% of n-heptane and 15% ethanol gave a close Cetane number and RON but a very different chemical composition in relative to diesel. Ethanol mechanism developed by Marinov et al. was used in this work [71]. The Cetane number and RON of diesel, n-heptane, toluene and ethanol were summarised in Table 4.2. The fuel's chemical composition, Cetane number and RON of diesel, the first mixture

and the second mixture were listed in Table 4.3. For fuels that have range of Cetane and RON values, an average value was used. RONs of diesel and ethanol were calculated with correlation below (Equation-4.1). Two surrogate mixtures were used in this study as shown in Figure 4.2. Cetane numbers and RONs of mixtures were calculated by formula stated as Equation 4.2.

*Table 4.2: List of Cetane numbers and RONs of various hydrocarbons.*

| Hydrocarbon | Cetane number | RON (Research Octane Number) |
|---|---|---|
| Diesel | 40-50 [72], 52 [73], avg=46 | 20.5 [Calculated] |
| n-heptane | 53 [74] | 0 [75, 76] |
| toluene | 18.3 [74] | 124 [75, 76] |
| Ethanol | 2 [74] | 125 [Calculated] |

$$CN = 54.6 - 0.42RON \qquad (4.1\ [73])$$

$$RON_{MIXTURE} = \sum \left(\text{Stoichiometric coefficient of hydrocarbon } x\ RON_{hydrocarbon}\right) \qquad (4.2\ [53])$$

*Table 4.3: Surrogate mixtures used in this study.*

| Surrogate Mixture | Fuel chemical composition | Cetane number | RON |
|---|---|---|---|
| Diesel | 80% parrafins, 20% aromatics (approximated) | 46 | 20.5 |
| Mixture-1 | 80% n-heptane, 20% toluene | 46 | 24.8 |
| Mixture-2 | 85% n-heptane, 15% ethanol | 45.4 | 18.8 |

Diesel combustion data from literature were scarce. Three sets of combustion data from shock tube and rapid compression machine experiments (Haylett shock tube diesel data [68], Hiroyasu RCM diesel data [77], Stringer shock tube diesel data

[70]) were selected to study the diesel surrogate fuel criteria. All the predictions were modelled via CHEMKIN homogeneous batch reactor model. The attempt of using n-heptane and toluene as surrogate fuels to diesel was made and the results were shown in Figure 4.4. The data of Stringer and Hiroyasu did not specify the fuel equivalence ratio. Thus the predictions in that range were made by fixing a fuel equivalence ratio which yielded the most consistent predictions in relative to the experimental values. For a fixed equivalence ratio of 0.3, the predicted results showed the most reasonable agreements as compared to the diesel combustion data. Figure 4.4 presented the results of ignition delay times calculated with the two binary kinetic mechanisms. The binary models were created by combining the two relevant surrogate fuels without including unique co-reactions involved. Model of mixture-1 predicted ignition delay time more accurate than model of mixture-2 especially at low temperature and low pressure conditions. Mixture-1 also predicted the whole ignition delay trend and cold flame intensity better than mixture-2 as compared to diesel. However the ID predictions of mixture-2 demonstrated that Cetane number and RON had strong relevance towards heat-release characteristic of combusted fuel. The predictions of mixture-2 which had similar Cetane number and RON as diesel were more accurate than the predictions of n-heptane which only had similar Cetane number as diesel as per shown in Figure 4.3. These results confirmed that fuel chemical composition, Cetane number and RON were accurate criteria to measure the compatibility of surrogate fuels. Henceforth, fuel blend of n-heptane and toluene with the proportion of

mixture-1 was chosen as the suitable blend that could represent diesel combustion.

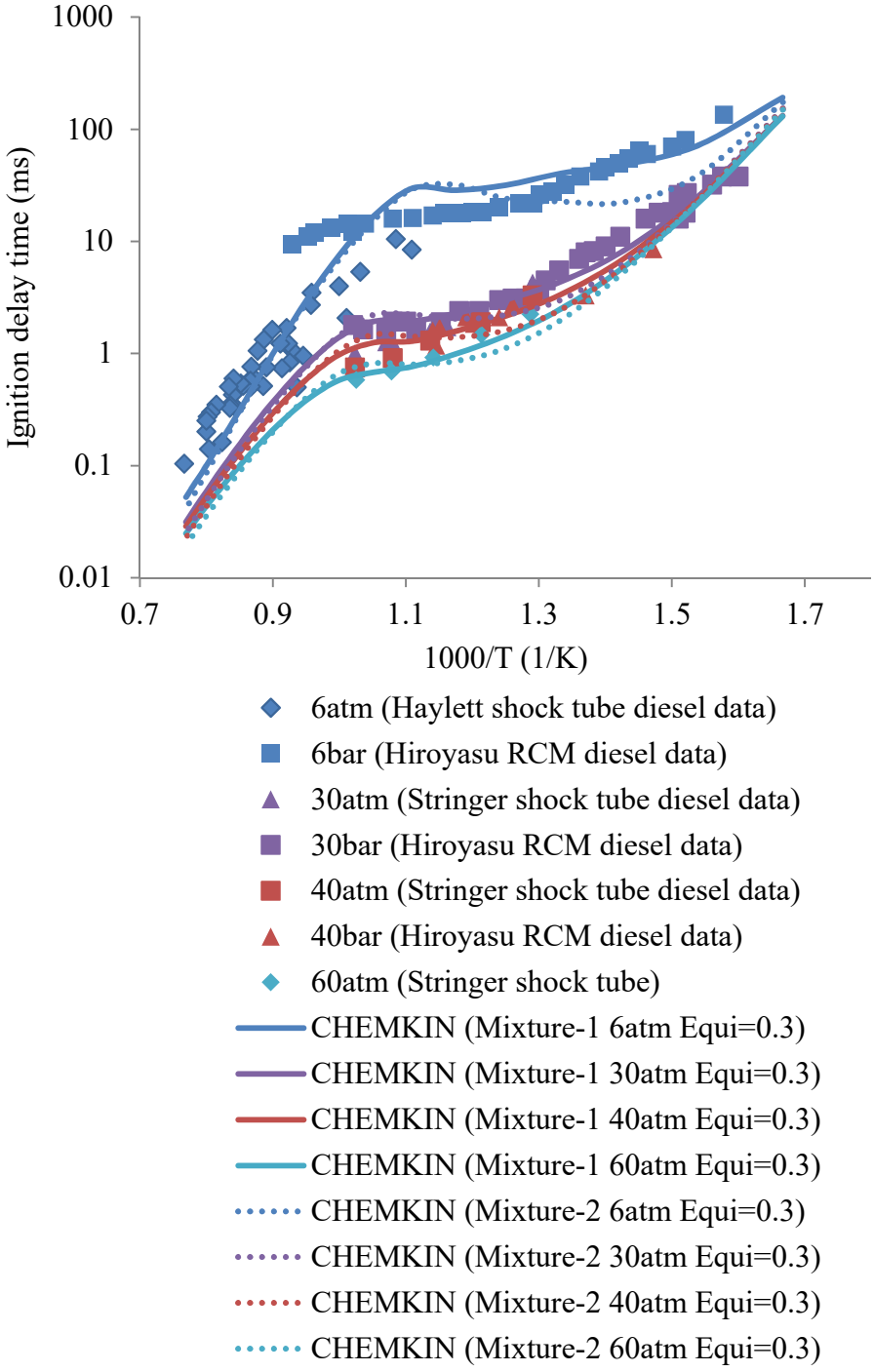


*Figure 4.4: Comparisons of predicted ignition delay times of Mixture-1 and Mixture-2 by CHEMKIN to previous diesel combustion data of shock tube and rapid compression machine (RCM).*

## 4.2 Development of gasoline surrogate model

Iso-octane and toluene were known to be relevant surrogate fuels to gasoline [52]. Iso-octane's chemical kinetic mechanism from LLNL website version LLNL-MI-421507 developed by Curran et al. [78] was used in this study. The accuracy of this Iso-octane kinetic model was validated with literature results of shock tube and RCM [79, 80, 81] as depicted in Figure 4.5. The same toluene's chemical kinetic mechanism from modelling work by Andrae et al. was used [56]. Chemical interaction among multiple single-component fuels can be regarded as competition of OH and $HO_2$ radicals [55]. Unique co-reactions found in this chemical interaction did not have significant effect on ignition delay time and combustion characteristics [55]. Thus, chemical kinetic mechanism of single-component surrogate fuels can be combined directly without considering the co-reactions involved. The iso-octane and toluene chemical kinetic mechanisms were combined to build a gasoline-surrogate kinetic model. This gasoline-surrogate model demonstrated reasonable good agreement with experimental data of shock tube and RCM from literature as shown in Figure 4.6. From this figure, gasoline generally had longer ignition delay than diesel. Gasoline's cool flame characteristics was less intense and present at lower temperatures as compared to diesel. The difference in temperature range of cool flame between diesel and gasoline raised the concern of the validity of the diesel and gasoline mechanisms in CI engine combustion. In a typical CI engine, combustion occurred at temperature of 800K to 1000K. This range of temperatures was where diesel exhibited its cool flame characteristics. Therefore cool flame characteristics for the diesel mechanism were more important than the gasoline mechanism. Hence the cool flame characteristics of diesel would have to be preserved during the mechanism reduction process.

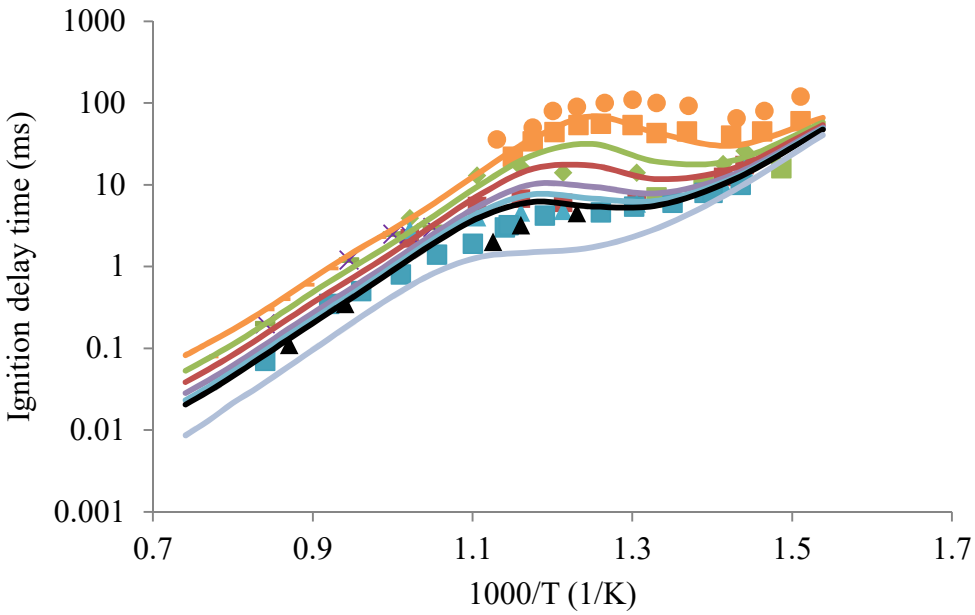


- 13bar, Equi=1 (Fieweger)
- 10.7-14.3bar, Equi=1 (Lille RCM)
- 12.6-16bar, Equi=1 (Lille RCM)
- 17bar, Equi=1 (Fieweger)
- 17-22.5bar, Equi=0.9 (Thornton RCM)
- 20bar, Equi=1 (MIT RCM)
- 22.7-30bar, Equi=0.9 (Thornton RCM)
- 34bar, Equi=1 (Fieweger)
- 34-45bar, Equi=0.9 (Thornton RCM)
- 40bar, Equi=1 (Fieweger)
- 45bar, Equi=1 (Fieweger)
- 14bar, Equi=1 (Prediction with Curran iso-octane mec)
- 20bar, Equi=1 (Prediction with Curran iso-octane mec)
- 26bar, Equi=1 (Prediction with Curran iso-octane mec)
- 34bar, Equi=1 (Prediction with Curran iso-octane mec)
- 40bar, Equi=1 (Prediction with Curran iso-octane mec)
- 45bar, Equi=1 (Prediction with Curran iso-octane mec)
- 100bar, Equi=1 (Prediction with Curran iso-octane mec)

*Figure 4.5: Predicted ignition delay times of iso-octane compared against literature results under various initial pressures and temperatures* ***[79, 80, 81]****.*

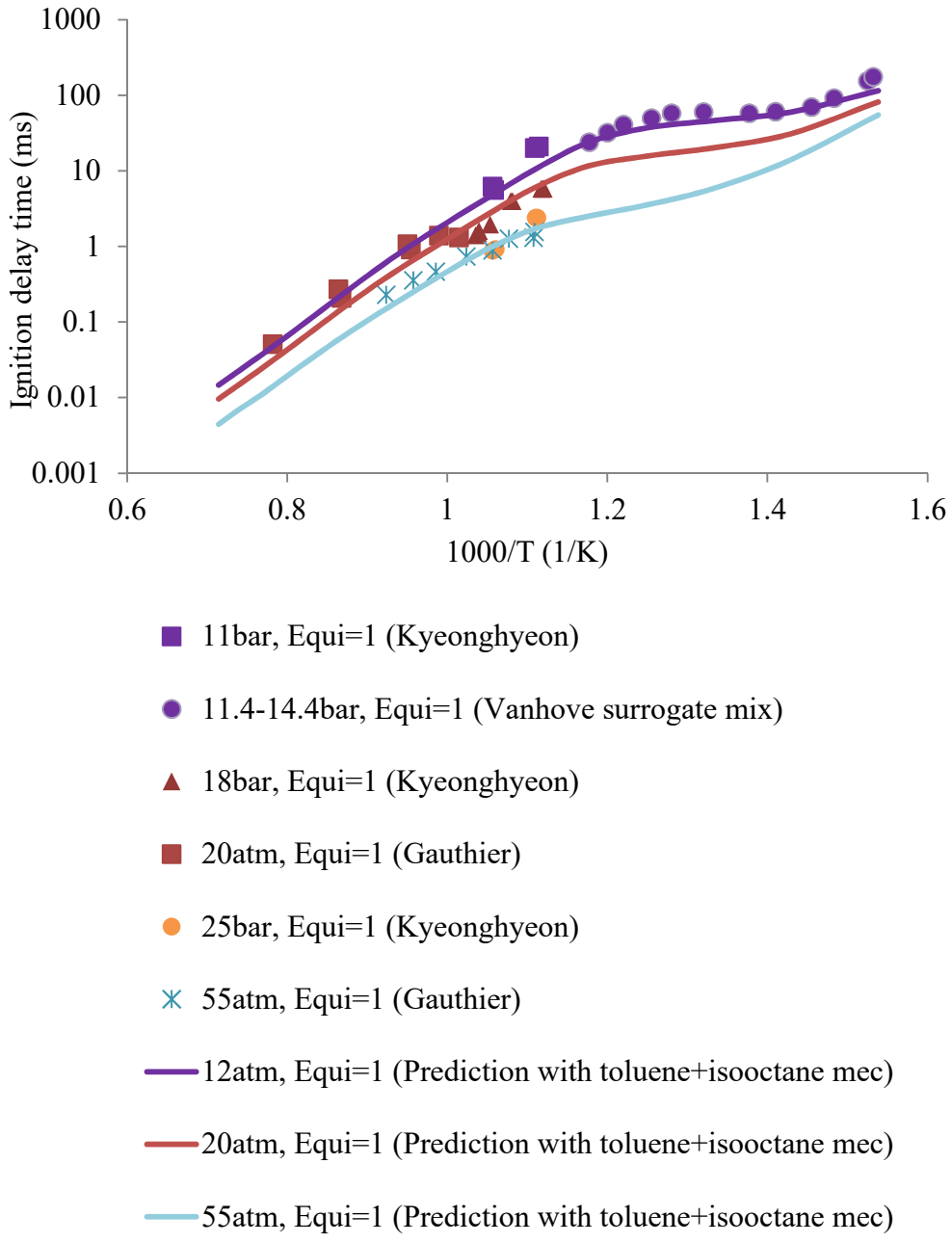


*Figure 4.6: Predicted ignition delay times by gasoline-surrogate kinetic model in comparison with literature gasoline data under various initial pressures and temperatures.*

### 4.3 Development of diesel-gasoline surrogate model

The reaction kinetics model of gasoline-diesel blends combined n-heptane, iso-octane and toluene in proportions fixed by the volumetric blend ratio and the surrogate fuel descriptions: 80% n-heptane/20% toluene for diesel and 70% iso-octane/30% toluene for gasoline. Although the n-heptane, isooctane and toluene mechanisms had only been validated under the pressure conditions of 4 to 55bar of homogeneous combustion due to the limited shock tube data and constant volume bomb data available, which were lower than pressure conditions of the engine experiment (68 to 88bar), but the mechanisms had been validated across a wide range of pressure conditions and shown accurate under these conditions. This demonstrated the mechanisms comprised of crucial reactions that take account of the change of pressures and may still be accurate at the pressure range of the experiment. This argument was supported by the mechanism' ability to predict ignition delay trends consistent to the engine experimental ones which was shown in later section. The predicted ID characteristics of a 50%/50%vol. diesel-gasoline surrogate fuel which comprised 40% n-heptane/35% iso-octane/25% toluene by volume were illustrated in Figure 4.7, for a range of simulated conditions covering pressures of 6 to 100 atm, and temperatures from 650 to 1350 K at a fixed $\phi = 4$. Although the surrogate fuel models had been validated for $\phi$ up to the stoichiometric condition, these mechanisms consisted of the vital enhanced third-body efficiencies of reactions which would allow them to be applied for conditions with $\phi > 1$ for appropriate qualitative studies. Also shown here were the predictions made with the extensively validated LLNL's gasoline surrogate model [13] published recently for the same surrogate fuel model composition, which showed similar prediction for the ID trend. This demonstrated that the interactions among the individual component in both the surrogate fuel models are comparable.

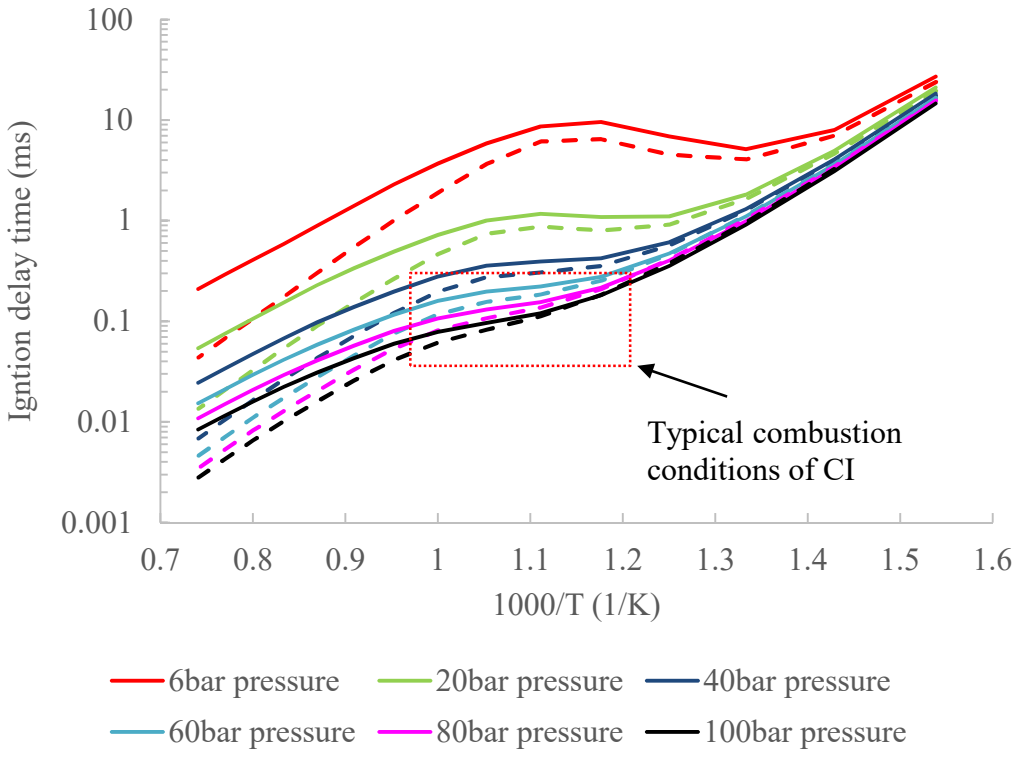


*Figure 4.7: Comparison of predicted ID period using the developed ternary kinetic model with 40/35/25 %vol. of n-heptane/iso-octane/toluene ratio (dashed lines) and the LLNL gasoline surrogate model* ***[13]*** *(solid lines) at* $\phi = 4$.

In calculating the chemical delay, the charge was assumed to be fully vaporised and premixed where the temperature and equivalence ratio must be specified. Prior to the onset of auto-ignition for typical diesel engine environment, the charge was assumed to have been homogeneously mixed and therefore, zero-dimensional (0-D) closed homogeneous batch reactor model was used in this study [82, 83]. Kook et al. [84] described the progress of combustion in a direct-injection compression ignition engine under various diluted intake air conditions by plotting the path of a fuel parcel in the equivalence ratio-temperature map corresponding to an adiabatic mixing process followed by low-temperature heat-release. This was given by Figure 4.8 which was also used to determine the operating conditions of the bulk air-fuel mixture in the CI engine for CHEMKIN kinetic modelling. From Figure 4.8, under undiluted intake air and ambient air temperature of 900 K conditions, adiabatic mixing reduced the mixture values of $\phi$ from 3.8 to 1.7 and increased the

mixture temperature from 750 K to 820 K. At 820 K, mixture temperatures for all the conditions deviated from the adiabatic mixing lines as heat-release of fuel begins. A combustible air-fuel mixture was present at this temperature. Hence, this temperature was taken as the initial temperature for the kinetic modelling. Figure 4.8 also demonstrated that the adiabatic mixing line was dependent on the level of dilution and the in-cylinder bulk-air temperature. The adiabatic mixing line for the same dilution level could be shifted to match the in-cylinder temperature of the test engine used in this study. For the test engine, at SOI of -4° ATDC, the in-cylinder temperature was approximately 1000 K and at this temperature, the equivalence ratio of the mixture was estimated to be 4. This was consistent with the value of $\phi$ = 4 at which combustion first occurred as noted by Dec [85], in studies of an optically accessed CI engine. Thus, this value was adopted in the kinetic modelling here.

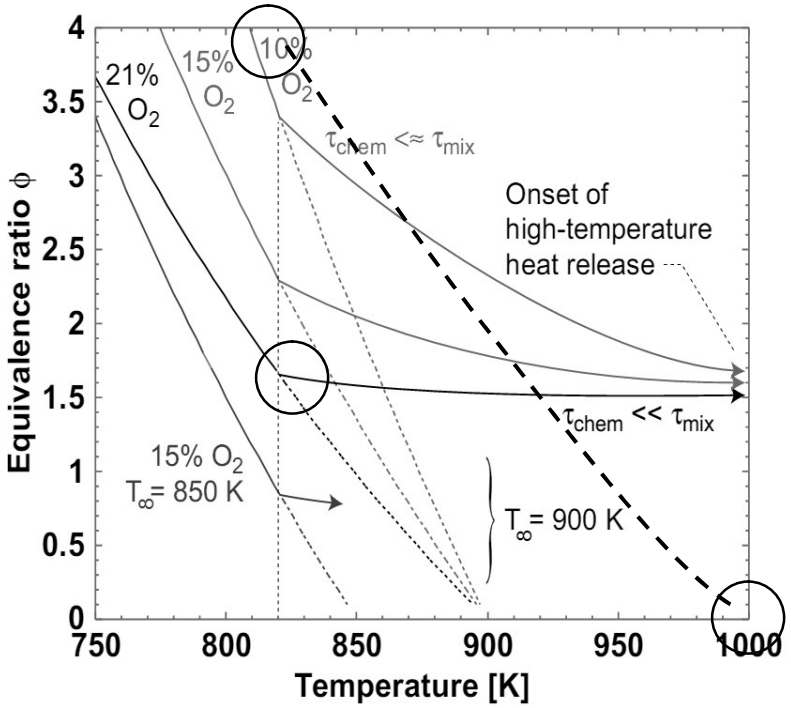


*Figure 4.8: The path of a fuel parcel in the equivalance ratio-temperature plot corresponding to an adiabatic mixing process followed by low-temperature heat release (adapted from **[84]**).*

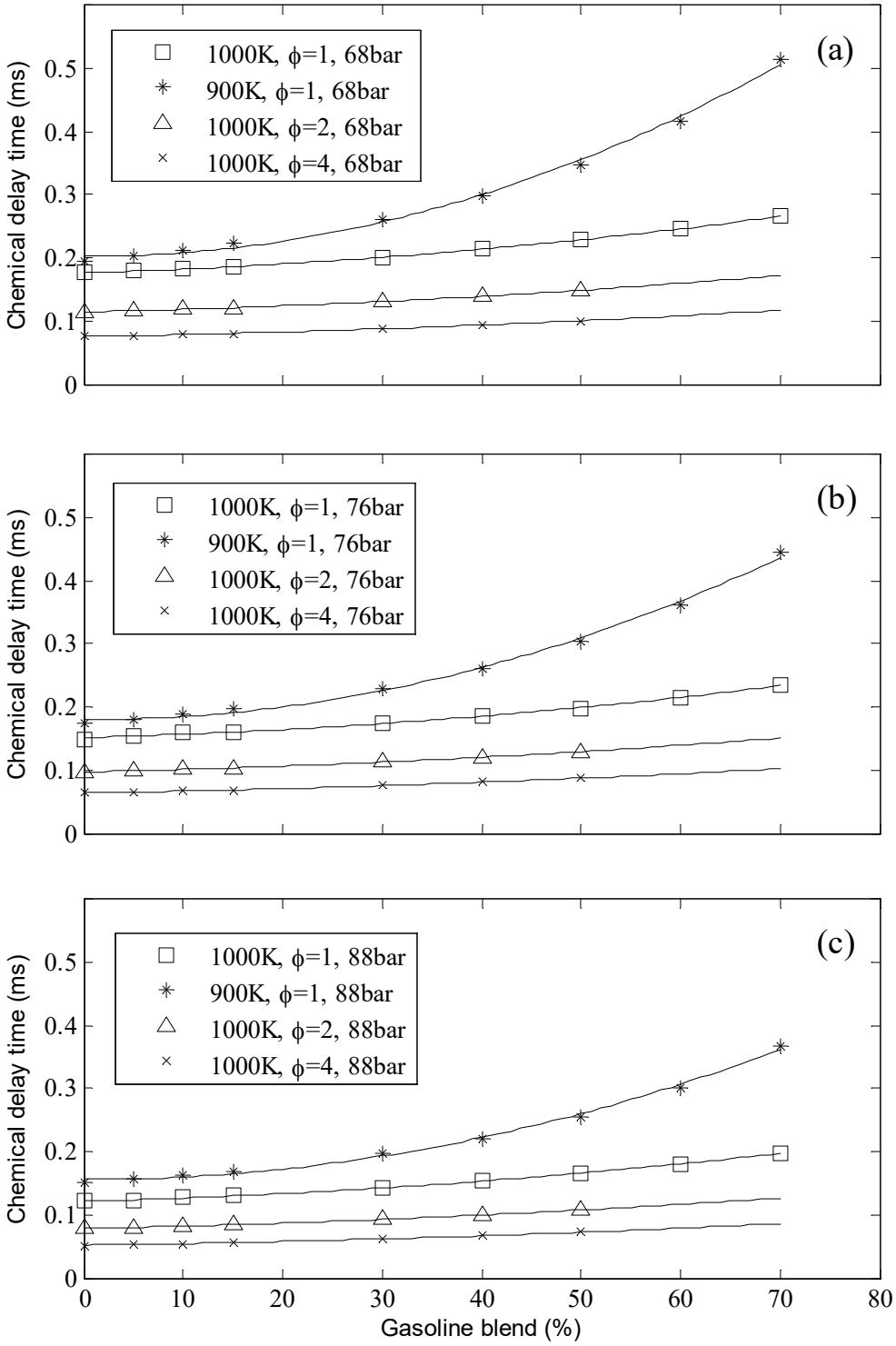


*Figure 4.9: ID periods predicted by CHEMKIN for diesel-gasoline blends under different speed-load conditions at (a) 2000 rev/min and 2.5 bar BMEP, (b) 2000 rev/min and 5 bar BMEP, and (c) 2000 rev/min and 8.5 bar BMEP.*

Predicted values of chemical delay were given in Figure 4.9 for the range of blends covered in the experimental work. The predictions covered three pressures (68 bar, 76 bar and 88 bar) corresponding to cylinder pressures during the ignition delay for the engine brake loads of 2.5, 5.0 and 8.5 bar BMEP. In each set of predictions, the same temperatures and equivalence ratio values were used and these included the targeted $\phi = 4$. As the gasoline fraction in the blends increased, the chemical delay increased, most significantly at lower values of temperature and equivalence ratio. The variations of the delay with blend ratio were observed to be similar at all three pressures. Figure 4.9 also showed that the difference in chemical delays predictions for $\phi$ values between 2 and 4 were insignificant. This justified the use of $\phi = 4$ for the simulations of all three engine loads, despite the fact that it varied from 3.5 to 4 according to the variation of in-cylinder temperatures from 950 K to 1050 K in practice. To compare with the experimental measurements taken on the test engine, using the results for the diesel fuelled case, a physical delay contribution was defined by subtracting the predicted chemical delay from the experimental total delay. The inferred physical delay reduced from 0.33 ms at the lightest load to 0.21 ms at the highest load; these were within the range of values found by extrapolating the trend lines in Figure 3.10a. At each fixed engine load, these physical delay values were assumed to be independent of proportion of gasoline in the fuel blend. As shown in Figure 4.10, the predicted variations of the total, and by implication the variations of the chemical delay contribution with blend proportions, then exhibited very similar trends as that obtained from the experiments.

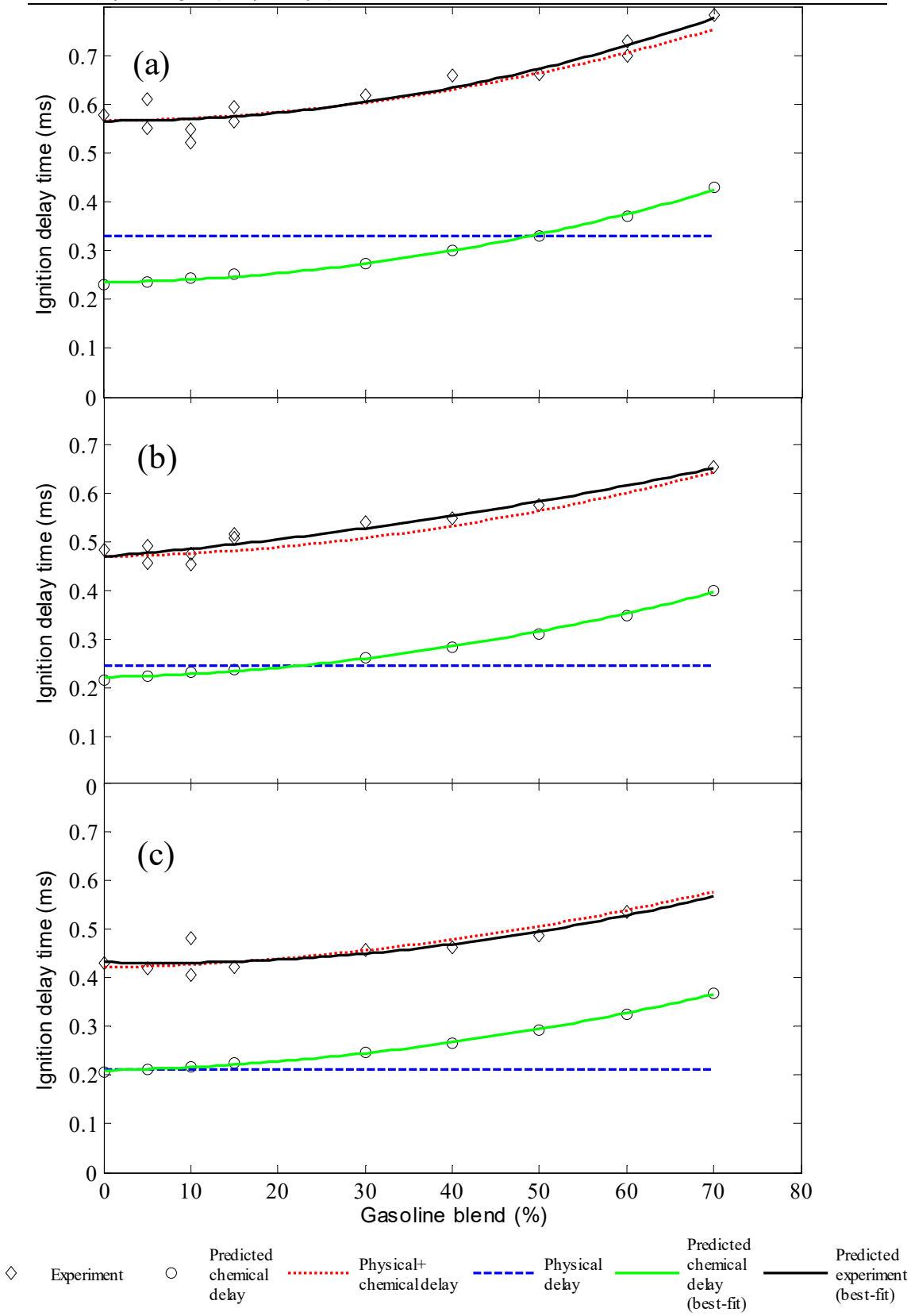


*Figure 4.10: Experimental and predicted ID periods for diesel-gasoline blends with an initial temperature of 820 K and mixture equivalence ratio of 4 under*

*different speed-load conditions of (a) 2000 rev/min and 2.5 bar BMEP, (b) 2000 rev/min and 5 bar BMEP, and (c) 2000 rev/min and 8.5 bar BMEP.*

The ID results for the gasoline-diesel blend with 50% gasoline and 50% diesel by volume which was known as G50 showed delay times less than half of the difference between delay times of pure diesel (D100) and delay times of pure gasoline (G100) as depicted in Figure 4.11. This observation indicated that the presence of diesel effectively accelerated the chemical rate of gasoline. Figure 4.12 showed the consumption of surrogate species which represented constituents such as alkanes (n-heptane/$NC_7H_{16}$), alkenes (iso-octane/$IC_8H_{18}$), and aromatics (toluene/$C_6H_5CH_3$) presence in diesel and gasoline for different D100, G50, and G100 at initial temperature of 900K and initial pressure of 76bar. Alkane comprised in diesel was shown to accelerate the consumption of alkene and aromatics. This could due to the fast breakdown rate of alkanes' molecules which leads to the higher production rate of active radicals such as OH and $H_2O_2$ that would help to consume fuel components of other chemical groups.

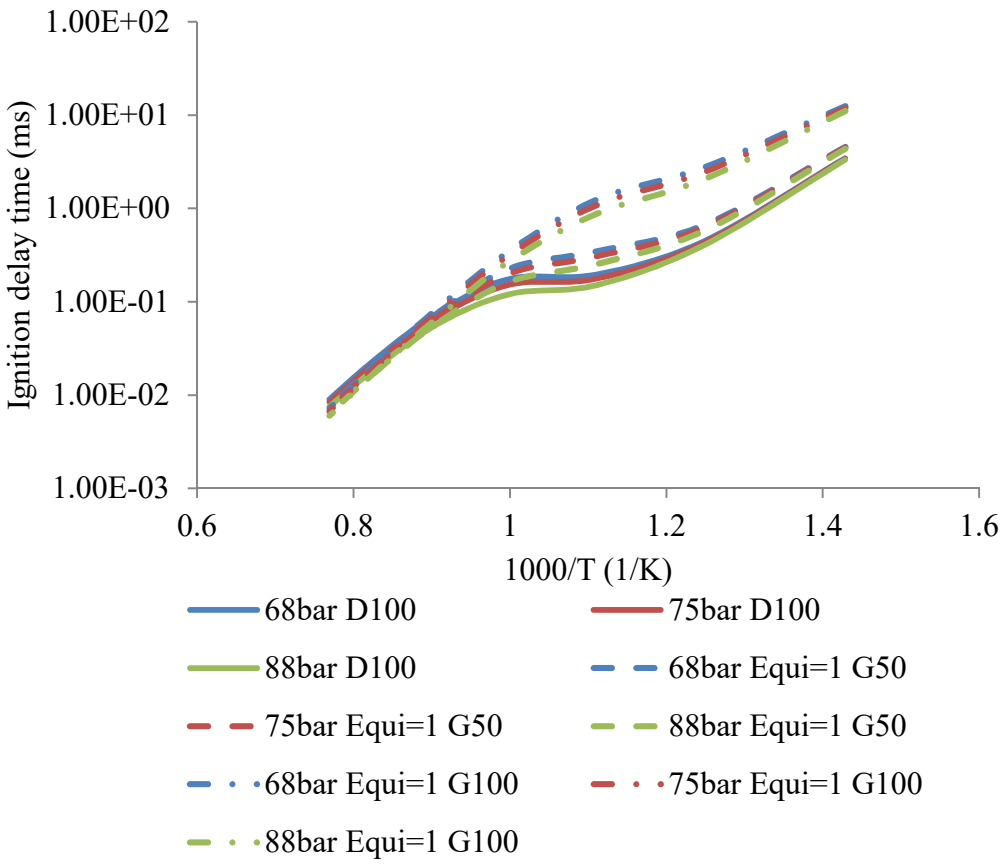


*Figure 4.11: Predicted ignition delay times of various fuel blends by CHEMKIN at three different pressures which emulate engine operating pressures.*

The CHEMKIN homogeneous batch reactor model was able to predict the gasoline blends' chemical delay periods with reasonable accuracy when the chemical kinetic mechanism comprised of n-heptane and toluene and the one comprised of n-heptane and iso-octane were used. Chemical delay was the main contribution to exponential increase of ignition delay period as gasoline blend was increased. The experiment found that gasoline application in CI engine struggled mostly at low engine speed and load conditions which the ignition delay periods were the longest. Maybe a dual-fuel CI engine that could run on diesel at low engine speed and load conditions and swap to gasoline at higher engine speed and load conditions would reap the benefits of gasoline combustion and yet maintain the reliability of a normal diesel engine by adjusting the chemical delay according to the engine speed-load conditions.

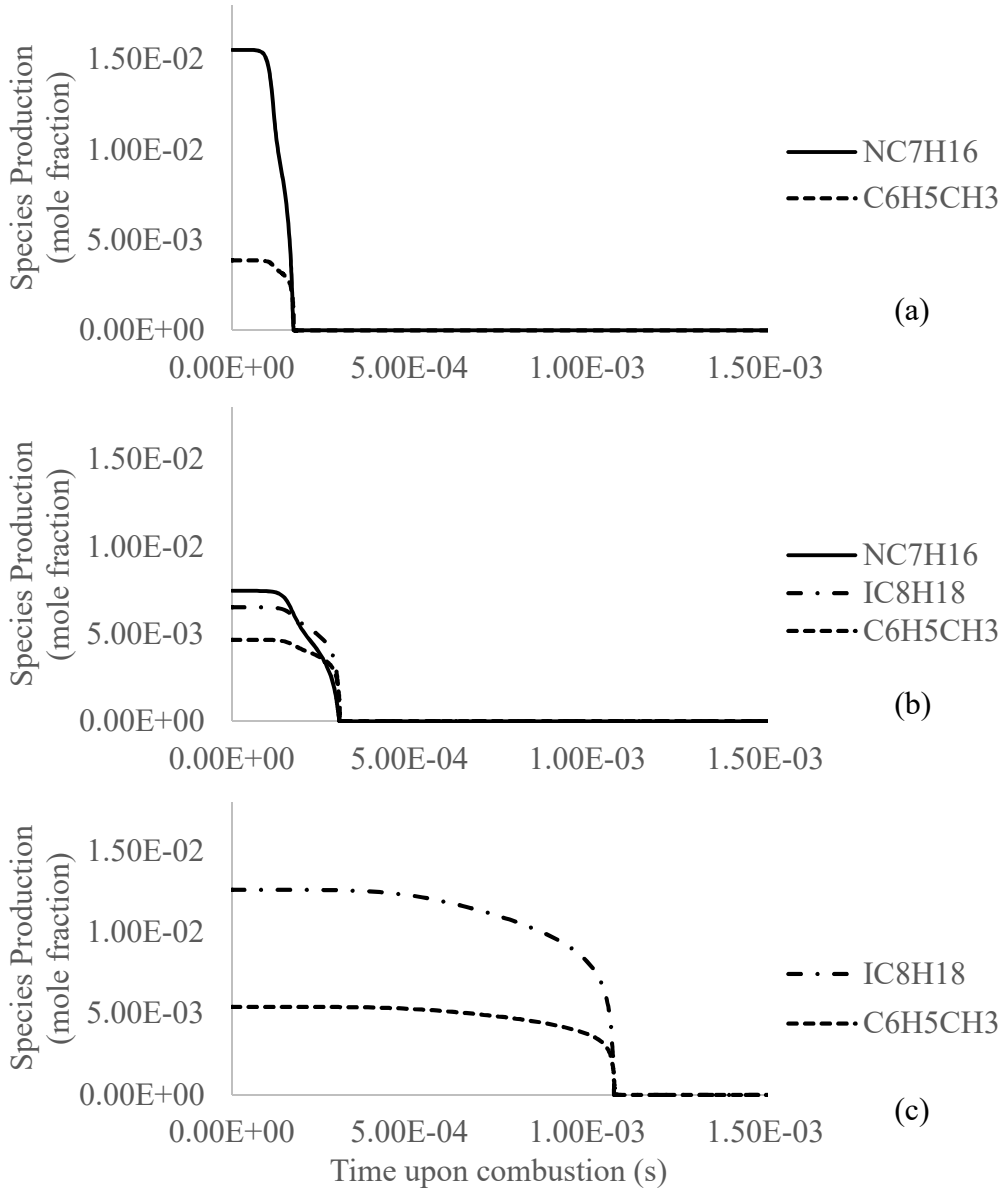


*Figure 4.12: Plot of mole fraction (mole) against time (s) simulated by CHEMKIN in homogeneous batch reactor model. (a) D100. (b) G50. (c) G100.*

# CHAPTER 5

## Binary chemical kinetic mechanism for CFD application

Chapter 3 and chapter 4 covered the experimental study of different diesel-gasoline fuel blends in a compression ignition engine and the theoretical study of chemical delay of the tertiary kinetic model comprised of n-heptane, iso-octane and toluene. Ignition delay period was shown to dictate the heat release rate and phase of combustion. Physical delay and chemical delay were postulated to be equally significant in the contribution to the total ignition delay. As the content of gasoline in blend was increased, the increase of ignition delay period was found to be attributed to the chemical delay. This led the desire to study gasoline combustion deeper with CFD simulation which require a reduced size chemical kinetic mechanism that could represent diesel and gasoline. Species size reductions of the detailed chemical kinetic mechanisms of all the three surrogate fuel components were done to reduce the calculation time of the chemical kinetic mechanisms. There were many existing reduction techniques and methodologies available from the literature.

### 5.1 Reduction of surrogate kinetic mechanism for diesel-gasoline blends

The conventional methods used to reduce the size of chemical kinetic mechanisms were based on absolute rate of production analysis, normalised sensitivity analysis, temperature sensitivity analysis and mole fraction of species analysis. Uncertainties such as the lack of information of the smallest time scales and destruction or production mode caused these methods to be ineffective in chemical kinetic reduction as compared to the newer methods. The computational singular perturbation (CSP), intrinsic low-dimensional manifolds (ILDM), and isomer lumping were the main newer methods that could tackle the weaknesses

experienced by the conventional methods. However, these reduction methods were not exactly simple and easy to be executed.

Therefore it was essential to understand the application of the reduced chemical kinetic mechanism before the choice of reduction technique was made. This had ensured the reduced chemical kinetic mechanism was optimised in size and accuracy. FLUENT CFD models suitable for modelling CI engine were evaluated. Diesel unsteady flamelet model in FLUENT CFD had the smaller species size allowed. This model only allowed chemical kinetic mechanism limited to 76species. This size was set as the targeted size for the reduced chemical kinetic mechanism for diesel-gasoline blends. Equivalence ratios of air-fuel mixture in this CI combustion were postulated to be between 2 to 4 [84]. Majority of the reduced chemical kinetic mechanisms available were developed and validated to be accurate at near stoichiometric conditions only; more relevant to conditions in spark-ignition and HCCI engines. The tested engine conditions also had combustion occurred in the temperature range of 850K to 1100K. Therefore the accuracy of the reduced mechanism was specifically validated to these equivalence ratio range and temperature range.

DRG reduction method was chosen for this work due to its simplicity and effectiveness towards reducing the size of chemical mechanisms according to the accuracy of predicted chemical delay in relative to the detailed chemical mechanisms. This work also did not require accurate prediction of species production rates as the focus had been on heat release characteristics of gasoline combustion. The DRG formula used was adopted from [59] and it was shown in Equation 5.11. The net rate of production, $\omega_i$ was calculated by deducting production rate of forward reaction, $\omega_{fi}$ to production rate of backward reaction, $\omega_{ri}$ as shown in Equation 5.12. This formula was written into an algorithm in MATLAB format to achieve semi-automatic reduction and skeletal mechanism compilation. Details of these algorithms will be explained in section 5.2.

$$\boldsymbol{r_{AB}} \equiv \frac{\sum_{i=1,I}|\boldsymbol{V_{A,i}\omega_i\delta_{Bi}}|}{\sum_{i=1,I}|\boldsymbol{V_{A,i}\omega_i}|} \qquad (5.11)$$

$$\boldsymbol{\omega_i = \omega_{fi} - \omega_{ri}} \quad (5.12)$$

$$\boldsymbol{r_{AB,S} \equiv \frac{\sum_{i=1,I}|V_{A,i}\omega_{i,S}\delta_{Bi}|}{\sum_{i=1,I}|V_{A,i}\omega_{i,S}|}} \quad (5.13)$$

$\delta_{Bi} = 1,0$ ; 1 if the ith reaction involves B, 0 otherwise.

The definition of the Delta ($\delta_{Bi}$) and stoichiometric coefficient ($V_{A,i}$) used in the DRG formula were straight forward ones.

In the kinetic calculation for combustion of any fuels, the production rates of reactions comprised in a mechanism change with time. This raised the question of ROPs at what time frame should be used as the input for DRG reduction algorithm. There were two approaches to define the production rates. First was the overall maximum net ROPs throughout the entire chemical kinetic calculation period. The second approach of defining the ROP inputs which was inspired by the unique heat release characteristics of n-heptane fuel. N-heptane generally exhibited four stages of combustions which were the initialisation, propagation, cool flame, and heat release as depicted in Fig. 5.1.1 [47]. The production rates of reactions were shown the highest at the heat release stage. Therefore if only the overall maximum production rates were considered like the first approach, many essential species for stages other than the heat release would have appeared to be redundant and eliminated.

The reduction of n-heptane with the ROP inputs defined by the second approach was carried out in four executions of the DRG algorithm with four sets of maximum net ROPs taken from every combustion stage instead of a single set, which resulted in four lists of species to be eliminated or kept. These lists were combined to give the net species to be eliminated. An additional subscript, S was added to the DRG formula to denote the stage of combustion as depicted in Equation 5.13. Later section explained the details of mechanism reduction algorithm built based on Equation 5.13 and the reduction process of the three surrogate components n-heptane, iso-octane and toluene. The chemical kinetic

mechanisms of iso-octane and toluene were reduced with the same method as n-heptane but with different stages of combustion. Iso-octane and toluene mechanisms exhibited 3-stages and 2-stages of combustions, respectively. Fig. 5.1.2 showed that regardless of the thresholds set against the normalised contribution ($\boldsymbol{r_{AB}}$), DRG reduction with the ROP inputs defined via the second approach were superior over the first. The 190species n-heptane skeletal mechanism reduced by the second approach predicted IDs more accurate than the 243species n-heptane skeletal mechanism reduced by the first approach.

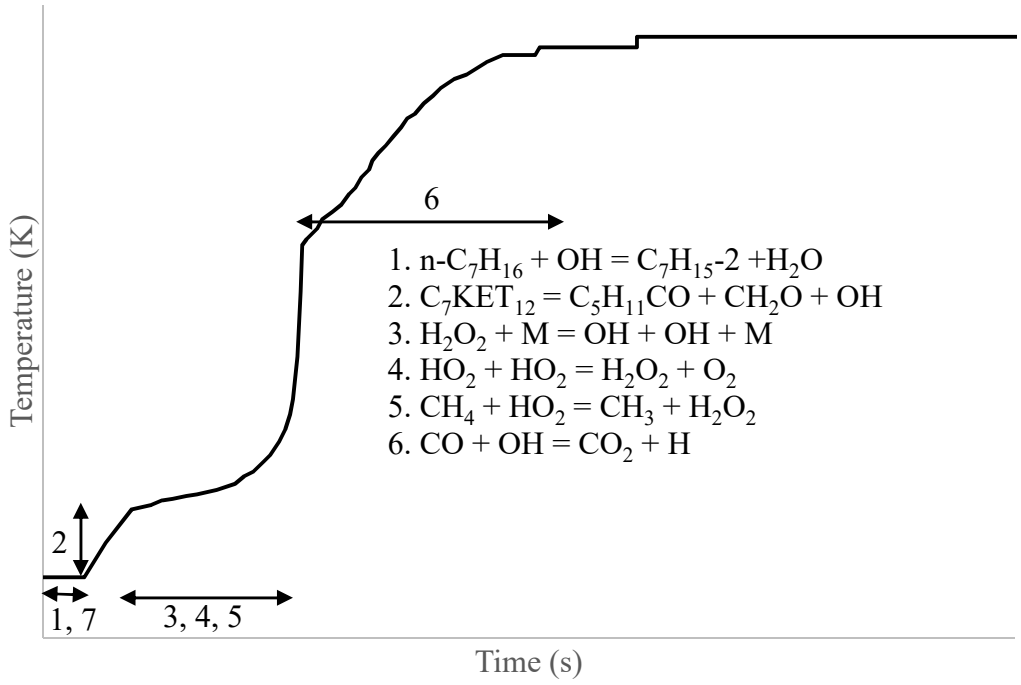


*Fig. 5.1.1: Temperature profile of n-heptane homogeneous combustion (adapted from **[47]**).*

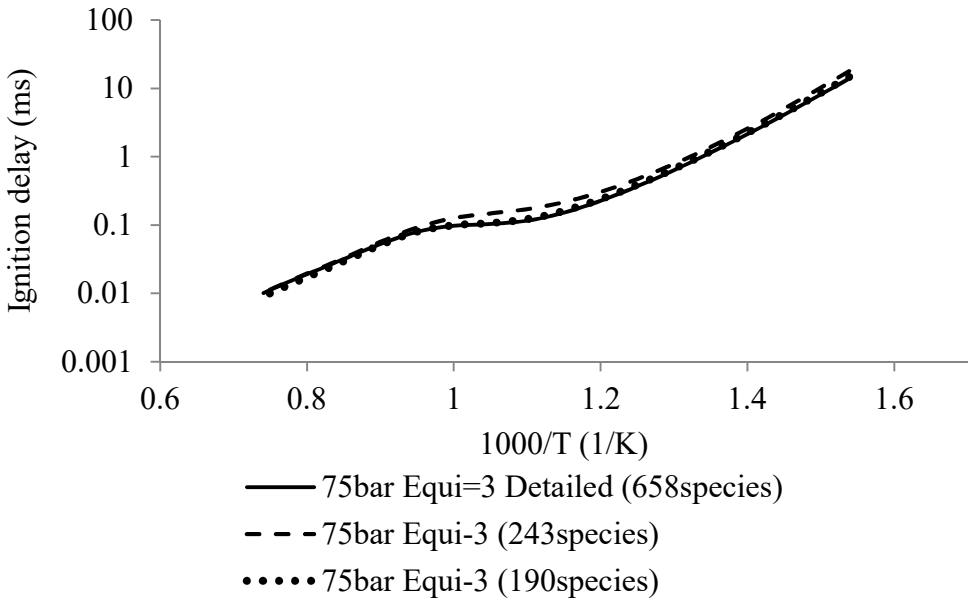


*Fig. 5.1.2: Ignition delay predicted with the ROPs of the first approach (243species) and the second approach (190species) via n-heptane mechanisms.*

**5.2 The reduction algorithms and step-by-step guide to execute the codes**

The algorithm of DRG was written in four steps and provided in the form of pseudo codes and MATLAB codes. The MATLAB codes were provided in Appendix A. The first step generated an array of stoichiometric coefficients ($V_{A,i}$) which was required by the DRG formula of Equation 5.13. The other variables of DRG, the net rate of productions ($\omega_i$), was generated manually by CHEMKIN homogeneous batch reactor model and the Delta ($\delta_{Bi}$) used to discriminate if species B were comprised in a reaction was taken into account by the regular expression search which would be explained in the pseudo codes of the DRG algorithm in section 5.2.1 of this thesis. Additional algorithm was included to identify reactants with stoichiometric coefficient of 2. The ROPs of these reactants needed to be multiplied by two as CHEMKIN only displayed ROPs of reactants in singular stoichiometric coefficient form. The second step constructed the graph similarly as [59] by evaluated the term $V_{A,i}\omega_i$ first but not the Delta ($\delta_{Bi}$) and counted the numerator and the denominator followed by the normalised contribution. In addition to Lu's algorithm, this step also recorded the coupling species of all predecessor species which had normalised contribution more than the set threshold.

The revised depth first search (RDFS) by Lu which searched for species pair through the entire graph with normalised contribution above threshold was not be required as the coupling species had already been identified through the second step. A more direct and active approach was adapted to complete the graph in the third step. The starting species were first determined followed by connecting all the subsequent coupling species and generated a list of retained species and a list of eliminated species at the end. The final or the forth step involved algorithm which removed the eliminated species and reactions and created the skeletal mechanism. A step-by-step instructions of implementing the MATLAB code for the DRG reduction had been given in Appendix B.

5.2.1 Pseudo codes

DRG()

#Step-1 Evaluate stoichiometric coefficients, VA, i from a list of reactions

*For each species i=1: no_species*
*For each reaction which consists of species i*
*Use regular expression search to mark either reactants with i and products with 10 dependent on the species being searched.*
*End for*
*Store the markings in a matrix in reference to the reactions.*
*End for*
*For each reaction products*
*If reactants/products consist $V_{A,i}$ of 2*
*Increase the marking by one to take account of CHEMKIN only displays ROPs of reactants in single molecule form.*
*End if*
*End for*

#Step-2 Graph Construction

*Import a list of ROPs generated by CHEMKIN*
*For each species pair A,B involved in the reactions*
*For each set of markings*
*If marking equals to 1,2 or 10*
*Count the numerator and denominator by adding the ROPs to the accumulated values*

*End if*
*If marking equals to 11*
*Count the numerator and denominator by adding the ROPs to the accumulated values*
*End if*
*End for*
*Evaluate $r_{AB}$ with the accumulated numerator and denominator.*
*If $r_{AB}$ is above the set threshold (ε)*
*Record species B as coupling species of species A in a matrix*
*End if*
*Reset the numerator and denominator counters*
*End for*

#Step-3 Graph Compilation
*Mark the species involved or the starting species with one*
*While number of species involved is increasing*
*Mark the coupling species of the starting species and the subsequent coupling species with one*

*Count the total number of species involved*
*End while*
*Generate a list of retained species and a list of eliminated species*

#Step-4 Create skeletal mechanism
*Import a list of eliminated species*
*Import the detailed chemical kinetic mechanism*
*Remove eliminated species and relevant reactions*
*Write the retained species and reactions to the skeletal mechanism*
*End*

## 5.3 Reduction methodology

### 5.3.1 Multiple-step DRG

Previously, all the fundamental DRG reduction knowledge and materials to build a skeletal chemical kinetic mechanism had been provided. A further reduction on the skeletal mechanism had been done through the multiple-step DRG followed by Arrhenius constants tuning. The basic DRG reduction involved only altering the

normalised contribution threshold to manipulate the eliminated species and reactions. A bigger normalised contribution threshold would eliminate more species. A drawback of DRG was said to be too aggressive in reducing species size [59]. That was overcome by divided the normal DRG reductions into multiple steps. This multiple-step DRG reduction recovered species comprised in mechanisms that were erroneously classified as too slow and unimportant.

In the multiple-step DRG reduction, the normalised contribution threshold was increased gradually from the starting value to the final value which induced ignition delay error less than 30%, with an increment of 0.01 for every interval. A starting threshold must produce a skeletal mechanism with ID error less than 10% and had been estimated to be around 0.1 based on experience. The methodology was illustrated in Figure5.3.1. Multiple sets of DRG reduction were performed according to the set intervals. If an interval increment resulted in relative ID error of more than 20% and usually consisted of many additional eliminated species, the threshold had to be reverted back to the previous value and the increment resolution for that specific interval was doubled. At each of the intervals, ignition delay error of the immediate reduced skeletal mechanism in relative to the previous one was evaluated. If the relative error was more than 5% error, the additional species eliminated during that interval would be tested one by one by CHEMKIN 0-D homogeneous batch reactor modelling. Any species that induced relative ignition delay error more than 5% would be recovered to the immediate mechanism before progressed to the next interval. The arrows and textboxes with dashed lines represented the loop cycles involved during each step of the multiple-step DRG when the conditions of relative error were fulfilled.

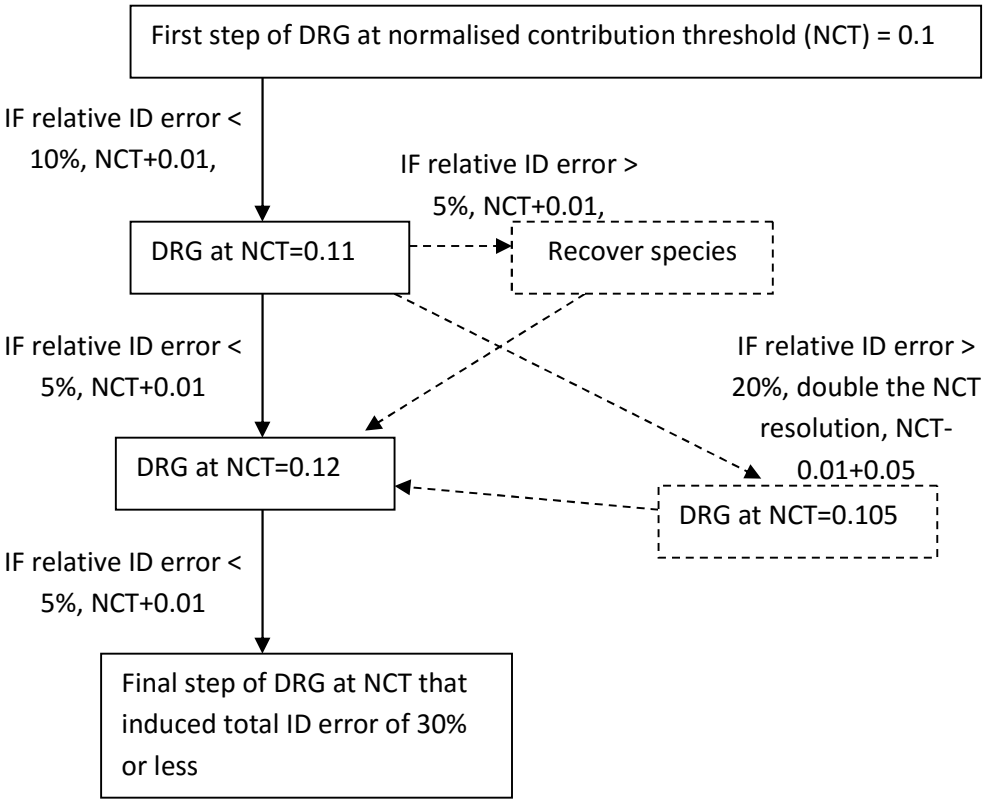


*Figure 5.3.1: Flow chart illustration of multiple-step DRG.*

5.3.2 Parametric adjustment of Arrhenius Constants

At this point, the leanest skeletal mechanisms with ID error less than 30% were constructed. In order to reduce the sizes of mechanisms further, the Arrhenius constants of reactions were adjusted to compensate additional errors caused by the further reduction. The targeted species for further reduction were the recovered species from the multiple-step DRG. The presence of vital reactions allowed the error to be compensated through the constants tuning of these reactions. Therefore sensitivity tests were performed on the Curran's 25 classes of reactions comprised in the mechanisms. The pre-exponential factors of every class of reactions had been evaluated. The reactions with the largest maximum rates of productions of each class were used for the sensitivity tests. The ROPs of the 25 classes of reactions were first generated before the sensitivity test. Both were done by the CHEMKIN 0-D batch reactor model. With the insight of the sensitivity of these reactions towards ignition delay, the error compensation was done accordingly. For example, the adjustment of the pre-exponential factors of the class-one

reactions which were sensitive towards high temperature combustion compensated IDs in the high temperature region. More details of tuning the reactions constants were explained in later section which included the sensitivity of reaction constants of each reaction class towards ignition delay for all the three surrogate fuels n-heptane, iso-octane and toluene.

A simple flow-chart illustration of the reduction via constant tuning was depicted in Figure5.3.2. The two vital inputs for this stage of reduction were the final skeletal mechanism and the list of relative ID errors of all the recovered species from the multiple-step DRG. The list of relative ID errors of all the recovered species was arranged in ascending order from the smallest error to the largest. The number of species that had to be eliminated was pre-determined according to the targeted species number estimated earlier. The exact number of species with the least errors was chosen from the arranged list of relative ID errors of all the recovered species. These chosen species were then eliminated from the final skeletal mechanism taken from the previous multiple-step DRG mechanism stage. This shredded final skeletal mechanism had to go through the 0-D CHEMKIN homogeneous batch reactor modelling for IDs, Arrhenius constants tuning of the vital 25 classes of reactions, and revised the species that could be eliminated again and again before it was taken as the reduced mechanism. Ideally, the reduced mechanism was expected to have the ability to predict IDs with error less than 30% as the multiple-step DRG stage. However the species limitation had forced the tolerance for ID error to increase. The validation of the IDs predicted by the reduced mechanism was hence focused on qualitative instead of quantitative and it was done visually. Ultimately the Arrhenius constants of the reduced mechanism of n-heptane, iso-octane and toluene had been readjusted again to match the IDs of diesel and gasoline. The IDs predicted by the mechanisms can be easily prolonged or delayed by increasing or decreasing the activation energy of the vital reactions. But the qualitative predictions of the IDs such as the cool-flame characteristics cannot be altered as easily via the adjustment of Arrhenius constants. Thus, the focus was paid on building the reduced mechanisms that bear the same cool-flame characteristics as the respective detailed mechanisms.

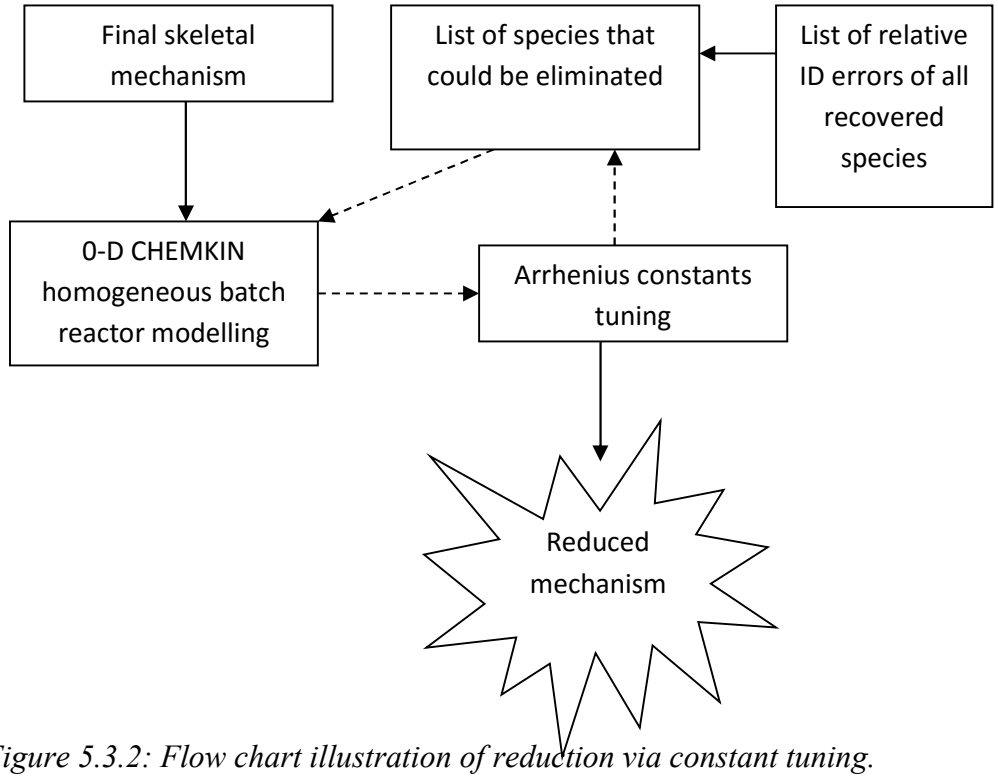


*Figure 5.3.2: Flow chart illustration of reduction via constant tuning.*

## 5.4 Reduction of n-heptane, iso-octane and toluene

The ultimate reduced diesel-gasoline chemical mechanism was developed for the CFD application specifically for predicting the ignition delay. Commercial CFD software, FLUENT 13.0 was selected to perform this task. The maximum species size of chemical mechanism that is allowed by FLUENT's diesel unsteady flamelet model is 76species. The mechanisms of the three single-component surrogate fuels were reduced to the smallest size possible with 30percent ID error or less in relative to the respective detailed mechanisms.

The detailed n-heptane mechanism consisted of 658species. The detailed iso-octane mechanism consisted of 878species. The detailed toluene mechanism consisted of 117species. These three components summed up to a total of 1653species without excluding the common species among the three mechanisms. This figure helped to estimate the size of each reduced component had to be. As the targeted final diesel-gasoline mechanism was limited to 76species, the n-heptane component was estimated to be 30species, the iso-octane component was estimated to be 40species, and the toluene mechanism was estimated to be 6species.

These were the initial estimated targeted species size for the three reduced surrogate fuels.

The detailed n-heptane mechanism was reduced first via a single-step DRG with normalised contribution thresholds (NCT) of 0.11 and 0.15 as shown in Figure 5.4.1. Both reductions resulted in two skeletal mechanisms comprised of 186species and 100species. The largest relative IDs errors between the two skeletal mechanisms and the detailed n-heptane mechanism were 13.8% and 121.2%, respectively. It was as expected that the ID error increased as the NCT increased. The ID error of the 100species n-heptane skeletal mechanism had already exceeded the pre-determined ID error limit. Hence the 100species n-heptane mechanism cannot be used for further reduction. As for the 186species skeletal mechanism, the reduction was continued via the multiple-step DRG. The multiple-step DRG reduction managed to bring down the size of the skeletal mechanism down to 97species with relative ID error peaked at 14.9%. Despite the skeletal mechanism reduced by the multiple-step DRG had 97species compared to the 100species skeletal mechanism reduced by the single-step DRG, the predicted IDs were far more accurate. This was the evidence that proved the multiple-step DRG is more superior to the single-step DRG. However, 97species was still very far from achieving the targeted size of 30species for n-heptane. The multiple-step DRG successfully shredded 89species from the first skeletal n-heptane mechanism and recovered a total of 84species which induced relative ID error more than 5%. The 84 recovered species were the potential species that could be removed.

The constant tuning reduction method had successfully reduced the 97species skeletal mechanism down to 48species with maximum ID error of 38% as compared to the detailed n-heptane mechanism. The process involved the adjustments of two class1 reactions' preexponential factor by 1E5 times and one class3 reaction's preexponential factor by 20 times. The exact reactions and the original and adjusted Arrhenius constants of these reactions were shown in Table 5.4.1.

*Table 5.4.1: Vital reactions that were adjusted to compensate the errors induced by additional species eliminated from the recovered species.*

| Reaction | Preexponential factor | Temperature exponent | Activation energy | Comments |
|---|---|---|---|---|
| NC7H16=> H+C7H15-2 | 1.300E+88 | -21.01 | 1.395E+05 | Original (class 1) |
| | 1.300E+93 | -21.01 | 1.395E+05 | Adjusted |
| NC7H16=> H+C7H15-3 | 1.300E+88 | -21.01 | 1.395E+05 | Original (class 1) |
| | 1.300E+93 | -21.01 | 1.395E+05 | Adjusted |
| C7H15-2=> PC4H9+C3H6 | 9.764E+18 | -1.79 | 3.136E+04 | Original (class 3) |
| | 1.9528E+20 | -1.79 | 3.136E+04 | Adjusted |

Figure 5.4.2 showed the effect of the two Class 1 reactions and the Class 3 reaction towards the IDs of n-heptane. The untuned 48species n-heptane mechanism predicted the IDs with reasonable accuracy at temperature below 950K. The ID error peaked at 28% for temperature below 950K. However the ID error increased to 200% for temperature went from 950K to 1350K. It was very apparent that ID errors for the high temperature region of the n-heptane combustion had to be reduced. Attempts of tuning the Curran's 25 classes of reactions had been done. Class 1 and Class 3 reactions were found to be sensitive to ID prediction in this temperature range. The constants tuning was executed by manual adjustment of the constants and the affected ID predictions were verified visually one by one.

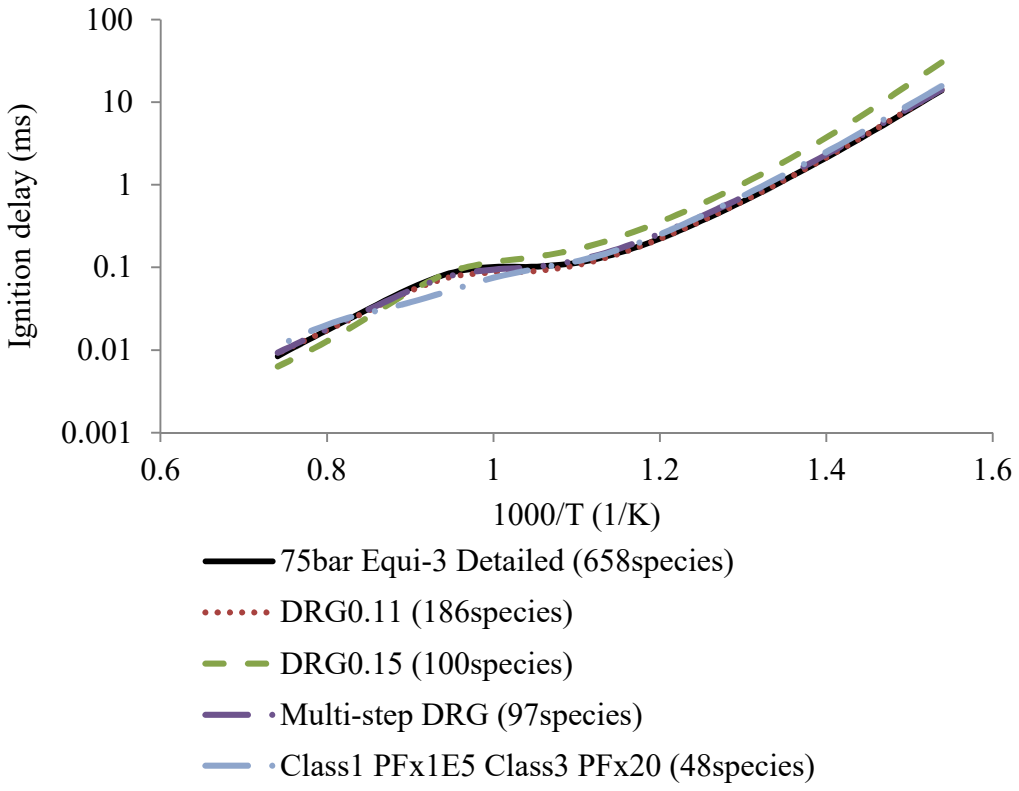


*Figure 5.4.1: Predicted ignition delay periods by detailed Nheptane mechanism (658species), skeletal mechanisms reduced with single-step DRG by NCT of 0.11 and 0.15 (186&100species) and multiple-step DRG (97species), and reduced mechanism constructed through constants tuning on top of the multiple-step DRG (48species).*

The detailed iso-octane mechanism was reduced first via a single-step DRG with normalised contribution thresholds (NCT) of 0.115 and 0.12 as shown in Figure5.4.3. Both reductions resulted in two skeletal mechanisms comprised of 254species and 218species. The largest relative IDs errors between the two skeletal mechanisms and the detailed iso-octane mechanism were 9.72% and 30.3%, respectively. It was as expected that the ID error increased as the NCT increased. The ID error of the 218species n-heptane skeletal mechanism had already exceeded the pre-determined ID error limit which was set at 30%. Hence the 218species n-heptane mechanism was not chosen to be reduced to any smaller one in size. As for the 254species skeletal mechanism, the reduction was continued via the

multiple-step DRG. The multiple-step DRG reduction managed to bring down the size of the skeletal mechanism down to 125species with relative ID error peaked at 17.2%. Despite the skeletal mechanism reduced by the multiple-step DRG had 125species compared to the 218species skeletal mechanism reduced by the single-step DRG, the predicted IDs were far more accurate. This had proven once again the multiple-step DRG was more superior to the single-step DRG. However, 125species was still very far from achieving the targeted size of 40species for iso-octane mechanism. The multiple-step DRG successfully shredded 134species from the first skeletal iso-octane mechanism and recovered a total of 108species which induced relative ID error more than 5%. The 108 recovered species were the potential species that could be removed.

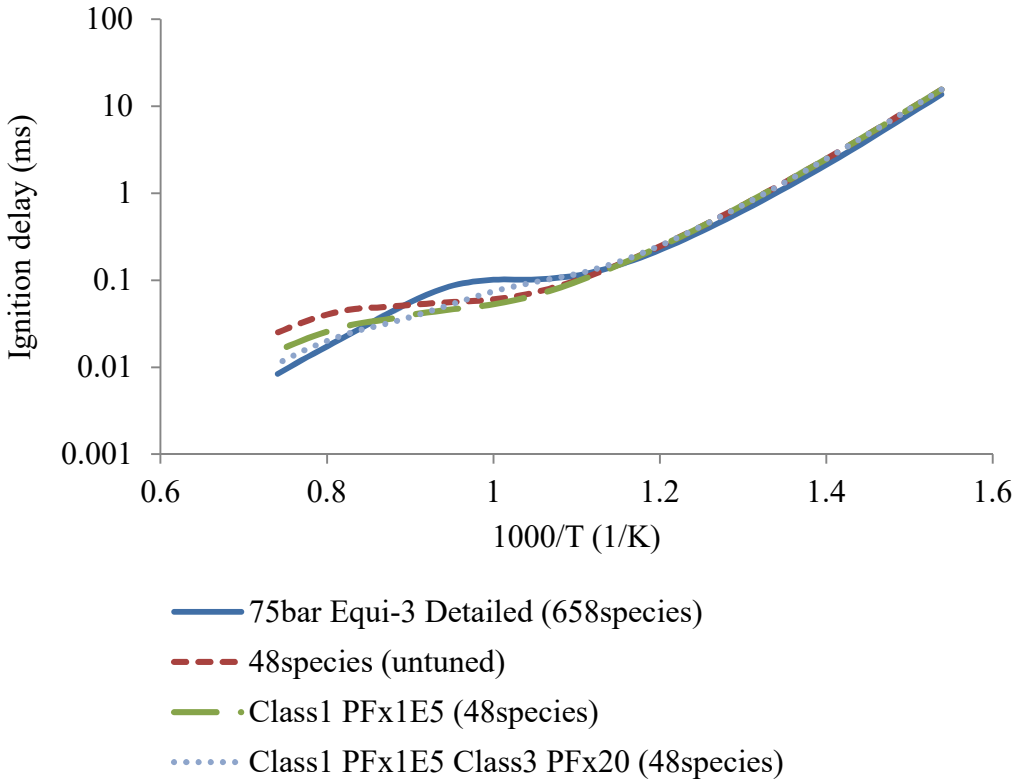


*Figure 5.4.2: The effect of class 1 and class 3 reactions on n-heptane mechanism.*

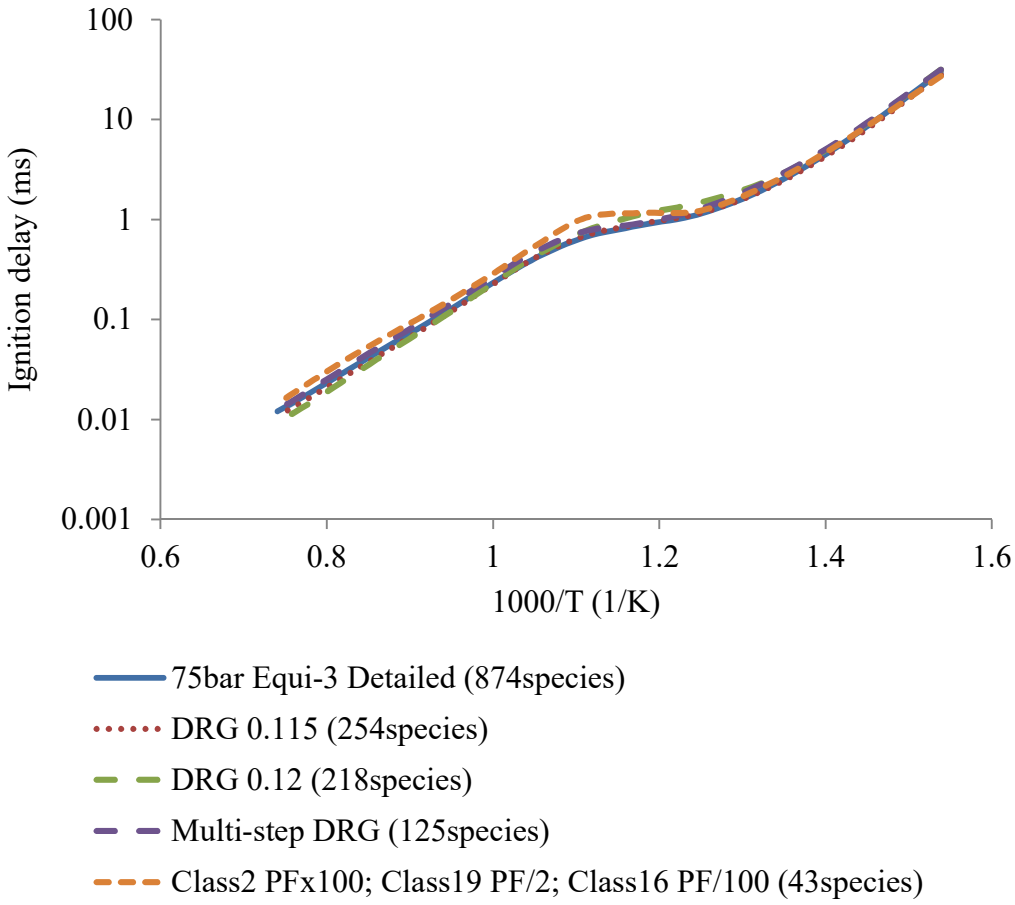


*Figure 5.4.3: Predicted ignition delay periods by detailed iso-octane mechanism (874species), skeletal mechanisms reduced with single-step DRG by NCT of 0.115 ad 0.12 (254&218species), skeletal mechanism reduced by multiple-step DRG (125species), and reduced mechanism constructed through constants tuning on top of the multiple-step DRG (43species).*

The constant tuning reduction method had successfully reduced the 125species skeletal mechanism down to 43species with maximum ID error of 56.1% as compared to the detailed iso-octane mechanism. The process involved the adjustments of two class2 reactions' preexponential factors by multiplying these preexponential factors by 100 times, one class16 reaction's preexponential factor by divided it by 100 times, and one class19 reaction's preexponential factor by divided it by 2. The exact reactions and the original and adjusted Arrhenius constants of these reactions were shown in Table 5.4.2.

*Table 5.4.2: Vital reactions that were adjusted to compensate the errors induced by additional species eliminated from the recovered species.*

| Reaction | Preexponential factor | Temperature exponent | Activation energy | Comments |
|---|---|---|---|---|
| IC8H18+H =>AC8H17+H2 | 7.341E+05 | 2.768 | 8.147E+03 | Original (class 2) |
| | 7.341E+07 | 2.768 | 8.147E+03 | Adjusted |
| IC8H18+OH <=>AC8H17+H2O | 2.630E+07 | 1.800 | 1.431E+03 | Original (class 2) |
| | 2.630E+09 | 1.800 | 1.431E+03 | Adjusted |
| AC8H17O2+AC8H17O2=>O2+AC8H17O+AC8H17O | 1.400E+16 | -1.610 | 1.860E+03 | Original (class 16) |
| | 1.400E+14 | -1.610 | 1.860E+03 | Adjusted |
| AC8H16OOH-B <=> IC8ETERAB+OH | 3.000E+11 | 0.000 | 1.425E+04 | Original (class 19) |
| | 1.500E+11 | 0.000 | 1.425E+04 | Adjusted |

Figure 5.4.4 showed the effect of the two Class 2 reactions, the Class 16 reaction, and Class 19 reaction towards the IDs of n-heptane. The untuned 43species iso-octane mechanism predicted the IDs with reasonable accuracy at high temperature above 950K. The ID error peaked at 50% for temperature above 950K. However the ID error increased to 232% for temperature below 950K. It was very apparent that ID errors for the low temperature region of the iso-octane combustion had to be reduced. Adjustments of the Curran's 25 classes of reactions had been done. Class 2, Class 16, and Class 19 reactions were found to be sensitive to ID prediction in this temperature range. The constants tuning was executed by manual adjustment of the constants and the affected ID predictions were verified visually one by one. The constants tuning successfully lowered the peak ID error down to only 56%. This impressive results of the iso-octane reduction by iso-octane demonstrated that even the errors induced by the recovered species from the

multiple-step DRG stage can be compensated with proper adjustments of Arrhenius constants of the Curran's 25 classes of reactions.

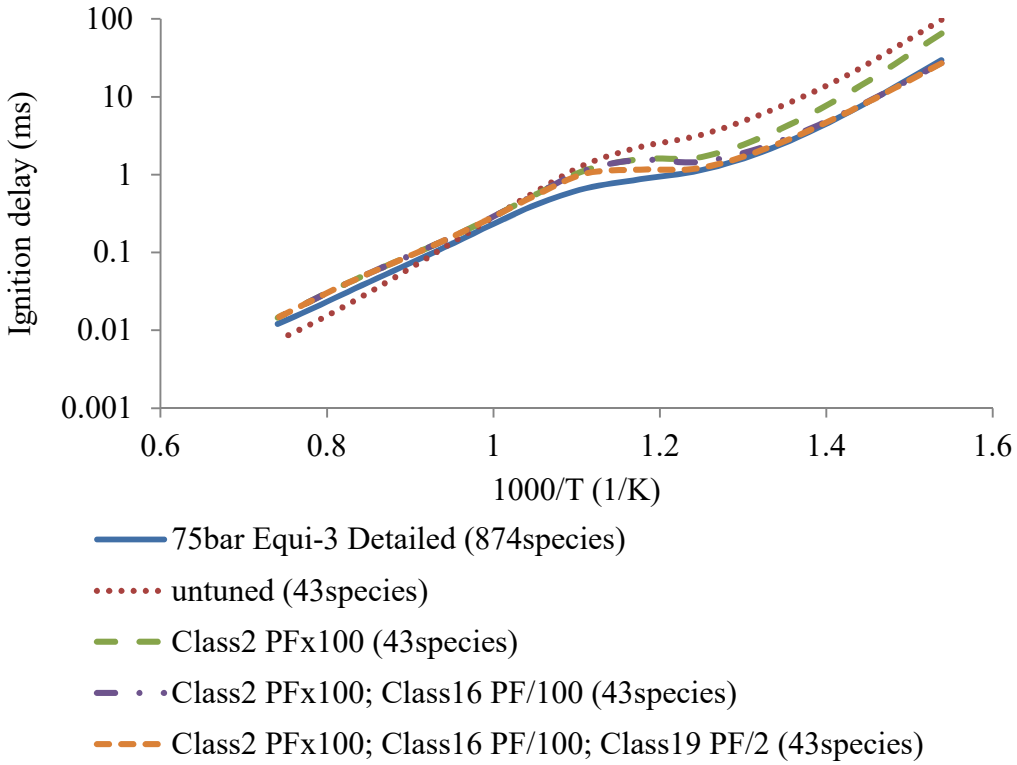


*Figure 5.4.4: The effect of class 2, class 16, and class 19 reactions on iso-octane mechanism.*

Toluene mechanism had a very simple ignition delay profile as compared to n-heptane and iso-octane as depicted in Figure 5.4.5. There was no cool-flame effect at all for toluene but only straight trend line of IDs in the logarithmic scale plot. The detailed toluene mechanism comprised of 117species. The detailed toluene mechanism was reduced first via a single-step DRG with normalised contribution thresholds (NCT) of 0.11 and 0.255. Both reductions resulted in two skeletal mechanisms comprised of 53species and 36species. The largest relative IDs errors between the two skeletal mechanisms and the detailed toluene mechanism were 5.4% and 58.9%, respectively. The ID error of the 36species toluene skeletal mechanism had already exceeded the pre-determined ID error limit which was set at 30%.

Hence the 36species n-heptane mechanism was not chosen to be reduced to any smaller one in size. As for the 53species skeletal mechanism, the reduction was continued via the multiple-step DRG. The multiple-step DRG reduction managed to bring down the size of the skeletal mechanism down to 33species with relative ID error peaked at 13.7%. This had proven once again the multiple-step DRG was more superior to the single-step DRG. The multiple-step DRG successfully shredded 20species from the first skeletal iso-octane mechanism and recovered a total of 13species which induced relative ID error more than 5%. However there was not any additional species that could be removed from the 13 recovered species without causing significant errors in IDs prediction. The toluene mechanism had been decided to be abandoned because it had linear ignition delay characteristics which could be replicated through the adjustments of Arrhenius constants of n-heptane and iso-octane mechanisms. The exclusion of toluene mechanism gave the ultimate diesel-gasoline mechanism additional space to include more reactions from n-heptane and iso-octane. This could actually improve the accuracy of the ultimate diesel-gasoline mechanism and let it be easier to achieve the targeted species size of 76.

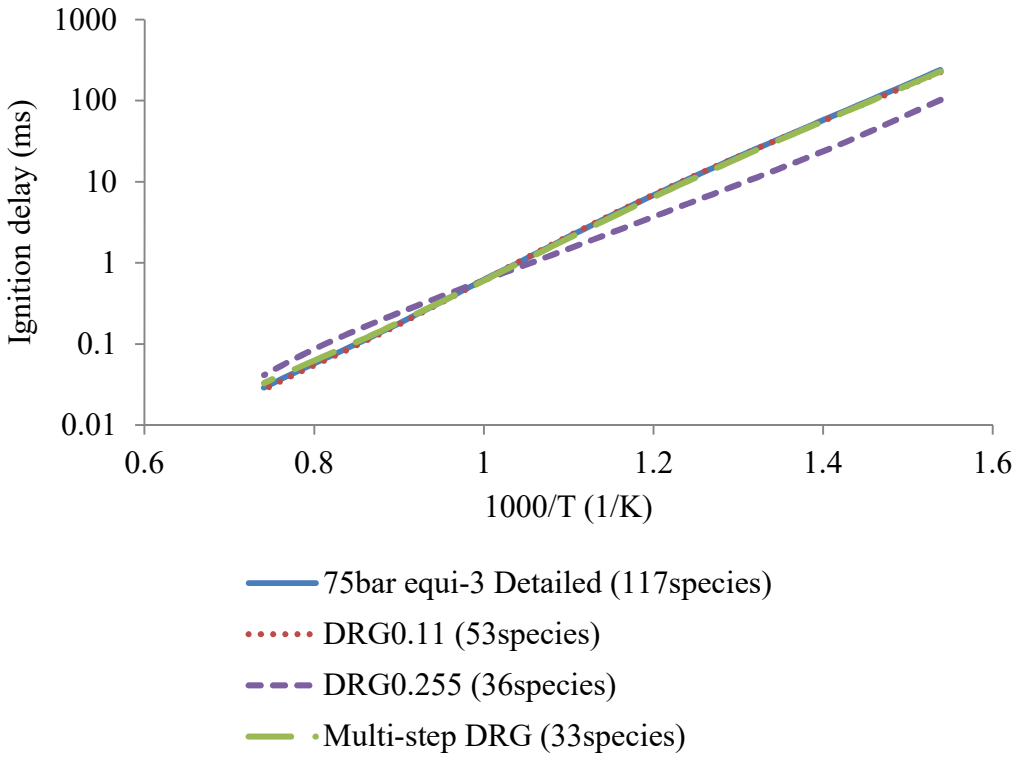


*Figure 5.4.5: Predicted ignition delay periods by detailed toluene mechanism (117species), skeletal mechanisms reduced with single-step DRG by NCT of 0.11 ad 0.255 (53&36species), and skeletal mechanism reduced by multiple-step DRG (33species).*

### 5.5 Binary diesel-gasoline mechanism

The diesel-gasoline mechanism had only two components made up by n-heptane and iso-octane as explained earlier. The challenge of combining these two mechanisms involved the limitation species size, the identification of the common species and reactions, and the addition of global reactions for diesel and other gasoline fuel blends. Another MATLAB algorithm given in Appendix C had been adapted from the species reduction algorithm to identify the common reactions and the unique reactions between the two mechanisms. It was crucial to prevent having repetitive common reactions when the two mechanisms were combined. This was to ensure the same reactions would not have been calculated twice and caused error in the IDs prediction.

Figure 5.5.1 listed down the entire process of how the ultimate diesel-gasoline mechanism was developed. As the toluene mechanism had been abandoned due to the species size limitation, the process only began with the detailed n-heptane mechanism and the detailed iso-octane mechanism. These two detailed mechanisms went through the multiple-step DRG reduction and the further reduction of the recovered species compensated Arrhenius constants tuning resulted in the 48species reduced n-heptane mechanism and the 43species reduced iso-octane mechanism as discussed in the earlier chapters. The unique species and common species between the two reduced mechanisms were listed down. The reduced n-heptane mechanism had 26 unique species. The reduced iso-octane mechanism had 21 unique species. Both reduced mechanism shared a total of 22 common species. The MATLAB algorithm had been used to identify the common reactions and unique reactions between the two reduced mechanisms.

The algorithm identified 133 unique n-heptane reactions, 165 unique iso-octane reactions and 139 common reactions. These unique and common reactions were stitched together and became the 69species binary n-heptane and isooctane mechanism. Global reactions were then added to this binary mechanism to represent the diesel, G30, G50 and G70 reactions. These global reactions linked up the n-heptane and iso-octane mechanisms for the predictions of diesel and other gasoline fuel blends especially made for CFD purpose.

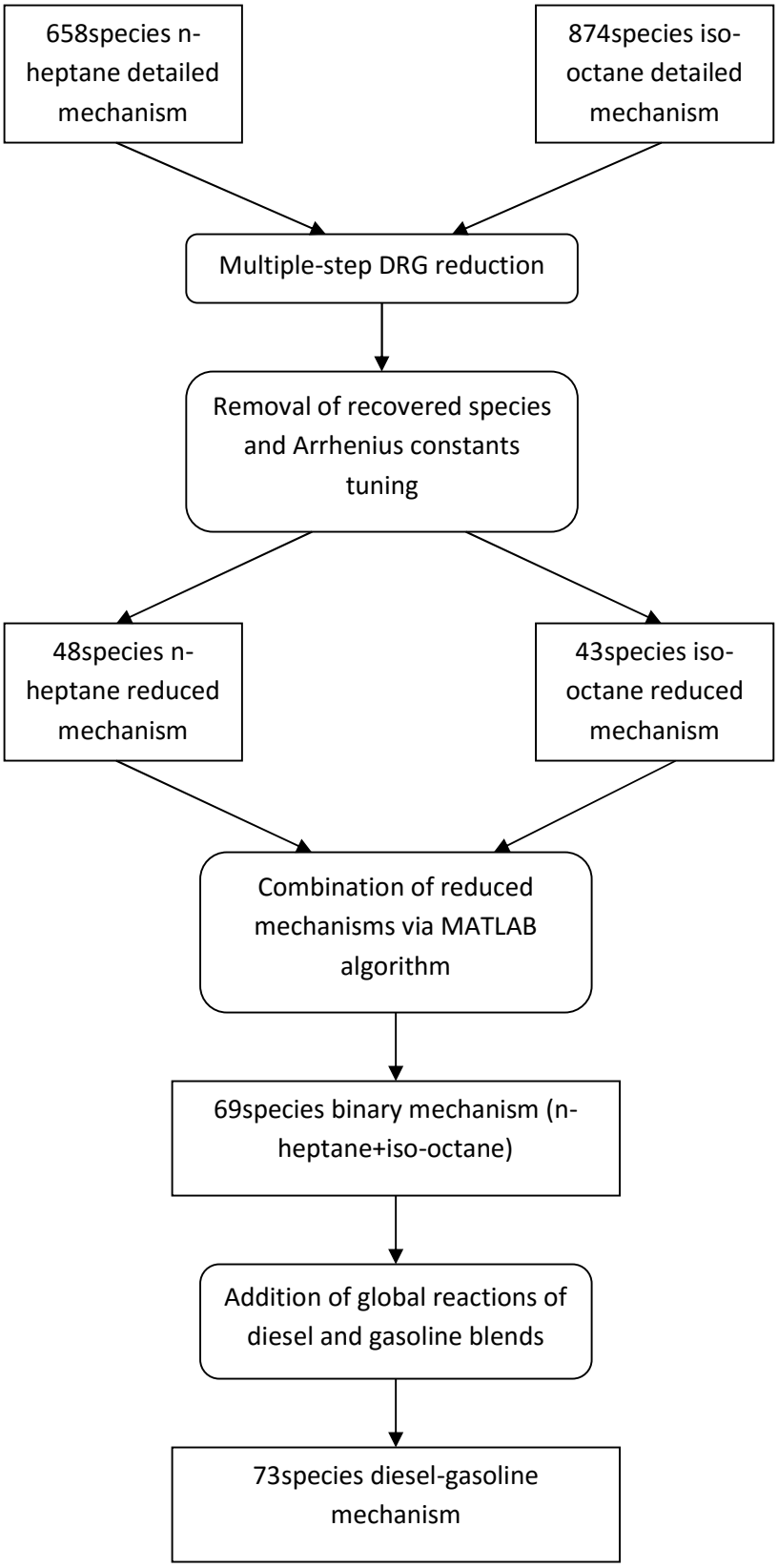


*Figure 5.5.1: The process of the development of the diesel-gasoline mechanism.*

The accuracy of the 73species diesel-gasoline mechanism in predicting IDs of n-heptane was shown in Figure 5.5.2. The validations were performed under pressures of 68bar to 88bar, equivalence ratios of 1 to 4, and temperatures of 650K to 1350K. The pressure conditions were determined according to the in-cylinder engine pressures near to TDC right before start of fuel injection. The validated equivalence ratios covered the richer combustion nature of compression-ignited type of combustion as compared to spark-ignited combustion. The validated temperature range was the standard validation range for chemical kinetic mechanism validation and it included the in-cylinder temperatures near to TDC across the engine speed-load conditions. It was apparent that the reduced diesel-gasoline mechanism had lost part of the essential reactions that govern the cool-flame characteristics of n-heptane. The largest ID error in relative to detailed n-heptane mechanism was 50.3% and it was induced by the prediction at pressure of 68bar, equivalence ratio of 1.0 and temperature of 1000K. Additional 49species were shredded from the 97species n-heptane skeletal mechanism despite the additional error increase from 14.9% to 38% for validations performed at equivalence ratio of 3. This effort had made the binary mechanism small enough to be practically used in CFD for feasible speed and predicted ID's accuracy.

The accuracy of the 73species diesel-gasoline mechanism in predicting IDs of iso-octane was shown in Figure 5.5.3. The validations were performed under the same conditions as the ones for n-heptane validations. There was a sudden spike in relative ID errors for the validations of low temperature combustion below 750K for equivalence ratio of 1. The spike caused the relative ID error to peak at 192.9%. Apart from this spike, the highest error was only 85.2% for all other conditions. Additional 82species were shredded from the 125species iso-octane skeletal mechanism despite the additional error increase from 14.9% to 56.1% for validations performed at equivalence ratio of 3.

Finally the 73species diesel-gasoline mechanism had been tested for its ability to predict the different gasoline fuel blends. Global reactions for diesel and three other gasoline fuel blends G30, G50 and G70 had been added to the mechanism.

Ideally, the global reactions for diesel and gasoline should each consist of 2moles of n-heptane and 2moles of iso-octane, as shown in Equation 5.51 and Equation 5.52, respectively. However, the global reactions of the other three fuel blends require the presence of other species with smaller carbon number to balance the reactions. Species such as $CH_4$ and $H_2$ had been included into the global reactions for the purpose of balancing the reactions. These two species had been selected because they appeared to be not affecting the predicted IDs. The diesel global reaction had hence been modified with the presence of both $CH_4$ and $H_2$ to assimilate the global reactions for G30, G50 and G70. These global reactions had been listed below as Equation 5.53, Equation 5.54, Equation 5.55, and Equation 5.56. All the global reactions comprised of the same Arrhenius constants. The exponential factor used was 5E10, the temperature exponent was zero and the activation energy was 28000. The complete mechanism was given in Appendix D.

$$\text{Diesel} \Rightarrow 2NC_7H_{16} \quad (5.51)$$

$$\text{Gasoline} \Rightarrow 2IC_8H_{18} \quad (5.52)$$

$$\text{Diesel} \Rightarrow 1.9NC_7H_{16}+0.7CH_4+0.4H_2 \quad (5.53)$$

$$\text{G30} \Rightarrow 1.4NC_7H_{16}+0.6IC_8H_{18}+0.4CH_4+0.1H_2 \quad (5.54)$$

$$\text{G50} \Rightarrow 1.1NC_7H_{16}+1.1IC_8H_{18}+0.5CH_4+0.3H_2 \quad (5.55)$$

$$\text{G70} \Rightarrow 0.6NC_7H_{16}+1.4IC_8H_{18}+0.6CH_4+0.4H_2 \quad (5.56)$$

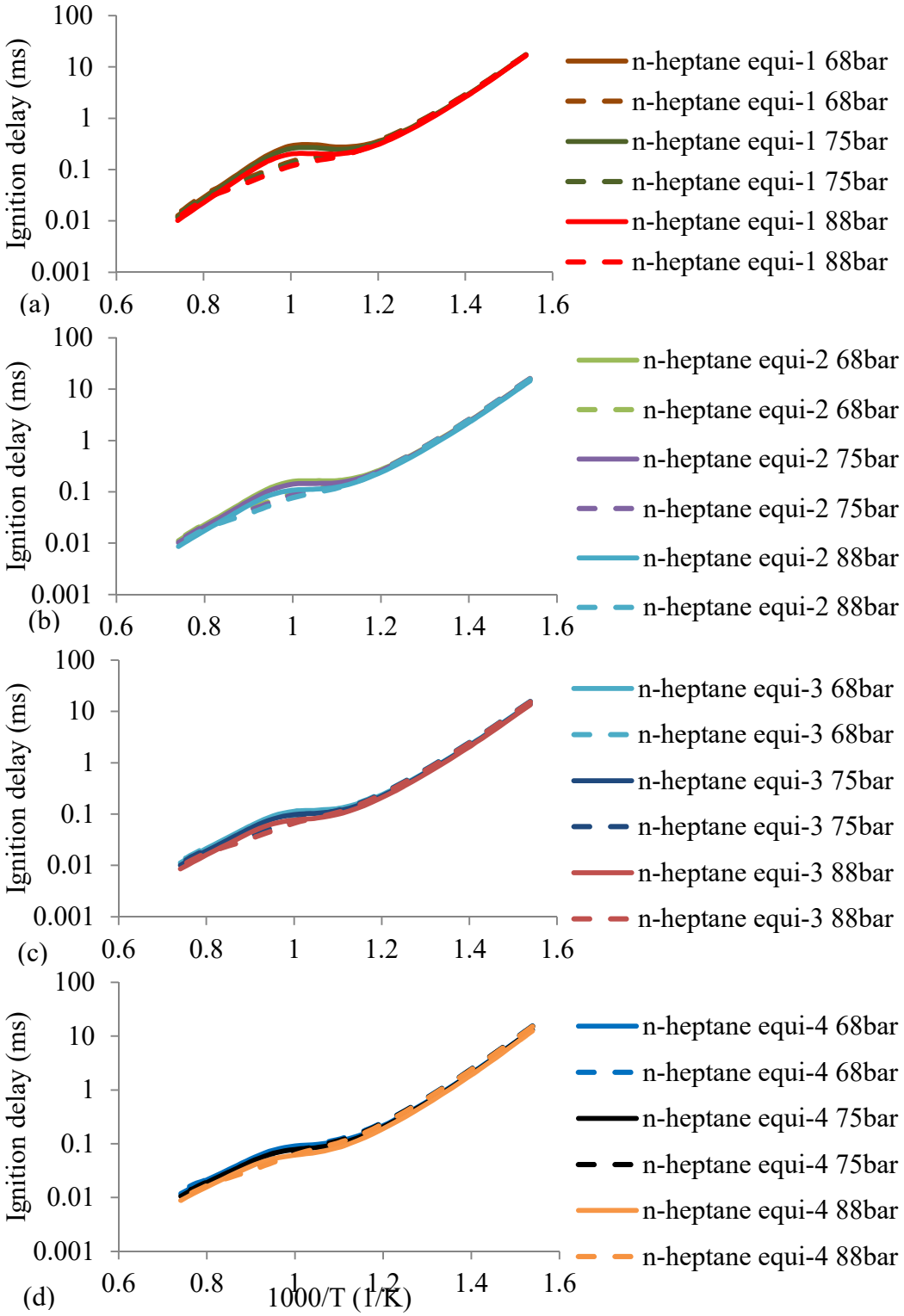


*Figure 5.5.2: Validation of IDs of n-heptane predicted by the 73species diesel-gasoline mechanism (dotted lines) against the IDs predicted by the detailed n-heptane mechanism (solid lines). (a) equi-1 (b) equi-2 (c) equi-3 (d) equi-4*

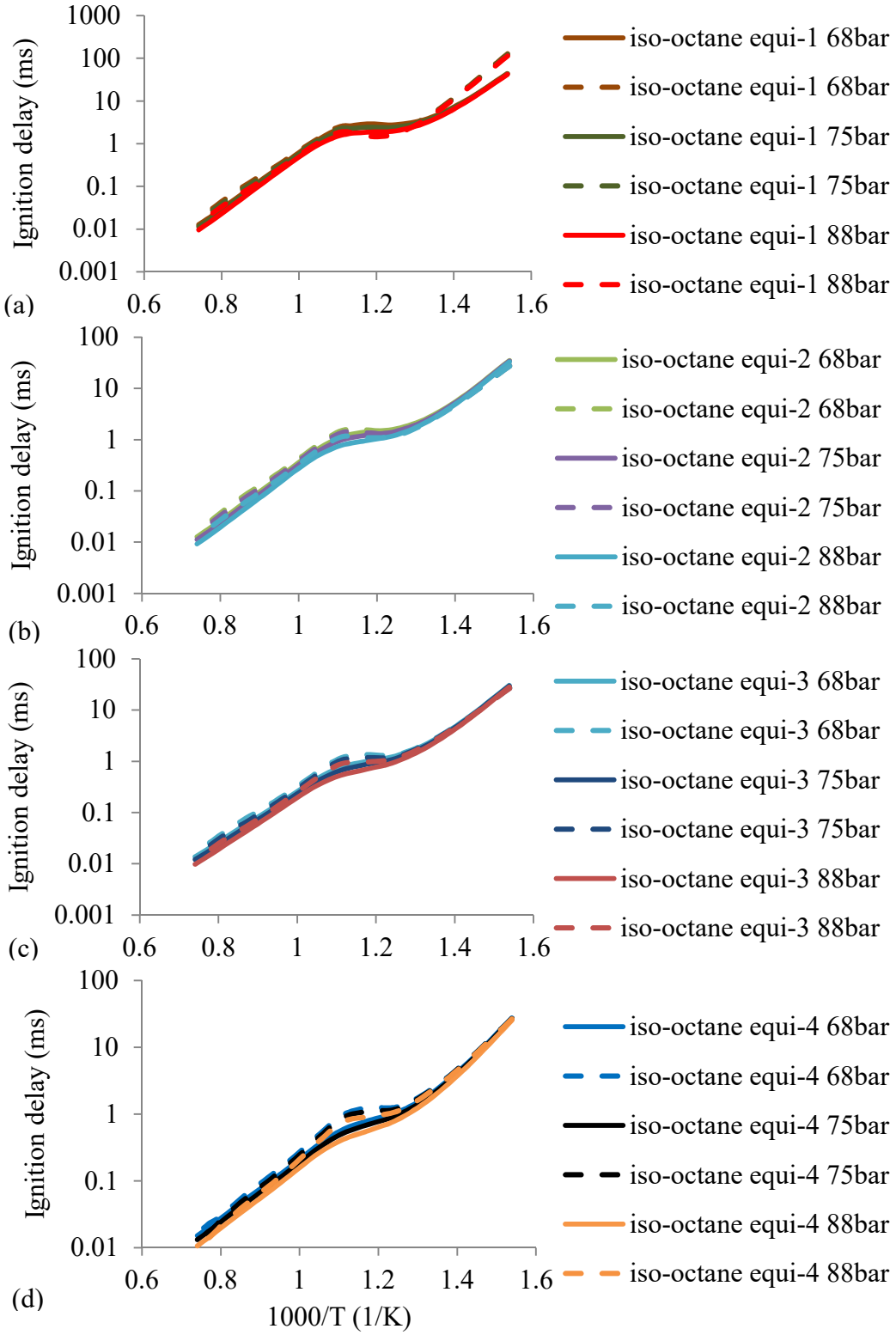


*Figure 5.5.3: Validation of IDs of iso-octane predicted by the 73species diesel-gasoline mechanism (dotted lines) against the IDs predicted by the detailed isooctane mechanism (solid lines). (a) equi-1 (b) equi-2 (c) equi-3 (d) equi-4*

These global reactions predicted ID times as depicted in Figure 5.5.4. The figure showed that fuel blends with higher gasoline content had longer IDs as per the finding of the experimental study. The constants of these global reactions may have to be adjusted again before it could be used for CFD application. The ID trend lines of all fuel blends would fall within the area enclosed by the iso-octane and n-heptane ID trend lines. The adjustments revolved around tuning the Arrhenius constants of the global reactions and the 25 class reactions of n-heptane and iso-octane reactions.

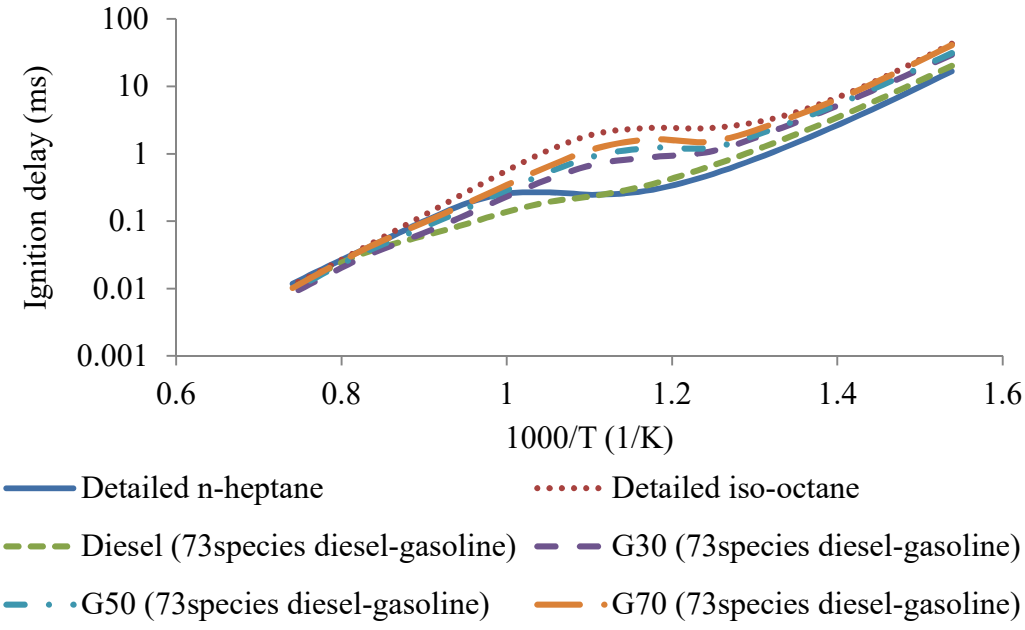


*Figure 5.5.4: Demonstration of ignition delays of different gasoline blends predicted by the 73species diesel-gasoline mechanism.*

DRG had been shown very effective in reducing size of detailed mechanisms. The programmed algorithm allowed the DRG reduction process to be executed repetitively and effortlessly. A hundred rounds of executions could easily be done in an hour time excluding the time spent on results analyses. This semi-automatic way of reduction allowed the ultimate binary diesel-gasoline mechanism to be built starting from detailed mechanisms of n-heptane and iso-octane. Having the detailed mechanisms as starting mechanisms actually allowed the ultimate binary mechanism to be the leanest and most accurate for the purpose of ignition delay

prediction because all the reactions comprised in it were chosen especially for this specific purpose. Therefore this advantage had led to creating a reliable reduced chemical kinetic mechanism that could predict ID periods accurately for diesel-gasoline blends. Having accurately ID predictions made this reduced chemical kinetic mechanism a model model to predict $NO_x$ and soot formations accurately in future CFD work. The development of this chemical kinetic mechanism reduction platform allowed many other surrogate mechanisms to be developed from relevant single-component detailed mechanism.

# CHAPTER 6

## Conclusion

Gasoline and diesel blends showed an exponential increase in ID as gasoline blend was increased from G0 to G80 for engine speed-load conditions of 2000rev/min 2.5bar BMEP, 2000rev/min 5bar BMEP, and 2000rev/min 8.5bar BMEP. The highest gasoline blend ever tested in this experiment was G80 at engine speed of 2000rev/min. The reason why the experiment did not carry on with gasoline blend beyond G80 was because G80 already exhibited behaviours of unstable combustion such as fluctuation in engine load and abnormal engine vibration when the engine was operated at lower engine speed of 1000rev/min. The extrapolated ID for 100% gasoline could go up to 14CAD for the engine speed-load condition of 2000rev/min 2.5bar BMEP and can go beyond 14CAD for cases with 1000rev/min. This extremely long extrapolated ID for 100% gasoline would have had the combustion phase shifted much later into the expansion stroke ATDC. This would have physical impact of having in-cylinder temperature too cold and fuel-air mixture too lean to have the gasoline burnt in the engine. This impact was not experienced by the cases with engine speed of 2000rev/min as the IDs were relative shorter as compared to 1000rev/min simply due to the more intense in-cylinder turbulence. Therefore the extremely long ID was the major reason for the unstable combustion of G80 at 1000rev/min and why G100 cannot run in this engine with the default SOI timing. The finding of exponential increase of IDs for gasoline blends had helped to understand the fact that G100 would have extremely long ID. The unstable combustion of G80 could have attributed to other factors such as fuel injection, fuel breakup, fuel vaporisation and fuel chemistry due to the different liquid physical properties of gasoline. These factors would be interesting to study in future work to validate if the factors actually had effect on the unstable combustion of G80.

However the different liquid physical properties did have effect on the pump-triggered type injection system used in this engine. The lower compressibility of gasoline caused the fuel to be injected later than diesel and in larger quantity for the same default ECU setting. The SOI timing was retarded up to 3degree CAD for G80. Therefore advancing the ECU timing for SOI would not help for this case. The experimental study found that there was always a physical delay period which varied from 0.29ms to 0.33ms before any sign of heat release. The physical delay period only varied with engine speed-load conditions but independent of gasoline blends. The change of engine brake thermal efficiencies were negligible as gasoline blend was increased. The values averaged at 24.2%, 33.8% and 39.8% for engine speed-load conditions of 2000rev/min 2.5bar BMEP, 2000rev/min 5bar BMEP and 2000rev/min 8.5bar BMEP, accordingly. The comparable thermal efficiencies of gasoline blends to diesel further supports gasoline to be feasible alternative fuel for CI engine. Future work can be focused on modification of engine ECU setting and equipment setup of CI engine to optimise performance of gasoline combustion in CI engine. The engine speeds and loads tested in this study were limited to extra-urban driving condition. Future work could cover speed-load conditions which are more relevant to urban driving condition.

Besides the comparable engine performance, $NO_x$ and soot formations were correlated to the proportions of premixed combustion and mixing-controlled combustion. The longer ignition delay of gasoline blends' combustion resulted in bigger premixed combustion and smaller mixing-controlled combustion. This phenomenon demonstrated the potential of gasoline combustion to defy the conventional soot-$NO_x$ trade-off of CI engine and be able to simultaneously reduce both $NO_x$ and soot formations. Future work could include the measure of $NO_x$ and PM emissions complemented by detailed $NO_x$ and soot formation study. Other emission-controlled strategies such as EGR and split injections could be applied to gasoline combustion in the future too. Discrimination of physical delay and chemical delay gave valuable insight to the proportions of premixed combustion and mixing-controlled combustion hence extended the understanding towards $NO_x$ and soot formations for gasoline blends' combustion. CHEMKIN's homogeneous

zero dimensional study with chemical kinetic mechanism developed for gasoline blend found that chemical delay was responsible for the exponential increase of ignition delay period as gasoline blend was increased. The increase of chemical delay for gasoline blend resulted in a leaner and bigger portion premixed combustion but smaller portion mixing-controlled combustion, which were ideal for the low $NO_x$ and low soot combustion. In the process of finding ways to predict chemical delay of gasoline combustion, a fast chemical delay prediction model by CHEMKIN had been established. Future work could employ this fast chemical delay prediction model to develop correlations that predict ID and $NO_x$-soot formations at even faster speed than the CHEMKIN model.

Extensive chemical kinetic mechanism reduction work had been done to develop the reduced mechanism that could be used in CFD to simulate the combustion chemistry of diesel-gasoline blends. This effort provided the key combustion model for future CFD work which could potentially find the relationships between physical-chemical delays and $NO_x$-soot formations in cylinder. A multi-stage ROP and a multiple-step DRG reduction techniques had been founded for effective chemical kinetic mechanism reduction. For a case with multi-stage ROP technique, the detailed n-heptane mechanism with 658species was reduced to 190species but the normal ROP approach resulted in 243species with similar level of ID accuracy. This was clear sign that the multi-stage ROP approach did 8% more reduction in species size than the normal approach. The multiple-step DRG technique managed to reduce the detailed n-heptane mechanism down to 97species as compared to 186species for the normal DRG. Both reduced n-heptane mechanisms had similar accuracy level of IDs. Multiple-step DRG reduced 13.5% more species than normal DRG.

In the midst of reducing the two-component diesel-gasoline chemical kinetic mechanism consisted of n-heptane and iso-octane mechanisms, a systematic semi-automatic reduction methodology with MATLAB algorithms had been founded. This reduction methodology had brought the n-heptane down to 97species with error peaked 14.9% relative to the detailed mechanism and iso-octane down to

125species with relative error peaked at 17.2%. The adjustment of Arrhenius constants allowed the n-heptane and iso-octane mechanisms to be finally reduced to 48species with relative error peaked at 38% and 43species with relative error peaked at 56.1%, respectively. Ultimately, the reduced n-heptane and iso-octane mechanisms were combined to build a 73species CFD-applicable diesel-gasoline reduced chemical kinetic mechanism equipped with global reactions for G30, G50 and G70. Future study could extend the theoretical study to CFD engine simulation and study in depth of the $NO_x$ and soot formations in sophisticated in-cylinder environment which involves breakup of fuel particle, air-fuel mixing, and complicated chemical reactions of fuel.

# REFERENCES

[1] Y. Chi and E. Kim, "Measurement of Droplet Size Distribution of Transient Diesel Spray," *SAE Technical paper 931949,* 1993.

[2] C. Yu, J. Wang, Z. Wang and S. Shuai, "Comparative study on Gasoline Homogeneous Charge Induced Ignition (HCII) by diesel and Gasoline/Diesel Blend Fuels (GDBF) combustion," *Fuel,* vol. 106, pp. 470-477, 2013.

[3] S. Ma, Z. Zheng, H. Liu, Q. Zhang and M. Yao, "Experimental investigation of the effects of diesel injection strategy on gasoline/diesel dual-fuel combustion," *Applied Energy,* vol. 109, pp. 202-212, 2013.

[4] R. Hanson, D. Splitter and R. Reitz, "Operating a heavy-duty direct-injection compression-ignition engine with gasoline for low emissions," *SAE Technical Paper 2009-01-1442,* 2009.

[5] G. Kalghatgi, P. Risberg and H. Angstrom, "Partially pre-mixed auto-ignition of gasoline to attain low smoke and low NOx at high load in a compression ignition engine and comparison with a diesel fuel," *SAE Technical Paper 2007-01-0006,* 2007.

[6] D. Han, A. Ickes, S. Bohac, Z. Huang and D. Asssanis, "HC and CO emissions of premixed low-temperature combustion fueled by blends of diesel and gasoline," *Fuel,* vol. 99, pp. 13-19, 2012.

[7] G. Chen, Y. Shen, Q. Zhang, M. Yao, Z. Zheng and H. Liu, "Experimental study on combustion and emission characteristics of a diesel engine fuelled with 2,5-dimethylfuran-diesel, n-butanol-diesel and gasoline-diesel blends," *Energy,* vol. 54, pp. 333-342, 2013.

[8] M. Sellnau, J. Sinnamon, K. Hoyer and H. Husted, "Gasoline direct injection compression ignition (GDCI)- Diesel-like efficiency with low CO2 emissions," *SAE Int. J. Engine,* vol. 4, pp. 2010-2022, 2011.

[9] S. Park, I. Youn, Y. Lim and C. Lee, "Influence of he mixture of gasoline and diesel fuels on droplet atomization, combustion, and exhaust emission characteristics in a compression ignition engine," *Fuel Processing Techology,*

vol. 106, pp. 392-401, 2012.

[10] A. Maghbouli, W. Yang, H. An, J. Li, S. Chou and K. Chua, "An advanced combustion model coupled with detailed chemical reaction mechanism for DI diesel engine simultion," *Applied Energy,* vol. 111, pp. 758-770, 2003.

[11] W. Pitz, N. Cernansky, F. Dryer, F. Egolfopoulos, J. Farrell, D. Friend and H. Pitsch, "Development of an experimental database and chemical kinetic models for surrogate gasoline fuels," *SAE Technical paper 2007-01-0175,* 2007.

[12] M. Sjögren, H. Li, U. Rannug and R. Westerholm, "A multivariate statistical analysis of chemical composition and physical characteristics of ten diesel fuels," *Fuel,* vol. 74, no. 7, pp. 983-989, 1995.

[13] M. Mehl, W. Pitz, C. Westbrook and H. Curran, "Kinetic modelling of gasoline surrogate components and mixtures under engine conditions," *Proc. Combust. Inst.,* vol. 33, pp. 193-200, 2011.

[14] J. Hernandez, J. Sanz-Argent, J. Benajes and S. Molina, "Selection of a diesel fuel surrogate for the prediction of auto-ignition under HCCI engine conditions," *Fuel,* vol. 87, pp. 655-665, 2008.

[15] J. Luo, M. Yao, H. Liu and B. Yang, "Experimental and numerical study on suitable diesel fuel surrogates in low temperature combustion conditions," *Fuel,* vol. 97, pp. 621-629, 2012.

[16] K. Lee, Y. Kim and K. Min, "Development of a reduced chemical kinetic mechanism for a gasoline surrogate for gasoline HCCI combustion," *Combust. Theor. Model,* vol. 15, pp. 107-124, 2011.

[17] J. Brakora, Y. Ra, R. Reitz, J. McFarlane and C. Daw, "Development and validation of a reduced reaction mechanism for biodiesel-fueled engine simulations," *SAE Technical paper 2008-01-1378,* 2008.

[18] V. Golovitchev and J. Yang, "Construction of combustion models for rapeseed methyl ester bio-diesel fuel for internal combustion engine applications," *Biotechnology advances,* vol. 27, no. 5, pp. 641-655, 2009.

[19] H. Ismail, H. Ng, S. Gan and T. Lucchini, "Computational study of biodiesel–diesel fuel blends on emission characteristics for a light-duty diesel engine

using OpenFOAM," *Applied Energy,* vol. 111, pp. 827-841, 2013.

[20] H. Ismail, H. Ng, X. Cheng, S. Gan, T. Lucchini and G. D'Errico, "Development of thermophysical and transport properties for the CFD simulations of in-cylinder biodiesel spray combustion," *Energy Fuels,* vol. 26, pp. 4857-4870, 2012.

[21] D. Montgomery and R. Reitz, "Effects of multiple injections and flexible control of boost and EGR on emissions and fuel consumption of a heavy-duty diesel engine," *SAE Technical paper 2001-01-0195,* 2001.

[22] A. Uludogan and D. Foster, "Modeling the effect of engine speed on the combustion process and emissions in a DI Diesel engine," *SAE Technical paper 962056,* 1996.

[23] B. Jayashankara and V. Ganesan, "Effect of fuel injection timing and intake pressure on the performance of a DI diesel engine- A parametric study using CFD," *Energy Conversion and Management,* vol. 51, pp. 1835-1848, 2010.

[24] X. Wang, Z. Huang, O. Kuti, W. Zhang and K. Nishida, "Experimental and analytical study on biodiesel and diesel spray characteristics under ultra-high injection pressure," *International Journal of Heat and Fluid Flow,* vol. 31, pp. 659-666, 2010.

[25] H. Kim, S. Park and C. Lee, "A study on the macroscopic spray behavior and atomization characteristics of biodiesel and dimethyl ether sprays under increased ambient pressure," *Fuel Processing Technology,* vol. 91, pp. 354-363, 2010.

[26] M. Tat, J. Van Gerpen, S. Soylu, M. Canakci, A. Monyem and S. Wormley, "The speed of sound and isentropic bulk modulus of biodiesel at 21C from atmospheric pressure to 35MPa," *Journal of the American Oil Chemists' Society,* vol. 77, pp. 285-289, 2000.

[27] F. Boudy and P. Seers, "Impact of physical properties of biodiesel on the injection process in a common-rail direct injection system," *Energy Conversion and Management,* vol. 50, pp. 2905-2912, 2009.

[28] J. Morón-Villarreyes, C. Soldi, A. de Amorim, M. Pizzolatti, P. de Mendonça and M. D'Oca, "Diesel/biodiesel proportion for by-compression ignition engines," *Fuel,* vol. 86, pp. 1977-1982, 2007.

[29] A. Demirbas, "Relationships derived from physical properties of vegetable oil and biodiesel fuels," *Fuel,* vol. 87, pp. 1743-1748, 2008.

[30] S. Takahashi, K. Wakimoto, N. Lida and D. Nikolic, "Effects of Aromatics Content and 90% Distillation Temperature of Diesel Fuels on Flame Temperature and Soot Formation," *SAE Technical paper 2001-01-1940,* 2001.

[31] J. Sun, J. Caton and T. Jacobs, "Oxides of nitrogen emissions from biodiesel-fuelled diesel engines," *Progress in Energy and Combustion Science,* vol. 36, pp. 677-695, 2010.

[32] A. Senatore, M. Cardone, V. Rocco and M. Prati, "A comparative analysis of combustion process in DI diesel engine fueled with biodiesel nd diesel fuel," *SAE Technical paper 2000-01-0691,* 2000.

[33] S. Hong, M. Wooldridge and D. Assanis, "Modeling of chemical and mixing effects on methane autoignition under direct-injection, stratefied charged conditions," *Proceedings of the combustion institute,* pp. 711-718, 2002.

[34] M. Gumus, "A comprehensive experimental investigation of combustion and heat release characteristics of a biodiesel (hazelnut kernel oil methyl ester) fueled direcct injection compression igntion engine," *Fuel,* vol. 89, pp. 2802-2814, 2010.

[35] M. Zheng, M. Mulenga, G. Reader, M. Wang, D. Ting and J. Tjong, "Biodiesel engine performance and emissions in low temperature combustion," *Fuel,* vol. 87, pp. 714-722, 2008.

[36] R. Radu, C. Petru, R. Edward and M. Gheorghe, "Fueling an DI agricultural diesel engine with waste oil biodiesel: Effects over injection, combustion and engine characteristics," *Energy and Conversion and Management,* vol. 50, pp. 2158-2166, 2009.

[37] J. Würmel, E. Silke, H. Curran, M. Ó Conaire and J. Simmie, "The effect of diluent gases on ignition dely times in the shock tube and in the rapid compression machine," *Combustion and flame,* vol. 151, pp. 289-302, 2007.

[38] U. Pfahl, K. Fieweger and G. Adomeit, "Self-ignition of diesel-relevant hydrocarbon-air mixtures under engine conditions," in *Symposium (International) on Combustion*, 1996.

[39] G. Mittal, M. Raju and C. Sung, "CFD modeling of two-stage ignition in a rapid compression machine: Assessment of zero-dimensional approach," *Combustion and flame,* vol. 157, pp. 1316-1324, 2010.

[40] C. Espey and J. Dec, "The effect of TDC temperature and density on the liquid-phase fuel penetration in a DI diesel engine," *SAE Technical paper 952456,* 1995.

[41] R. Payri, F. Salvador, J. Gimeno and L. Zapata, "Diesel nozzle geometry influence on spray liquid-phase fuel penetration in evaporative conditions," *Fuel,* vol. 87, pp. 1165-1176, 2008.

[42] H. Suh, S. Park and C. Lee, "Effect of piezo-driven injection system on the macroscopic and microscopic atomization characteristics of diesel fuel spray," *Fuel,* vol. 86, pp. 2833-2845, 2007.

[43] S. Moon, Y. Matsumoto, K. Nishida and J. Gao, "Gas entrainment characteristics of diesel spray injected by a group-hole nozzle," *Fuel,* vol. 89, pp. 3287-3299, 2010.

[44] S. Martinez-Martinez, F. Sanchez-Cruz, J. Riesco-Avila, A. Gallegos-Muñoz and S. Aceves, "Liquid penetration length in direct diesel fuel injection," *Applied Thermal Engineering,* vol. 28, pp. 1756-1762, 2008.

[45] S. Sazhin, C. Crua, D. Kennaird and M. Heikal, "The initial stage of fuel spray penetration," *Fuel,* vol. 82, pp. 875-885, 2003.

[46] C. Lee and S. Park, "An experimental and numerical study on fuel atomization characteristics of high-pressure diesel injection sprays," *Fuel,* Vols. 2417-2423, p. 81, 2002.

[47] S. Singh, R. Reitz and M. Musculus, "Comparison of the characteristic time (CTC), repesentative interactive flamelet (RIF), and direct integration with detailed chemistry combustion models against optical diagnostic data for multi-mode combustion in a heavy-duty DI diesel engine," *SAE Technical paper 2006-01-0055,* 2006.

[48] Q. Zheng, H. Zhang and D. Zhang, "A computational study of combustion in compression ignition natural gas engine with separated chamber," *Fuel,* vol. 84, pp. 1515-1523, 2005.

[49] A. Patel, S. Kong and R. Reitz, "Development and validation of a reduced reaction mechanism for HCCI engine simulations," *SAE Technical paper 2004-01-0558,* 2004.

[50] B. Zhong and J. Xi, "Reduced kinetic mechanism of n-heptane oxidation in modeling polycyclic aromatic hydrocarbon formation in opposed-flow diffusion flames," *Frontiers of Energy and Power Engineering in China,* vol. 2, pp. 326-332, 2008.

[51] ANSYS® Academic Research, Release 14.0, Fluent's User Guide.

[52] CHEMKIN-CFD overview (2009), CHEMKIN-CFD Q&A.

[53] S. Hong, D. Assanis, M. Wooldridge, H. Im, E. Kurtz and H. Pitsch, "Modeling of Diesel combustion and NO emissions based on a modified Eddy dissipation concept," *SAE SP,* pp. 59-72, 2004.

[54] M. Yahyaoui, N. Djebaïli-Chaumeix, P. Dagaut, C. Paillard and S. Gail, "Experimental and modelling study of gasoline surrogate mixtures oxidation in jet stirred reactor and shock tube," *Proceedings of the combustion institute,* vol. 31, pp. 385-391, 2007.

[55] C. Naik, W. Pitz, M. Sjöberg, J. Dec, J. Orme, H. Curran, J. Simmie and C. Westbrook, "Detailed chemical kinetic modeling of surrogate fuels for gasoline and application to an HCCI engine," in *2005 Joint Meeting of the US Sections of The Combustion Institute*, 2005.

[56] A. Saylam, M. Ribaucour, W. Pitz and R. Minetti, "Reduction of large detailed chemical kinetic mechanisms for autoignition using joint analyses of reaction rates and sensitivities," *International Journal of Chemicl Kinetics,* vol. 39, pp. 181-196, 2007.

[57] G. Vanhove, G. Petit and R. Minetti, "Experimental study of the kinetic interactions in the low-temperature autoignition of hydrocarbon binary mixtures and a surrogate fuel," *Combustion and flame,* vol. 145, pp. 521-532, 2006.

[58] J. Andrae, P. Björnbom, R. Cracknell and G. Kalghatgi, "Autoignition of toluene reference fuels at high pressures modeled with detailed chemical kinetics," *Combustion and flame,* vol. 149, pp. 2-24, 2007.

[59] F. Maroteaux and L. Noel, "Development of a reduced n-heptane oxidation mechanism for HCCI combustion modeling," *Combustion and flame,* vol. 146, pp. 246-267, 2006.

[60] T. Lu and C. Law, "A directed relation graph method for mechanism reduction," *Proceedings of the combustion institute,* vol. 30, pp. 1333-1341, 2005.

[61] T. Lu and C. Law, "On the applicability of directed relation graphs to the reduction of reaction mechanisms," *Combustion and flame,* vol. 146, pp. 472-483, 2006.

[62] T. Lu, P. Max, Z. Luo, S. Sarathy, W. Pitz, S. Som and D. Longman, "Directed relation graph with expert knowledge for skeletal mechanism reduction," in *7th US National Combustion Meeting*, 2011.

[63] L. Hildingsson, B. Johansson, G. Kalghatgi and A. Harrison, "Some effects of fuel autoignition quality and volatility in premixed compression ignition engines," *SAE Int. J. Engines,* vol. 3, pp. 440-460, 2010.

[64] D. Assanis, Z. Filipi, S. Fiveland and M. Syrimis, "A methodology for cycle-by-cycle transient heat release analaysis in a turbocharged direct injection diesel engine," *SAE Technical paper 2000-01-1185,* 2000.

[65] H. Curran, P. Gaffuri, W. Pitz and C. Westbrook, "A comprehensive modelling study of n-heptane oxidation," *Combust. Flame,* vol. 114, pp. 149-177, 1998.

[66] H. Shen, J. Vanderover and M. Oehlschlaeger, "A shock tube study of auto-ignition of toluene/air mixtures at high pressures," *Proceedings of the Combustion Institute,* vol. 32, pp. 165-172, 2009.

[67] D. Davidson, B. Gauthier and R. Hanson, "Shock tube ignition measurements of iso-octane/air and toluene/air at high pressures," *Proc. Combust. Inst.,* vol. 30, pp. 1175-1182, 2005.

[68] R. Seiser, H. Pitsch, K. Seshadri, W. Pitz and H. Curran, "Extinction and autoignition of n-heptane in counterflow configuration," *Proceedings of the Combustion Institute,* vol. 28, no. 2, pp. 2029-2037, 2000.

[69] G. Mittal and C. Sung, "Autoignition of toluene and benzene at elevated pressures in a rapid compression machine," *Combustion and Flame,* pp. 355-

368, 2007.

[70] D. Haylett, P. Lappas, D. Davidson and R. Hanson, "Application of an aerosol shock tube to the measurement of diesel ignition delay times," *Proceedings of the combustion institute,* vol. 32, pp. 477-484, 2009.

[71] N. Arai, G. Higuchi and H. Hiroyasu, "Ignition delay of diesel fuel and compound fuels," *Trans. JSME,* vol. 1345, pp. 50-453, 1984.

[72] F. Stringer, A. Clarke and J. Clarke, "The spontaneous ignition of hydrocarbon fuels in a flowing system," in *Proceedings of the Institution of Mechanical Engineers*, 1969.

[73] N. Marinov, "A detailed chemical kinetic model for high temperature ethanol oxidation," *Shock,* vol. 3, p. 2, 1999.

[74] J. Farrell, N. Cernansky, F. Dryer, C. Law, D. Friend, C. Hergart, R. McDavid, A. Patel, C. Mueller and H. Pitsch, "Development of an Experimental Database and Kinetic Models for Surrogate Diesel Fuels," *SAE Technical paper 2007-01-0201,* 2007.

[75] T. Gautam, "Auto-ignition Quality of Practical Fuels and Implications for Fuel Requirements of Future SI and HCCI Engines," *SAE Technical paper 2005-01-0239,* 2005.

[76] J. Michael, D. Joshua and L. Robert, "Conpendium of Experimental Cetane Number Data, NREL/SR-540-36805," 2004.

[77] G. Hobson, Modern Petroleum Technology 5th Edition Part II, Wiley, 1984, p. 786.

[78] C. Satterfield, Heterogeneous Catalysis in Practice, Wiley, 1980, p. 241.

[79] H. Hiroyasu, "Diesel engine combustion and its modeling," in *Proceedings of 1st International Symposium on Diagnostics and Modeling of Combustion in internal Combustion Engines*, Tokyo, Japan, 1985.

[80] H. Curran, P. Gaffuri, W. Pitz and C. Westbrook, "A comprehensive modeling study of iso-octane oxidation," *Combustion and flame,* vol. 129, pp. 253-280, 2002.

[81] K. Fieweger, R. Blumenthal and G. Adomeit, "Self-ignition of SI engine

model fuels: a shock tube investigation at high pressure," *Combustion and Flame,* vol. 109, pp. 599-619, 1997.

[82] R. Minetti, M. Carlier, M. Ribaucour, E. Therssen and L. Sochet, "Comparison of oxidation and autoignition of the two primary reference fuels by rapid compression," in *Symposium (International) on Combustion*, 1996.

[83] J. Griffiths, P. Halford-Maw and D. Rose, "Fundamental features of hydrocarbon autoignition in a rapid compression machine," *Combustion and Flame,* vol. 95, pp. 291-306, 1993.

[84] G. D'Errico, D. Ettorre and T. Lucchini, "Simplified and detailed chemistry modeling of constant-volume diesel combustion experiments," *SAE Technical paper 2008-01-0954,* 2008.

[85] S. Kook, C. Bae, P. Miles, D. Choi and L. Pickett, "The influence of charge dilution and injection timing on low-temperature diesel combustion and emissions," *SAE Technical paper 2005-01-3837,* 2005.

[86] J. Dec, "A conceptual model of DI diesel combustion based on laser sheet imaging," *SAE Technical paper 970873,* 1997.

[87] J. Andrae, T. Brinck and G. Kalghatgi, "HCCI experiments with toluene reference fuels modelled by a semidetailed chemical kinetic model," *Combust. Flame,* pp. 696-712, 2008.

# APPENDIX A

**MATLAB codes**

#Step-1 Evaluate stoichiometric coefficients, $V_{A,i}$ from a list of reactions

```
%scan species
fid = fopen('species_all.txt');
file_lines = textscan(fid,'%s','Delimiter','\n','BufSize',100000);
single_line = file_lines{1};

%scan reactions
fid1 = fopen('mec.inp');
file_lines1 = textscan(fid1,'%s','Delimiter','\n','BufSize',100000);
single_line1 = file_lines1{1};

no_species=658;
num_reactions=2827;
firstpart='(?<![\w])\d?';
secondpart='(?![\w])';
species_regexp=cell(no_species,1);
species_in_reaction=zeros(num_reactions,no_species);

for i=1:no_species
species_regexp{i}={firstpart, char(single_line(i)), secondpart};
species_regexp1=cell2mat(species_regexp{i});

for k=1:num_reactions
if(regexp(char(reactions{k}),species_regexp1)>0)

if(regexp(char(reactions{k}),species_regexp1)<regexp(char(reactions{k}),'
='))
species_in_reaction(k,i)=1;
end

if(regexp(char(reactions{k}),species_regexp1)>regexp(char(reactions{k}),'
='))
species_in_reaction(k,i)=10;
end
end

end
```

```
end
%Amend the confusion between ch2 and ch2(s)

for k=1:num_reactions
a=regexp(char(reactions{k}),'ch2(s');
b=regexp(char(reactions{k}),'ch2');

if a>0
species_in_reaction(k,29)=1;
species_in_reaction(k,26)=0;

end
c=size(b);
if c(1,2)>1

species_in_reaction(k,26)=1;
end

end

%Create an array to gather stoichiometric coefficients required for
DRG's
%input
firstpart1='(?<![\w])\d?2'; % add \s if there is space after stoic 2
species_regexp2=cell(no_species,1);
stoic_coeff=zeros(num_reactions,no_species);

for i=1:no_species
species_regexp2{i}={firstpart1, char(single_line(i)),secondpart};
species_regexp3=cell2mat(species_regexp2{i});
for k=1:num_reactions
if(regexp(char(reactions{k}),species_regexp3)>0)
 stoic_coeff(k,i)=1;
end

end
end

stoic_coeff1=stoic_coeff+species_in_reaction;
```

#Step-2 Graph Construction

```
%Run matlab code "Create_array_of_stoic_coeff_for_DRG

stoic_coeff2=stoic_coeff1;
%Export rop_gv from excel "list of rop"
```

```
%Identify reactions consist of targeted species for DRG (begin with OH or species
6)
%Calculate coupling coefficient of DRG
species_to_keep=zeros(1,no_species);
matrix_Rab=zeros(no_species,no_species);
coupling_coeff_matrix=zeros(no_species,no_species);
for s=1:no_species
   count=1;
for i=1:no_species
sum_rop_A=0;
sum_rop_AB=0;

   if i==s
      continue;
   end
   for k=1:num_reactions
      if((stoic_coeff2(k,s)==1)||(stoic_coeff2(k,s)==10)||(stoic_coeff2(k,s)==2))
         sum_rop_A=sum_rop_A+abs(rop_gv(k)*1);
      end
      if(stoic_coeff2(k,s)==11)
         sum_rop_A=sum_rop_A+abs(rop_gv(k)*2);

      end
      if((stoic_coeff2(k,s)>0)&&(stoic_coeff2(k,i)>0))
         if((stoic_coeff2(k,i)==1)||(stoic_coeff2(k,i)==10)||(stoic_coeff2(k,i)==2))
         sum_rop_AB=sum_rop_AB+abs(rop_gv(k)*1);

         end
         if(stoic_coeff2(k,i)==11)
         sum_rop_AB=sum_rop_AB+abs(rop_gv(k)*2);
         end
      end
   end
   Rab=sum_rop_AB/sum_rop_A;
   matrix_Rab(count,s)=Rab;
   if(Rab>0.3)
      species_to_keep(1,i)=1;
      coupling_coeff_matrix(count,s)=i;
      count=count+1;
   end
end

end
```

#Step-3 Graph Compilation

```
k=5;    %species number for OH
k_1=5;  %same as k
count=1;
count1=1;
num_species=1;
num_species1=0;
species_involved=zeros(no_species,1);
%species_involved(1,1)=1;
species_involved(7,1)=1;    %species that must be kept N2
species_involved(6,1)=1;    %H2O
species_involved(10,1)=1;   %Ar
species_involved(12,1)=1;   %CO2
species_involved(81,1)=1;   %HE

reaction_path=zeros(no_species,no_species);



while num_species>num_species1
      num_species1=num_species;
      for z=1:no_species
          if z>1
             k=z;
          end
          if z==5 %species number of OH
             continue;
          end
          if(species_involved(z)==1)
          for i=1:no_species
             for m=1:no_species
             if(coupling_coeff_matrix(i,k)==m)
                species_involved(m)=1;
                if k_1-k>0 || k_1-k<0
                   count=count+1;
                   count1=1;
                end
                reaction_path(count1,count)=m;
                count1=count1+1;
                k_1=k;
             end
             end
          end
          end
      end
      num_species=sum(species_involved);
```

```
        k=1;
end
%Create arrays of species to be kept and removed (above DRG threshold).
counter=1;
counter1=1;
species_to_keep1=cell(no_species,1);
species_to_remove1=cell(no_species,1);
for i=1:no_species
   if(species_involved(i)==1)
      species_to_keep1(counter)=single_line(i);
      counter=counter+1;
   else
      species_to_remove1(counter1)=single_line(i);
      counter1=counter1+1;
   end
end
```

#Step-4 Create skeletal mechanism

```
% Open the file with fopen function
fid = fopen('mec.inp');

% didnt work, delimited by whitespace
%output = textscan(fid,'%s')

% reads in the text file, one line per row in the output data
file_lines = textscan(fid,'%s','Delimiter','\n','BufSize',100000);

% move text into one layer deep cell structure
single_line = file_lines{1};
single_line0=single_line;

% start line
start_line=33;%1st line of reaction.
end_line=412;  %Where the End is located.

start_line_species=17; %First line of species
end_line_species=28; %Last line of species

equals_present = zeros(end_line - start_line,1);

% pull out a line at a time, search for = on that line.
for i=start_line:end_line
  if(cell2mat(regexp(single_line(i),'=')) > 0)
     equals_present(i+1-start_line) = 1;
  end
```

```
end
%Input of no. of redundant species.
firstpart='(?<![\w])\d?\<';
secondpart='\>(?![\w])';
secondpart1='[-]\>(?![\w])';
I = input ('\n Enter number of species to be eliminated: \n\n');
equals_present1 = ones(end_line - start_line,1);
fid1 = fopen('unwanted species.txt');
file_lines1 = textscan(fid1,'%s','Delimiter','\n','BufSize',100000);
single_line1 = file_lines1{1};
%sort single_line1 or list of unwanted species so that species with '-'
%always comes after species without it.
counter3=1;
single_line4=cell(I,1);
for i=1:I
   if(regexp(char(single_line1(i)),'[-]')>0)
      single_line4(counter3)=single_line1(i);
      counter3=counter3+1;

   end
end

%Isolate species with (S) from list of species to be eliminated
record_s_species=zeros(I,1);
for j=1:I
   if(regexp(char(single_line1(j)),'(S')>0)
      record_s_species(j)=1;
   end
end
single_line2=cell(I,1);
single_line3=cell(I,1);
counter1=1;
counter2=1;
for j=1:I
   if record_s_species(j)==0
      single_line2(counter1)=single_line1(j);
      counter1=counter1+1;
   end
   if record_s_species(j)==1
      single_line3(counter2)=single_line1(j);
      counter2=counter2+1;
   end
end
%Change CH2(S) to CH2(S to be used in regular expression search
for j=1:counter2-1
```

```
    single_line3{j}=regexprep(single_line3{j},')','');
end

%Input of redundant species and convert species names to the form of
%regular expressions.
counter=0;
for j=1:counter1-1
%species_to_be_eliminated = input ('\n Enter species to be eliminated (uppercase:
\n\n','s');
species_to_be_eliminated = single_line2{j};
Regexp_species={firstpart, species_to_be_eliminated, secondpart};
species_regexp_included=cell2mat(Regexp_species);
species_regexp_included2=cell2mat({species_to_be_eliminated, '[-]'});

    %Generate a matrix of zeros and ones- zeros indicate the reactions which
    %comprised of unwanted species.
    for k=start_line:end_line-1
        if(cell2mat(regexp(single_line(k),species_regexp_included)) > 0)
            equals_present1(k+1-start_line) = 0;
            claim1=char(single_line{k});
            new_claim1=regexprep(claim1,species_regexp_included,'#');
            single_line0{k}=new_claim1;
           counter=counter+1;
           %Eliminate similarity matches such as IC5H11CO and IC5H11CO-B
           re_sub=regexp(char(single_line{k}),species_regexp_included2);
           re_sub1=size(re_sub);
           if re_sub>0
              if re_sub1(1,2)==1
              equals_present1(k+1-start_line)=1;
              single_line0{k}=claim1;
              end
           end
        end
        %Eliminate confusion between species such as CH2 and CH2(S).
        %CH2(S) will no longer be mistaken as CH2.
        if regexp(char(single_line0{k}),'#(S')>0
            equals_present1(k+1-start_line)=1;
            if regexp(char(single_line0{k}),'(?<![\w])\d?#(?![\w])')>0
                equals_present1(k+1-start_line)=0;
            end
        end
        single_line0{k}=single_line{k};
    end

%    Eliminate unwanted species in list of species of mechanism
```

```
    for q=start_line_species:end_line_species
      if(cell2mat(regexp(single_line(q),species_regexp_included)) > 0)
          claim=char(single_line{q});
          new_claim=regexprep(claim,species_regexp_included,'#');
          single_line{q}=new_claim;
      end
      re_sub2=regexp(char(single_line0{q}),species_regexp_included2);
      re_sub3=size(re_sub2);
       if re_sub2>0
            if re_sub3(1,2)==1
            single_line{q}=claim;
            end
       end

       if regexp(char(single_line{q}),'#(S')>0
          single_line{q}=claim;
       end
       if regexp(char(single_line{q}),'#')>0
          single_line{q}=regexprep(single_line{q},'#','');
       end

    end


end
%Eliminate reactions with species (S)

for j=1:counter2-1
    Regexp_species1={firstpart, single_line3{j}, secondpart};
    species_regexp_included1=cell2mat(Regexp_species1);
    for k=start_line:end_line-1
        if(cell2mat(regexp(single_line(k),species_regexp_included1)) > 0)
          equals_present1(k+1-start_line) = 0;

        end

    end

    for q=start_line_species:end_line_species
      if(cell2mat(regexp(single_line(q),species_regexp_included1)) > 0)
          claim=char(single_line{q});
          new_claim=regexprep(claim,species_regexp_included1,'#');
          single_line{q}=new_claim;
      end
      if regexp(char(single_line{q}),'#)')>0
          single_line{q}=regexprep(single_line{q},'#)','');
```

```
      end

    end

end

%Make sure reactions with species (-) are eliminated
for j=1:counter3-1
    species_regexp_included3=cell2mat({firstpart, single_line4{j}, secondpart});
    for k=start_line:end_line-1
        if regexp(single_line{k},species_regexp_included3)>0
            equals_present1(k+1-start_line)=0;
        end
    end
    for q=start_line_species:end_line_species
        if(cell2mat(regexp(single_line(q),species_regexp_included3)) > 0)
          claim=char(single_line{q});
          new_claim=regexprep(claim,species_regexp_included3,'');
          single_line{q}=new_claim;
        end
    end

end


unwanted_reactions=cell(counter,1);
B=1;
for A=1:end_line-start_line
    if(equals_present1(A))==0
        unwanted_reactions(B)=single_line(A+start_line-1);
        B=B+1;
    end
end

%Generate matrix of zeros and ones which indentify wanted species.
equals_present2 = zeros(end_line - start_line,1);
for L=start_line:end_line-1
    if((equals_present(L+1-start_line)>0)&&(equals_present1(L+1-start_line)>0))

        equals_present2(L+1-start_line)=1;

    end
end


equals_present3=zeros(end_line - start_line+1,1);
```

```
for M=start_line:end_line-1
   if((equals_present3(M+1-start_line)==0)&&(equals_present(M+1-
start_line)==1)&&(equals_present2(M+1-start_line)==1))

      equals_present3(M+2-start_line)=1;
   else
      if((equals_present3(M+1-start_line)==1)&&(equals_present(M+1-
start_line)==0)&&(equals_present2(M+1-start_line)==0))

      equals_present3(M+2-start_line)=1;
      else
         if((equals_present3(M+1-start_line)==1)&&(equals_present(M+1-
start_line)==1)&&(equals_present2(M+1-start_line)==1))
            equals_present3(M+2-start_line)=1;
         else

         end

      end
  end



end


for N=1:end_line-start_line-1
   equals_present3(N)=equals_present3(N+1);

end

single_line_final=cell(end_line,1);
for O=1:start_line-1
   single_line_final(O)=single_line(O);
end

for O=start_line:end_line-1
   if (equals_present3(O-start_line+1)==1)
      single_line_final(O)=single_line(O);
   else
       single_line_final(O)={''};
   end

end
single_line_final(end_line)=single_line(end_line);
```

```
fid = fopen('mec_modified.inp','wt');

for Z=1:end_line
fprintf(fid,'%s\n',char(single_line_final(Z)));
 end
```

# APPENDIX B

**Step-by-step guide for semi-automatic reduction via the MATLAB codes**

#Step-1 Evaluate stoichiometric coefficients, $V_{A,i}$ from a list of reactions

1) Create a list of all species present in the mechanism with one species per row and name it species_all.txt.
2) Copy the Step-1 MATLAB code and place it into the same folder as the list of all species and the detailed kinetic mechanism which must be renamed to mec.inp.
3) Edit the number of species and the number of reactions in the MATLAB code which are denoted as "no_species" and "num_reactions", accordingly.
4) Execute the MATLAB code.

#Step-2 Graph Construction

5) Import a list of ROPs as an array variable into MATLAB.
6) Copy the Step-2 MATLAB code and place it into the folder.
7) Set the DRG threshold in the code which the normalised contribution (Rab) must be more than it.
8) Execute the MATLAB code.

#Step-3 Graph Compilation

9) Copy the Step-3 MATLAB code and place it into the folder.
10) Run the MATLAB code and retrieve a list of retained species and a list of eliminated species.

#Step-4 Create skeletal mechanism

11) Export the list of eliminated species as a text file to the same folder and name it unwanted species.txt.
12) Create an empty mechanism file with the name mec_modified.inp and place it into the folder.

13) Copy the Step-4 MATLAB code and place it into the folder.
14) Edit the variables which define the location of species and reactions comprised in the detailed chemical kinetic mechanism. The "start_line" and the "end_line" define the first line of the reaction and the line when "End" is located in the mechanism. The "start_line_species" and the "end_line_species" define the first line of species and the last line of species, accordingly.
15) Execute the MATLAB code and generate a skeletal mechanism written into the file mec_modified.inp.

# APPENDIX C

```
% Open the file with fopen function
fid = fopen('mec.inp');

% reads in the text file, one line per row in the output data
file_lines = textscan(fid,'%s','Delimiter','\n','BufSize',100000);

% move text into one layer deep cell structure
single_line = file_lines{1};


% start line
start_line=37;%1st line of reaction.
end_line=369;  %Where the End is located.

equals_present = zeros(end_line - start_line,1);

% pull out a line at a time, search for = on that line.
for i=start_line:end_line
 if(cell2mat(regexp(single_line(i),'=')) > 0)
    equals_present(i+1-start_line) = 1;
 end

end
%Input of no. of wanted species.
firstpart='(?<![\w])\d?\<';
secondpart='\>(?![\w])';
secondpart1='[-]\>(?![\w])';
I = input ('\n Enter number of species to be captured: \n\n');
equals_present1 = zeros(end_line - start_line,1);
fid1 = fopen('wanted species.txt');
file_lines1 = textscan(fid1,'%s','Delimiter','\n','BufSize',100000);
single_line1 = file_lines1{1};
%Input of no. of unwanted species to be substracted.
K = input ('\n Enter number of species to be substracted: \n\n');
fid2 = fopen('substracted species.txt');
file_lines2 = textscan(fid2,'%s','Delimiter','\n','BufSize',100000);
single_line2 = file_lines2{1};
%Input of redundant species and convert species names to the form of
%regular expressions.


for j=1:I

species_to_be_captured = single_line1{j};
Regexp_species={firstpart, species_to_be_captured, secondpart};
species_regexp_included=cell2mat(Regexp_species);
```

```
    %Generate a matrix of zeros and ones- zeros indicate the reactions which
    %comprised of wanted species.
    for k=start_line:end_line-1
        if(cell2mat(regexp(single_line(k),species_regexp_included)) > 0)
            equals_present1(k+1-start_line) = 1;




        end

    end
end

for j=1:K

species_to_be_substracted = single_line2{j};
Regexp_species1={firstpart, species_to_be_substracted, secondpart};
species_regexp_included2=cell2mat(Regexp_species1);

    %Generate a matrix of zeros and ones- zeros indicate the reactions which
    %comprised of wanted species.
    for k=start_line:end_line-1
        if(cell2mat(regexp(single_line(k),species_regexp_included2)) > 0)
            equals_present1(k+1-start_line) = 0;




        end

    end
end


%Generate matrix of zeros and ones which identify wanted species.
equals_present2 = zeros(end_line - start_line,1);
for L=start_line:end_line-1
    if((equals_present(L+1-start_line)>0)&&(equals_present1(L+1-start_line)>0))

        equals_present2(L+1-start_line)=1;

    end
end


equals_present3=zeros(end_line - start_line+1,1);

for M=start_line:end_line-1
    if((equals_present3(M+1-start_line)==0)&&(equals_present(M+1-
start_line)==1)&&(equals_present2(M+1-start_line)==1))

        equals_present3(M+2-start_line)=1;
    else
```

```
      if((equals_present3(M+1-start_line)==1)&&(equals_present(M+1-
start_line)==0)&&(equals_present2(M+1-start_line)==0))

      equals_present3(M+2-start_line)=1;
      else
         if((equals_present3(M+1-start_line)==1)&&(equals_present(M+1-
start_line)==1)&&(equals_present2(M+1-start_line)==1))
            equals_present3(M+2-start_line)=1;
         else

         end

      end
  end



end

for N=1:end_line-start_line-1
   equals_present3(N)=equals_present3(N+1);

end

single_line_common=cell(end_line,1);
counter=1;

for O=start_line:end_line-1
   if (equals_present3(O-start_line+1)==1)
      single_line_common(counter)=single_line(O);
      counter=counter+1;
   end

end
single_line_common(end_line)=single_line(end_line);
fid = fopen('common reactions.inp','wt');

for Z=1:counter-1
fprintf(fid,'%s\n',char(single_line_common(Z)));
end

single_line_unique=cell(end_line,1);
counter=1;

for O=start_line:end_line-1
   if (equals_present3(O-start_line+1)==0)
      single_line_unique(counter)=single_line(O);
      counter=counter+1;
   end

end
single_line_unique(end_line)=single_line(end_line);
fid = fopen('unique reactions.inp','wt');
```

```
for Z=1:counter-1
fprintf(fid,'%s\n',char(single_line_unique(Z)));
end
```

# APPENDIX D

```
!73species diesel-gasoline mechanism
ELEMENTS
C H N O

END
SPECIES
G50 G30 G70 Diesel
!common species
H       H2    O    O2    OH
H2O     N2    HO2  H2O2  CO
CO2     CH2O  HCO  CH3O  CH3O2H
CH3O2   CH4   CH3  C2H6  CH2CO
CH3COCH2  C3H6

!Unique Nheptane species
C2H5       C2H4       C2H3        CH3CHO
C2H5CHO    C4H7OOH1-4  C4H7O1-4   PC4H9
C2H5COCH2  NC3H7CHO   C5H10-1    C5H9O1-3    NC3H7COCH2
NC7H16     C7H15-2    C7H15-3    C7H15O2-2   C7H15O2-3
C7H14OOH2-4  C7H14OOH3-5  C7H14OOH4-2  C7H14OOH2-4O2  C7H14OOH3-
5O2
NC7KET24   NC7KET35   NC7KET42

!Unique Isooctane species
IC3H7      C3H5-T     IC4H9       IC4H8
IC4H7      IC4H7O     IC3H7CHO    TC3H6CHO    IC4H7OH
YC7H15     IC8H18     AC8H17      CC8H17      DC8H17
AC8H17O2   AC8H17O    DC8H17O     AC8H16OOH-B  IC8ETERAB
AC8H16OOH-BO2  IC8KETAB

END

REACTIONS

G10+0.5O2=>1.8NC7H16+0.2IC8H18+0.8CO+0.3H2+0.1O2 5.00E+10 0.0 21000
G20+0.5O2=>1.6NC7H16+0.4IC8H18+0.6CO+0.1H2+0.2O2 5.00E+10 0.0 21000
!G30+0.6O2=>1.4NC7H16+0.6IC8H18+0.4CO2+0.4H2O 5.00E+10 0.0 20800
!G30=>1.4NC7H16+0.6IC8H18+0.4C+0.8H 5.00E+10 0.0 20800
G30=>1.4NC7H16+0.6IC8H18+0.4CH4+0.1H2 5.00E+10 0.0 28000
!G50+0.5O2=>NC7H16+IC8H18+CO   5.00E+10 0.0 21000
!G50+0.5O2=>0.95NC7H16+0.95IC8H18+0.75CO+0.35H2+0.125O2   5.00E+10 0.0
21000
G50=>1.1NC7H16+1.1IC8H18+0.5CH4+0.3H2 5.00E+10 0.0 28000
```

```
!Diesel=>2NC7H16                5.00E+09 0.5 25300
!Diesel+1.5O2=>2NC7H16+CO2+H2O          5.00E+10 0.0 20000
!Diesel+O2=>2NC7H16+2H2O 5.00E+10 0.0 20000
!Diesel+0.5O2=>2NC7H16+CO               5.00E+10 0.0 23000
Diesel=>1.9NC7H16+0.7CH4+0.4H2 5.00E+10 0.0 28000
G70=>0.6NC7H16+1.4IC8H18+0.6CH4+0.4H2 5.00E+10 0.0 28000
!*****************************************
!**********Common reactions***************
!*****************************************
H+O2=>O+OH 3.547E+15 -0.406 1.660E+04                   !PFx 3.547E+15
O+OH=>H+O2 1.027E+13 -0.015 -1.330E+02
O+H2=>H+OH 5.080E+04 2.670 6.292E+03
H+OH=>O+H2 2.637E+04 2.651 4.880E+03
OH+H2=>H+H2O 2.160E+08 1.510 3.430E+03
H+H2O=>OH+H2 2.290E+09 1.404 1.832E+04
O+H2O=>OH+OH 2.970E+06 2.020 1.340E+04
OH+OH=>O+H2O 1.454E+05 2.107 -2.904E+03
H2+M=>H+H+M 4.577E+19 -1.400 1.044E+05
H2/2.5/ H2O/12/ CO/1.9/ CO2/3.8/
H+H+M=>H2+M 1.145E+20 -1.676 8.200E+02
H2/2.5/ H2O/12/ CO/1.9/ CO2/3.8/
O2+M=>O+O+M 4.420E+17 -0.634 1.189E+05
H2/2.5/ H2O/12/ CO/1.9/ CO2/3.8/ CH4/2/ C2H6/3/
O+O+M=>O2+M 6.165E+15 -0.500 0.000E+00
H2/2.5/ H2O/12/ CO/1.9/ CO2/3.8/ CH4/2/ C2H6/3/
OH+M=>O+H+M 9.780E+17 -0.743 1.021E+05
H2/2.5/ H2O/12/ CO/1.5/ CO2/2/ CH4/2/ C2H6/3/
O+H+M=>OH+M 4.714E+18 -1.000 0.000E+00
H2/2.5/ H2O/12/ CO/1.5/ CO2/2/ CH4/2/ C2H6/3/
H2O+M=>H+OH+M 1.907E+23 -1.830 1.185E+05
H2/.73/ H2O/12/ CH4/2/ C2H6/3/
H+OH+M=>H2O+M 4.500E+22 -2.000 0.000E+00
H2/.73/ H2O/12/ CH4/2/ C2H6/3/
H+O2(+M)<=>HO2(+M) 1.475E+12 0.600 0.000E+00
LOW / 3.4820E+16 -4.1100E-01 -1.1150E+03 /
TROE / 5.0000E-01 1.0000E-30 1.0000E+30 1.0000E+10 / !Troe Fall-off reaction
H2/1.3/ H2O/14/ CO/1.9/ CO2/3.8/ CH4/2/ C2H6/3/
HO2+H=>H2+O2 1.660E+13 0.000 8.230E+02
H2+O2=>HO2+H 3.166E+12 0.348 5.551E+04
HO2+H=>OH+OH 7.079E+13 0.000 2.950E+02
OH+OH=>HO2+H 2.028E+10 0.720 3.684E+04
HO2+O=>OH+O2 3.250E+13 0.000 0.000E+00
OH+O2=>HO2+O 3.217E+12 0.329 5.328E+04
HO2+OH=>H2O+O2 1.973E+10 0.962 -3.284E+02
H2O+O2=>HO2+OH 3.989E+10 1.204 6.925E+04
H2O2+O2=>HO2+HO2 1.136E+16 -0.347 4.973E+04
DUP
HO2+HO2=>H2O2+O2 1.030E+14 0.000 1.104E+04
DUP
H2O2+O2=>HO2+HO2 2.141E+13 -0.347 3.728E+04
DUP
```

HO2+HO2=>H2O2+O2 1.940E+11 0.000 -1.409E+03
DUP
H2O2(+M)<=>OH+OH(+M) 2.951E+14 0.000 4.843E+04
LOW / 1.2020E+17 0.0000E+00 4.5500E+04 /
TROE / 5.0000E-01 1.0000E-30 1.0000E+30 1.0000E+10 / !Troe Fall-off reaction
H2/2.5/ H2O/12/ CO/1.9/ CO2/3.8/ CH4/2/ C2H6/3/
H2O2+H=>H2O+OH 2.410E+13 0.000 3.970E+03
H2O+OH=>H2O2+H 1.265E+08 1.310 7.141E+04
H2O2+H=>H2+HO2 2.150E+10 1.000 6.000E+03
H2+HO2=>H2O2+H 3.716E+07 1.695 2.200E+04
H2O2+O=>OH+HO2 9.550E+06 2.000 3.970E+03
OH+HO2=>H2O2+O 8.568E+03 2.676 1.856E+04
H2O2+OH=>H2O+HO2 2.000E+12 0.000 4.272E+02
DUP
H2O+HO2=>H2O2+OH 3.665E+10 0.589 3.132E+04
DUP
H2O2+OH=>H2O+HO2 1.700E+18 0.000 2.941E+04
DUP
H2O+HO2=>H2O2+OH 3.115E+16 0.589 6.030E+04
DUP
CO+O(+M)<=>CO2(+M) 1.800E+10 0.000 2.384E+03
LOW / 1.3500E+24 -2.7880E+00 4.1910E+03 / !Lindemann Fall-off reaction
H2/2/ O2/6/ H2O/6/ CO/1.5/ CO2/3.5/ CH4/2/ C2H6/3/
CO+O2=>CO2+O 1.050E+12 0.000 4.254E+04
CO2+O=>CO+O2 8.035E+15 -0.800 5.123E+04
CO+OH=>CO2+H 2.230E+05 1.890 -1.158E+03
CO2+H=>CO+OH 5.896E+11 0.699 2.426E+04
CO+HO2=>CO2+OH 3.010E+13 0.000 2.300E+04
CO2+OH=>CO+HO2 2.280E+16 -0.470 8.497E+04
HCO+M=>H+CO+M 4.750E+11 0.660 1.487E+04
H2/2/ H2O/12/ CO/1.5/ CO2/2/ CH4/2/ C2H6/3/
H+CO+M=>HCO+M 3.582E+10 1.041 -4.573E+02
H2/2/ H2O/12/ CO/1.5/ CO2/2/ CH4/2/ C2H6/3/
HCO+O2=>CO+HO2 7.580E+12 0.000 4.100E+02
CO+HO2=>HCO+O2 1.198E+12 0.309 3.395E+04
HCO+H=>CO+H2 7.340E+13 0.000 0.000E+00
CO+H2=>HCO+H 2.212E+12 0.656 8.823E+04
HCO+O=>CO+OH 3.020E+13 0.000 0.000E+00
CO+OH=>HCO+O 4.725E+11 0.638 8.682E+04
HCO+O=>CO2+H 3.000E+13 0.000 0.000E+00
CO2+H=>HCO+O 1.241E+18 -0.553 1.122E+05
HCO+OH=>CO+H2O 1.020E+14 0.000 0.000E+00
CO+H2O=>HCO+OH 3.259E+13 0.551 1.031E+05
HCO+CH3=>CH4+CO 2.650E+13 0.000 0.000E+00
CH4+CO=>HCO+CH3 7.286E+14 0.211 8.977E+04
HCO+HO2=>CH2O+O2 2.499E+14 -0.061 1.392E+04
CH2O+O2=>HCO+HO2 8.070E+15 0.000 5.342E+04
HCO+HO2=>CO2+H+OH 3.000E+13 0.000 0.000E+00
CO2+H+OH=>HCO+HO2 0.000E+00 0.000 0.000E+00
CH2O+CO=>HCO+HCO 9.186E+13 0.370 7.304E+04
HCO+HCO=>CH2O+CO 1.800E+13 0.000 0.000E+00

HCO+HCO=>H2+CO+CO 3.000E+12 0.000 0.000E+00
H2+CO+CO=>HCO+HCO 0.000E+00 0.000 0.000E+00
HCO+H(+M)<=>CH2O(+M) 1.090E+12 0.480 -2.600E+02
LOW / 1.3500E+24 -2.5700E+00 1.4250E+03 /
TROE / 7.8240E-01 2.7100E+02 2.7550E+03 6.5700E+03 / !Troe Fall-off reaction
H2/2/ H2O/6/ CO/1.5/ CO2/2/ CH4/2/ C2H6/3/
CO+H2(+M)<=>CH2O(+M) 4.300E+07 1.500 7.960E+04
LOW / 5.0700E+27 -3.4200E+00 8.4348E+04 /
TROE / 9.3200E-01 1.9700E+02 1.5400E+03 1.0300E+04 / !Troe Fall-off reaction
H2/2/ H2O/6/ CO/1.5/ CO2/2/ CH4/2/ C2H6/3/
CH2O+OH=>HCO+H2O 7.820E+07 1.630 -1.055E+03
HCO+H2O=>CH2O+OH 4.896E+06 1.811 2.903E+04
CH2O+H=>HCO+H2 5.740E+07 1.900 2.740E+03
HCO+H2=>CH2O+H 3.390E+05 2.187 1.793E+04
CH2O+O=>HCO+OH 6.260E+09 1.150 2.260E+03
HCO+OH=>CH2O+O 1.919E+07 1.418 1.604E+04
CH2O+CH3=>HCO+CH4 3.830E+01 3.360 4.312E+03
HCO+CH4=>CH2O+CH3 2.063E+02 3.201 2.104E+04
CH2O+HO2=>HCO+H2O2 7.100E-03 4.517 6.580E+03
HCO+H2O2=>CH2O+HO2 2.426E-02 4.108 5.769E+03
CH3O(+M)<=>CH2O+H(+M) 6.800E+13 0.000 2.617E+04
LOW / 1.8670E+25 -3.0000E+00 2.4307E+04 /
TROE / 9.0000E-01 2.5000E+03 1.3000E+03 1.0000E+99 / !Troe Fall-off reaction
H2/2/ H2O/6/ CO/1.5/ CO2/2/ CH4/2/ C2H6/3/
CH3O+O2=>CH2O+HO2 4.380E-19 9.500 -5.501E+03
CH2O+HO2=>CH3O+O2 1.416E-20 9.816 2.108E+04
CH3O+CH3=>CH2O+CH4 1.200E+13 0.000 0.000E+00
CH2O+CH4=>CH3O+CH3 6.749E+13 0.218 8.281E+04
CH3O+H=>CH2O+H2 2.000E+13 0.000 0.000E+00
CH2O+H2=>CH3O+H 1.233E+11 0.664 8.127E+04
CH3O+HO2=>CH2O+H2O2 3.010E+11 0.000 0.000E+00
CH2O+H2O2=>CH3O+HO2 1.074E+12 -0.031 6.527E+04
CH3+H(+M)<=>CH4(+M) 1.270E+16 -0.600 3.830E+02
LOW / 2.4770E+33 -4.7600E+00 2.4440E+03 /
TROE / 7.8300E-01 7.4000E+01 2.9400E+03 6.9600E+03 / !Troe Fall-off reaction
H2/2/ H2O/6/ CO/1.5/ CO2/2/ CH4/2/ C2H6/3/
CH4+H=>CH3+H2 6.140E+05 2.500 9.587E+03
CH3+H2=>CH4+H 6.730E+02 2.946 8.047E+03
CH4+OH=>CH3+H2O 5.830E+04 2.600 2.190E+03
CH3+H2O=>CH4+OH 6.776E+02 2.940 1.554E+04
CH4+O=>CH3+OH 1.020E+09 1.500 8.600E+03
CH3+OH=>CH4+O 5.804E+05 1.927 5.648E+03
CH4+HO2=>CH3+H2O2 1.130E+01 3.740 2.101E+04
CH3+H2O2=>CH4+HO2 7.166E+00 3.491 3.468E+03
CH3+OH=>CH2O+H2 8.000E+09 0.500 -1.755E+03
CH2O+H2=>CH3+OH 1.066E+12 0.322 6.821E+04
CH3+OH=>CH3O+H 6.943E+07 1.343 1.120E+04
CH3O+H=>CH3+OH 1.500E+12 0.500 -1.100E+02
CH3+HO2=>CH3O+OH 1.000E+12 0.269 -6.875E+02
CH3O+OH=>CH3+HO2 6.190E+12 0.147 2.455E+04
CH3+HO2=>CH4+O2 1.160E+05 2.230 -3.022E+03

CH4+O2=>CH3+HO2 2.018E+07 2.132 5.321E+04
CH3+O=>CH2O+H 5.540E+13 0.050 -1.360E+02
CH2O+H=>CH3+O 3.830E+15 -0.147 6.841E+04
CH3+O2=>CH3O+O 7.546E+12 0.000 2.832E+04
CH3O+O=>CH3+O2 4.718E+14 -0.451 2.880E+02
CH3+O2=>CH2O+OH 2.641E+00 3.283 8.105E+03
CH2O+OH=>CH3+O2 5.285E-01 3.477 5.992E+04
CH3+O2(+M)<=>CH3O2(+M) 7.812E+09 0.900 0.000E+00
LOW / 6.8500E+24 -3.0000E+00 0.0000E+00 /
TROE / 6.0000E-01 1.0000E+03 7.0000E+01 1.7000E+03 / !Troe Fall-off reaction
CH3O2+CH2O=>CH3O2H+HCO 1.990E+12 0.000 1.166E+04
CH3O2H+HCO=>CH3O2+CH2O 1.323E+14 -0.853 9.259E+03
CH4+CH3O2=>CH3+CH3O2H 1.810E+11 0.000 1.848E+04
CH3+CH3O2H=>CH4+CH3O2 2.233E+12 -0.694 -6.550E+02
CH3O2+CH3=>CH3O+CH3O 5.080E+12 0.000 -1.411E+03
CH3O+CH3O=>CH3O2+CH3 1.967E+12 0.176 2.807E+04
CH3O2+HO2=>CH3O2H+O2 2.470E+11 0.000 -1.570E+03
CH3O2H+O2=>CH3O2+HO2 5.302E+14 -0.792 3.552E+04
CH3O2+CH3O2=>O2+CH3O+CH3O 1.400E+16 -1.610 1.860E+03
O2+CH3O+CH3O=>CH3O2+CH3O2 0.000E+00 0.000 0.000E+00
CH3O2+H=>CH3O+OH 9.600E+13 0.000 0.000E+00
CH3O+OH=>CH3O2+H 1.720E+09 1.019 4.078E+04
CH3O2+O=>CH3O+O2 3.600E+13 0.000 0.000E+00
CH3O+O2=>CH3O2+O 2.229E+11 0.628 5.752E+04
CH3O2H=>CH3O+OH 6.310E+14 0.000 4.230E+04
CH3O+OH=>CH3O2H 2.514E+06 1.883 -2.875E+03
CH3+CH3(+M)<=>C2H6(+M) 9.214E+16 -1.170 6.358E+02
LOW / 1.1350E+36 -5.2460E+00 1.7050E+03 /
TROE / 4.0500E-01 1.1200E+03 6.9600E+01 1.0000E+10 / !Troe Fall-off reaction
H2/2/ H2O/6/ CO/1.5/ CO2/2/ CH4/2/ C2H6/3/
H2+CH3O2=>H+CH3O2H 1.500E+14 0.000 2.603E+04
H+CH3O2H=>H2+CH3O2 1.688E+18 -1.140 8.434E+03
CH2CO+H=>CH3+CO 1.100E+13 0.000 3.400E+03
CH3+CO=>CH2CO+H 2.400E+12 0.000 4.020E+04
CH3COCH2=>CH2CO+CH3 1.000E+14 0.000 3.100E+04
CH2CO+CH3=>CH3COCH2 1.000E+11 0.000 6.000E+03
C3H6+O=>CH2CO+CH3+H 2.500E+07 1.760 7.600E+01
CH2CO+CH3+H=>C3H6+O 0.000E+00 0.000 0.000E+00

!****************************************
!**********Nheptane reactions**************
!****************************************

!
C2H5+H(+M)<=>C2H6(+M) 5.210E+17 -0.990 1.580E+03
LOW / 1.9900E+41 -7.0800E+00 6.6850E+03 /
TROE / 8.4200E-01 1.2500E+02 2.2190E+03 6.8820E+03 / !Troe Fall-off reaction
H2/2/ H2O/6/ CO/1.5/ CO2/2/ CH4/2/ C2H6/3/
C2H6+H=>C2H5+H2 1.150E+08 1.900 7.530E+03
C2H5+H2=>C2H6+H 1.062E+04 2.582 9.760E+03

C2H6+O=>C2H5+OH 3.550E+06 2.400 5.830E+03
C2H5+OH=>C2H6+O 1.702E+02 3.063 6.648E+03
C2H6+OH=>C2H5+H2O 1.480E+07 1.900 9.500E+02
C2H5+H2O=>C2H6+OH 1.450E+04 2.476 1.807E+04
C2H6+O2=>C2H5+HO2 6.030E+13 0.000 5.187E+04
C2H5+HO2=>C2H6+O2 2.921E+10 0.334 -5.930E+02
C2H6+CH3=>C2H5+CH4 1.510E-07 6.000 6.047E+03
C2H5+CH4=>C2H6+CH3 1.273E-08 6.236 9.817E+03
C2H6+HO2=>C2H5+H2O2 3.460E+01 3.610 1.692E+04
C2H5+H2O2=>C2H6+HO2 1.849E+00 3.597 3.151E+03
C2H6+CH3O2=>C2H5+CH3O2H 1.940E+01 3.640 1.710E+04
C2H5+CH3O2H=>C2H6+CH3O2 2.017E+01 3.182 1.734E+03
C2H4+H(+M)<=>C2H5(+M) 1.081E+12 0.454 1.822E+03
LOW / 1.2000E+42 -7.6200E+00 6.9700E+03 /
TROE / 9.7500E-01 2.1000E+02 9.8400E+02 4.3740E+03 / !Troe Fall-off reaction
H2/2/ H2O/6/ CO/1.5/ CO2/2/ CH4/2/ C2H6/3/
C2H5+C2H3=>C2H4+C2H4 6.859E+11 0.110 -4.300E+03
C2H4+C2H4=>C2H5+C2H3 4.820E+14 0.000 7.153E+04
CH3+C2H5=>CH4+C2H4 1.180E+04 2.450 -2.921E+03
CH4+C2H4=>CH3+C2H5 2.390E+06 2.400 6.669E+04
C2H5+H=>CH3+CH3 9.690E+13 0.000 2.200E+02
CH3+CH3=>C2H5+H 2.029E+09 1.028 1.051E+04
C2H5+H=>C2H4+H2 2.000E+12 0.000 0.000E+00
C2H4+H2=>C2H5+H 4.440E+11 0.396 6.807E+04
C2H5+O=>CH3CHO+H 1.100E+14 0.000 0.000E+00
CH3CHO+H=>C2H5+O 1.033E+17 -0.500 7.742E+04
C2H5+O2=>C2H4+HO2 7.561E+14 -1.010 4.749E+03
DUP
C2H4+HO2=>C2H5+O2 8.802E+14 -0.962 1.813E+04
DUP
C2H5+O2=>C2H4+HO2 4.000E-01 3.880 1.362E+04
DUP
C2H4+HO2=>C2H5+O2 4.656E-01 3.928 2.700E+04
DUP
C2H5+O2=>CH3CHO+OH 8.265E+02 2.410 5.285E+03
CH3CHO+OH=>C2H5+O2 2.247E+03 2.301 6.597E+04
CH3CHO=>CH3+HCO 7.687E+20 -1.342 8.695E+04
CH3+HCO=>CH3CHO 1.750E+13 0.000 0.000E+00
C2H3+H(+M)<=>C2H4(+M) 1.360E+14 0.173 6.600E+02
LOW / 1.4000E+30 -3.8600E+00 3.3200E+03 /
TROE / 7.8200E-01 2.0750E+02 2.6630E+03 6.0950E+03 / !Troe Fall-off reaction
H2/2/ H2O/6/ CO/1.5/ CO2/2/ CH4/2/ C2H6/3/
C2H4+H=>C2H3+H2 5.070E+07 1.930 1.295E+04
C2H3+H2=>C2H4+H 1.602E+04 2.436 5.190E+03
C2H4+O=>CH3+HCO 8.564E+06 1.880 1.830E+02
CH3+HCO=>C2H4+O 3.297E+02 2.602 2.614E+04
C2H4+OH=>C2H3+H2O 1.800E+06 2.000 2.500E+03
C2H3+H2O=>C2H4+OH 6.029E+03 2.400 9.632E+03
C2H4+CH3=>C2H3+CH4 6.620E+00 3.700 9.500E+03
C2H3+CH4=>C2H4+CH3 1.908E+00 3.760 3.280E+03
C2H4+O2=>C2H3+HO2 4.000E+13 0.000 5.820E+04

C2H3+HO2=>C2H4+O2 6.626E+10 0.158 -4.249E+03
C2H4+CH3O2=>C2H3+CH3O2H 2.230E+12 0.000 1.719E+04
C2H3+CH3O2H=>C2H4+CH3O2 7.929E+12 -0.634 -8.167E+03
C2H3+O2=>CH2O+HCO 8.500E+28 -5.312 6.500E+03
CH2O+HCO=>C2H3+O2 3.994E+27 -4.883 9.345E+04
C2H5CHO=>C2H5+HCO 1.496E+27 -3.205 8.704E+04
C2H5+HCO=>C2H5CHO 1.810E+13 0.000 0.000E+00
C3H6=>C2H3+CH3 2.730E+62 -13.280 1.232E+05
C2H3+CH3=>C3H6 6.822E+53 -11.779 2.055E+04
C3H6+O=>C2H5+HCO 1.580E+07 1.760 -1.216E+03
C2H5+HCO=>C3H6+O 9.188E+01 2.725 2.311E+04
C3H6+H=>C2H4+CH3 2.300E+13 0.000 2.547E+03
C2H4+CH3=>C3H6+H 7.272E+07 1.271 1.120E+04
PC4H9=>C2H5+C2H4 3.504E+12 0.463 2.947E+04
C2H5+C2H4=>PC4H9 1.320E+04 2.480 6.130E+03
C5H9O1-3=>C2H5CHO+C2H3 1.417E+18 -1.560 2.334E+04
C2H5CHO+C2H3=>C5H9O1-3 1.000E+11 0.000 9.600E+03
NC7H16=>H+C7H15-2 1.300E+93 -21.01 1.395E+05 !class 1 PFx1e5
1.300E+88
H+C7H15-2=>NC7H16 2.263E+83 -20.31 4.083E+04
NC7H16=>H+C7H15-3 1.300E+93 -21.01 1.395E+05 !class 1 PFx1e5
1.300E+88
H+C7H15-3=>NC7H16 2.263E+83 -20.31 4.083E+04
NC7H16+H=>C7H15-2+H2 2.600E+06 2.40 4.471E+03
C7H15-2+H2=>NC7H16+H 1.807E+01 3.38 9.318E+03
NC7H16+H=>C7H15-3+H2 2.600E+06 2.40 4.471E+03
C7H15-3+H2=>NC7H16+H 1.807E+01 3.38 9.318E+03
NC7H16+O=>C7H15-2+OH 9.540E+04 2.71 2.106E+03
C7H15-2+OH=>NC7H16+O 3.481E-01 3.67 5.541E+03
NC7H16+O=>C7H15-3+OH 9.540E+04 2.71 2.106E+03
C7H15-3+OH=>NC7H16+O 3.481E-01 3.67 5.541E+03
NC7H16+OH=>C7H15-2+H2O 4.900E+06 2.00 -5.960E+02 !REACTION
CLASS 2 max rop at main=0.9452217 P.F A.E REAC12
C7H15-2+H2O=>NC7H16+OH 3.624E+02 2.87 1.914E+04
NC7H16+OH=>C7H15-3+H2O 4.900E+06 2.00 -0.5960E+03 !REACTION
CLASS 2 max rop at main=0.9452804 P.F A.E- -5.960E+02
C7H15-3+H2O=>NC7H16+OH 3.624E+02 2.87 1.914E+04
NC7H16+HO2=>C7H15-2+H2O2 1.264E+02 3.37 1.372E+04
C7H15-2+H2O2=>NC7H16+HO2 4.982E-01 3.66 2.562E+03
NC7H16+HO2=>C7H15-3+H2O2 1.264E+02 3.37 1.372E+04
C7H15-3+H2O2=>NC7H16+HO2 4.982E-01 3.66 2.562E+03
NC7H16+CH3=>C7H15-2+CH4 5.410E+04 2.26 7.287E+03
C7H15-2+CH4=>NC7H16+CH3 3.432E+02 2.79 1.367E+04
NC7H16+CH3=>C7H15-3+CH4 5.410E+04 2.26 7.287E+03
C7H15-3+CH4=>NC7H16+CH3 3.432E+02 2.79 1.367E+04
NC7H16+O2=>C7H15-2+HO2 2.800E+13 0.00 5.015E+04
C7H15-2+HO2=>NC7H16+O2 1.000E+09 0.63 3.090E+02
NC7H16+O2=>C7H15-3+HO2 2.800E+13 0.00 5.015E+04
C7H15-3+HO2=>NC7H16+O2 1.000E+09 0.63 3.090E+02
NC7H16+C2H5=>C7H15-2+C2H6 1.000E+11 0.00 1.040E+04
C7H15-2+C2H6=>NC7H16+C2H5 1.000E+11 0.00 1.290E+04

```
NC7H16+C2H5=>C7H15-3+C2H6 1.000E+11 0.00 1.040E+04
C7H15-3+C2H6=>NC7H16+C2H5 1.000E+11 0.00 1.290E+04
NC7H16+C2H3=>C7H15-2+C2H4 8.000E+11 0.00 1.680E+04
C7H15-2+C2H4=>NC7H16+C2H3 2.000E+12 0.00 2.420E+04
NC7H16+C2H3=>C7H15-3+C2H4 8.000E+11 0.00 1.680E+04
C7H15-3+C2H4=>NC7H16+C2H3 2.000E+12 0.00 2.420E+04
NC7H16+CH3O2=>C7H15-2+CH3O2H 2.037E+01   3.58  1.481E+04
C7H15-2+CH3O2H=>NC7H16+CH3O2 1.562E+00   3.42  2.054E+03
NC7H16+CH3O2=>C7H15-3+CH3O2H 2.037E+01   3.58  1.481E+04
C7H15-3+CH3O2H=>NC7H16+CH3O2 1.562E+00   3.42  2.054E+03
NC7H16+C7H15-2=>C7H15-3+NC7H16 1.000E+11 0.00 1.040E+04
C7H15-3+NC7H16=>NC7H16+C7H15-2 1.000E+11 0.00 1.040E+04
C7H15-2=>PC4H9+C3H6 1.9528E+20  -1.79  3.136E+04
        !REACTION CLASS 3 max rop at main=1.414783 P.Fx20 9.764E+18
PC4H9+C3H6=>C7H15-2 1.000E+11 0.00 8.200E+03
C7H15-2=>C7H15-3 9.587E+08 1.39 3.970E+04
C7H15-3=>C7H15-2 9.587E+08 1.39 3.970E+04
C7H15O2-2=>C7H15-2+O2 1.357E+23 -2.36 3.767E+04
C7H15-2+O2=>C7H15O2-2 7.540E+12 0.00 0.000E+00
C7H15O2-3=>C7H15-3+O2 1.357E+23 -2.36 3.767E+04
C7H15-3+O2=>C7H15O2-3 7.540E+12 0.00 0.000E+00
C7H15O2-2<=>C7H14OOH2-4 2.500E+10 0.00 2.045E+04
        !REACTION CLASS 12 max rop at main=0.0431867 P.F A.E
C7H15O2-3<=>C7H14OOH3-5 2.500E+10 0.00 2.045E+04
        !REACTION CLASS 12 max rop at main=0.02375319 P.F
C7H14OOH2-4=>OH+CH3CHO+C5H10-1 1.548E+12   0.59  3.009E+04
OH+CH3CHO+C5H10-1=>C7H14OOH2-4 0.000E+00 0.00 0.000E+00
C7H14OOH4-2=>OH+NC3H7CHO+C3H6 6.186E+13   0.09  3.084E+04
OH+NC3H7CHO+C3H6=>C7H14OOH4-2 0.000E+00 0.00 0.000E+00
C7H14OOH2-4O2=>C7H14OOH2-4+O2 1.389E+23 -2.38 3.760E+04
C7H14OOH2-4+O2=>C7H14OOH2-4O2 7.540E+12 0.00 0.000E+00
C7H14OOH3-5O2=>C7H14OOH3-5+O2 1.389E+23 -2.38 3.760E+04
C7H14OOH3-5+O2=>C7H14OOH3-5O2 7.540E+12 0.00 0.000E+00
C7H14OOH2-4O2<=>NC7KET24+OH 1.250E+10 0.00 1.745E+04
        !REACTION CLASS 23
C7H14OOH3-5O2<=>NC7KET35+OH 1.250E+10 0.00 1.745E+04
        !REACTION CLASS 23
NC7KET24=>NC3H7CHO+CH3COCH2+OH 1.000E+16 0.00 3.900E+04
        !REACTION CLASS 24
NC3H7CHO+CH3COCH2+OH=>NC7KET24 0.000E+00 0.00 0.000E+00
NC7KET35=>C2H5CHO+C2H5COCH2+OH 1.000E+16 0.00 3.900E+04
        !REACTION CLASS 24
C2H5CHO+C2H5COCH2+OH=>NC7KET35 0.000E+00 0.00 0.000E+00
NC7KET42=>CH3CHO+NC3H7COCH2+OH 1.000E+16 0.00 3.900E+04
        !REACTION CLASS 24
CH3CHO+NC3H7COCH2+OH=>NC7KET42 0.000E+00 0.00 0.000E+00
C4H7OOH1-4=>C4H7O1-4+OH 2.021E+20 -1.53 4.704E+04
C4H7O1-4+OH=>C4H7OOH1-4 2.000E+13 0.00 0.000E+00
C2H5COCH2=>CH2CO+C2H5 1.000E+14 0.000 3.500E+04
CH2CO+C2H5=>C2H5COCH2 1.000E+11 0.000 0.000E+00
```

```
!****************************************
!***********Isooctane reactions*************
!****************************************
IC3H7=>H+C3H6 6.919E+13 -0.025 3.769E+04
H+C3H6=>IC3H7 2.640E+13 0.000 2.160E+03
IC3H7+O2=>C3H6+HO2 4.500E-19 0.000 5.020E+03
C3H6+HO2=>IC3H7+O2 2.000E-19 0.000 1.750E+04
IC3H7+OH=>C3H6+H2O 2.410E+13 0.000 0.000E+00
C3H6+H2O=>IC3H7+OH 2.985E+12 0.570 8.382E+04
C3H6=>C3H5-T+H 5.620E+71 -16.580 1.393E+05
C3H5-T+H=>C3H6 4.260E+68 -16.164 3.008E+04
C3H6+O=>C3H5-T+OH 6.030E+10 0.700 7.632E+03
C3H5-T+OH=>C3H6+O 9.483E+06 1.373 5.760E+02
C3H6+OH=>C3H5-T+H2O 1.110E+06 2.000 1.451E+03
C3H5-T+H2O=>C3H6+OH 3.565E+03 2.586 1.070E+04
C3H6+HO2=>C3H5-T+H2O2 9.000E+03 2.500 2.359E+04
C3H5-T+H2O2=>C3H6+HO2 1.577E+03 2.497 1.941E+03
C3H6+H=>C3H5-T+H2 4.050E+05 2.500 9.794E+03
C3H5-T+H2=>C3H6+H 1.227E+02 3.192 4.150E+03
C3H6+O2=>C3H5-T+HO2 1.400E+12 0.000 6.070E+04
C3H5-T+HO2=>C3H6+O2 2.224E+09 0.344 3.690E+02
C3H6+CH3=>C3H5-T+CH4 8.400E-01 3.500 1.166E+04
C3H5-T+CH4=>C3H6+CH3 2.322E-01 3.746 7.552E+03
C3H5-T+O2=>CH3COCH2+O 3.810E+17 -1.360 5.580E+03
CH3COCH2+O=>C3H5-T+O2 2.000E+11 0.000 1.750E+04
IC4H9=>IC4H8+H 3.371E+13 0.124 3.366E+04
IC4H8+H=>IC4H9 6.250E+11 0.510 2.620E+03
IC4H9=>C3H6+CH3 9.504E+11 0.773 3.070E+04
C3H6+CH3=>IC4H9 1.890E+03 2.670 6.850E+03
IC4H9+O2=>IC4H8+HO2 1.070E+00 3.710 9.322E+03
IC4H8+HO2=>IC4H9+O2 4.158E-02 4.024 2.715E+04
IC3H7CHO=>TC3H6CHO+H 2.304E+18 -0.910 9.200E+04
TC3H6CHO+H=>IC3H7CHO 2.000E+14 0.000 0.000E+00
IC3H7CHO=>IC3H7+HCO 1.129E+17 -0.030 7.976E+04
IC3H7+HCO=>IC3H7CHO 1.810E+13 0.000 0.000E+00
IC3H7CHO+HO2=>TC3H6CHO+H2O2 8.000E+10 0.000 1.192E+04
TC3H6CHO+H2O2=>IC3H7CHO+HO2 3.366E+12 -0.420 1.105E+04
IC3H7CHO+OH=>TC3H6CHO+H2O 1.684E+12 0.000 -7.810E+02
TC3H6CHO+H2O=>IC3H7CHO+OH 1.194E+13 -0.090 2.981E+04
IC4H8=>C3H5-T+CH3 1.920E+66 -14.220 1.281E+05
C3H5-T+CH3=>IC4H8 1.561E+56 -12.293 2.610E+04
IC4H8=>IC4H7+H 3.070E+55 -11.490 1.143E+05
IC4H7+H=>IC4H8 1.428E+55 -11.738 2.640E+04
IC4H8+H=>C3H6+CH3 5.680E+33 -5.720 2.000E+04
C3H6+CH3=>IC4H8+H 6.093E+26 -4.209 2.720E+04
IC4H8+H=>IC4H7+H2 3.400E+05 2.500 2.492E+03
IC4H7+H2=>IC4H8+H 6.320E+04 2.528 1.816E+04
IC4H8+O=>CH2CO+CH3+CH3 3.330E+07 1.760 7.600E+01
CH2CO+CH3+CH3=>IC4H8+O 0.000E+00 0.000 0.000E+00
IC4H8+O=>IC4H7+OH 1.206E+11 0.700 7.633E+03
IC4H7+OH=>IC4H8+O 1.164E+10 0.709 2.189E+04
```

IC4H8+CH3=>IC4H7+CH4 4.420E+00 3.500 5.675E+03
IC4H7+CH4=>IC4H8+CH3 7.495E+02 3.082 2.289E+04
IC4H8+HO2=>IC4H7+H2O2 1.928E+04 2.600 1.391E+04
IC4H7+H2O2=>IC4H8+HO2 2.073E+06 1.933 1.358E+04
IC4H8+O2=>IC4H7+HO2 6.000E+12 0.000 3.990E+04
IC4H7+HO2=>IC4H8+O2 5.848E+12 -0.320 8.830E+02
IC4H8+C3H5-T=>IC4H7+C3H6 7.940E+11 0.000 2.050E+04
IC4H7+C3H6=>IC4H8+C3H5-T 5.592E+20 -1.270 8.017E+04
IC4H8+OH=>IC4H7+H2O 5.200E+06 2.000 -2.980E+02
IC4H7+H2O=>IC4H8+OH 1.025E+07 1.922 3.027E+04
IC4H8+O=>IC3H7+HCO 1.580E+07 1.760 -1.216E+03
IC3H7+HCO=>IC4H8+O 4.538E+00 3.060 2.169E+04
IC4H8+CH3O2=>IC4H7+CH3O2H 1.928E+04 2.600 1.391E+04
IC4H7+CH3O2H=>IC4H8+CH3O2 4.034E+07 1.488 1.199E+04
IC4H7+O2=>CH3COCH2+CH2O 7.140E+15 -1.210 2.105E+04
CH3COCH2+CH2O=>IC4H7+O2 1.700E+12 -0.407 8.825E+04
CH3O2+IC4H7=>CH3O+IC4H7O 7.000E+12 0.000 -1.000E+03
CH3O+IC4H7O=>CH3O2+IC4H7 2.138E+11 0.349 1.506E+04
IC4H7+HO2=>IC4H7O+OH 7.000E+12 0.000 -1.000E+03
IC4H7O+OH=>IC4H7+HO2 3.418E+12 0.050 1.082E+04
IC4H7O=>C3H5-T+CH2O 2.925E+21 -2.391 3.559E+04
C3H5-T+CH2O=>IC4H7O 1.000E+11 0.000 1.260E+04
TC3H6CHO+H2=>IC3H7CHO+H 2.160E+05 2.380 1.899E+04
IC3H7CHO+H=>TC3H6CHO+H2 1.319E+05 2.470 3.550E+03
IC4H7OH=>IC4H7O+H 5.969E+16 -0.560 1.059E+05
IC4H7O+H=>IC4H7OH 4.000E+13 0.000 0.000E+00
IC4H7O+H2=>IC4H7OH+H 9.050E+06 2.000 1.783E+04
IC4H7OH+H=>IC4H7O+H2 7.160E+05 2.440 1.631E+04
IC4H7OH=>IC4H7+OH 7.310E+16 -0.410 7.970E+04
IC4H7+OH=>IC4H7OH 3.000E+13 0.000 0.000E+00
IC4H7O+CH2O=>IC4H7OH+HCO 1.150E+11 0.000 1.280E+03
IC4H7OH+HCO=>IC4H7O+CH2O 3.020E+11 0.000 1.816E+04
TC3H6CHO+CH2O=>IC3H7CHO+HCO 2.520E+08 1.900 1.819E+04
IC3H7CHO+HCO=>TC3H6CHO+CH2O 1.229E+07 1.990 1.742E+04
TC3H6CHO+IC4H8=>IC3H7CHO+IC4H7 4.700E+02 3.300 1.984E+04
IC3H7CHO+IC4H7=>TC3H6CHO+IC4H8 6.613E+00 3.390 8.672E+03
TC3H6CHO+HO2=>IC3H7CHO+O2 3.675E+12 0.000 1.310E+03
IC3H7CHO+O2=>TC3H6CHO+HO2 1.236E+14 -0.240 4.335E+04
IC4H7O+IC4H8=>IC4H7OH+IC4H7 2.700E+11 0.000 4.000E+03
IC4H7OH+IC4H7=>IC4H7O+IC4H8 1.000E+10 0.000 9.000E+03
YC7H15=>IC3H7+IC4H8 2.220E+20 -2.060 3.247E+04
IC3H7+IC4H8=>YC7H15 5.000E+10 0.000 9.200E+03
IC8H18=>AC8H17+H 5.748E+17 -0.360 1.012E+05
AC8H17+H=>IC8H18 1.000E+14 0.000 0.000E+00
IC8H18=>CC8H17+H 1.146E+19 -0.941 9.543E+04
CC8H17+H=>IC8H18 1.000E+14 0.000 0.000E+00
IC8H18=>DC8H17+H 1.919E+17 -0.360 1.004E+05
DC8H17+H=>IC8H18 1.000E+14 0.000 0.000E+00
IC8H18=>YC7H15+CH3 1.635E+27 -2.794 8.393E+04
YC7H15+CH3=>IC8H18 1.630E+13 0.000 -5.960E+02

IC8H18+H=>AC8H17+H2 7.341E+07 2.768 8.147E+03 !class2-reaction2
P.F x100
AC8H17+H2=>IC8H18+H 5.100E+01 3.404 1.048E+04
IC8H18+H=>CC8H17+H2 6.020E+05 2.400 2.583E+03
CC8H17+H2=>IC8H18+H 2.097E+00 3.617 1.071E+04
IC8H18+H=>DC8H17+H2 1.880E+05 2.750 6.280E+03
DC8H17+H2=>IC8H18+H 3.911E+01 3.386 9.417E+03
IC8H18+O=>AC8H17+OH 8.550E+03 3.050 3.123E+03
AC8H17+OH=>IC8H18+O 3.118E-01 3.666 4.048E+03
IC8H18+O=>CC8H17+OH 3.830E+05 2.410 1.140E+03
CC8H17+OH=>IC8H18+O 7.003E-01 3.607 7.858E+03
IC8H18+O=>DC8H17+OH 2.853E+05 2.500 3.645E+03
DC8H17+OH=>IC8H18+O 3.116E+01 3.116 5.370E+03

IC8H18+OH<=>AC8H17+H2O 2.630E+09 1.800 1.431E+03 !class2-reaction1
P.F x100
IC8H18+OH=>CC8H17+H2O 1.700E+06 1.900 -1.450E+03
CC8H17+H2O=>IC8H18+OH 6.301E+01 3.011 2.157E+04
IC8H18+OH=>DC8H17+H2O 1.780E+07 1.800 1.431E+03 !class2-reaction3
DC8H17+H2O=>IC8H18+OH 3.940E+04 2.330 1.946E+04
IC8H18+CH3=>AC8H17+CH4 4.257E-14 8.060 4.154E+03
AC8H17+CH4=>IC8H18+CH3 2.699E-15 8.250 8.031E+03
IC8H18+CH3=>CC8H17+CH4 6.010E-10 6.360 8.930E+02
CC8H17+CH4=>IC8H18+CH3 1.911E-12 7.131 1.056E+04
IC8H18+CH3=>DC8H17+CH4 1.470E-01 3.870 6.808E+03
DC8H17+CH4=>IC8H18+CH3 2.791E-02 4.060 1.148E+04
IC8H18+HO2<=>AC8H17+H2O2 61.2 3.59 17160
IC8H18+HO2<=>CC8H17+H2O2 433.2 3.01 12090
IC8H18+HO2<=>DC8H17+H2O2 40.8 3.59 17160
IC8H18+O2=>AC8H17+HO2 6.300E+13 0.000 5.076E+04
AC8H17+HO2=>IC8H18+O2 2.296E+10 0.288 -1.592E+03
IC8H18+O2=>CC8H17+HO2 7.000E+12 0.000 4.606E+04
CC8H17+HO2=>IC8H18+O2 1.279E+08 0.869 -4.990E+02
IC8H18+O2=>DC8H17+HO2 4.200E+13 0.000 5.076E+04
DC8H17+HO2=>IC8H18+O2 4.584E+10 0.288 -7.920E+02
IC4H8+IC4H9=>AC8H17 6.090E+02 2.48 8.520E+03 !!!!4.000E+02 2.500 8.520E+03
AC8H17=>IC4H8+IC4H9 2.458E+14 -0.14 2.678E+04
AC8H17=>DC8H17 1.390E+11 0.000 1.540E+04
DC8H17=>AC8H17 4.163E+11 0.000 1.620E+04
AC8H17=>CC8H17 3.708E+11 0.000 2.040E+04
CC8H17=>AC8H17 1.859E+10 0.581 2.619E+04
IC8H18+CH3O2<=>AC8H17+CH3O2H 2.079 3.97 18280
IC8H18+CH3O2<=>CC8H17+CH3O2H 136.6 3.12 13190
IC8H18+CH3O2<=>DC8H17+CH3O2H 1.386 3.97 18280
AC8H17O2=>AC8H17+O2 3.465E+20 -1.653 3.572E+04
AC8H17+O2=>AC8H17O2 4.520E+12 0.000 0.000E+00
AC8H17+AC8H17O2=>AC8H17O+AC8H17O 7.000E+12 0.000 -1.000E+03
AC8H17O+AC8H17O=>AC8H17+AC8H17O2 6.479E+13 -0.155 2.936E+04
DC8H17+AC8H17O2=>DC8H17O+AC8H17O 7.000E+12 0.000 -1.000E+03
DC8H17O+AC8H17O=>DC8H17+AC8H17O2 3.252E+13 -0.155 2.856E+04
AC8H17+HO2=>AC8H17O+OH 7.000E+12 0.000 -1.000E+03

```
AC8H17O+OH=>AC8H17+HO2 2.180E+15 -0.508 2.588E+04
DC8H17+HO2=>DC8H17O+OH 7.000E+12 0.000 -1.000E+03
DC8H17O+OH=>DC8H17+HO2 1.094E+15 -0.508 2.508E+04
AC8H17+CH3O2=>AC8H17O+CH3O 7.000E+12 0.000 -1.000E+03
AC8H17O+CH3O=>AC8H17+CH3O2 1.364E+14 -0.209 3.012E+04
DC8H17+CH3O2=>DC8H17O+CH3O 7.000E+12 0.000 -1.000E+03
DC8H17O+CH3O=>DC8H17+CH3O2 6.844E+13 -0.209 2.932E+04
AC8H17O2+CH3O2=>AC8H17O+CH3O+O2 1.400E+16 -1.610 1.860E+03
AC8H17O+CH3O+O2=>AC8H17O2+CH3O2 0.000E+00 0.000 0.000E+00
AC8H17O2+AC8H17O2=>O2+AC8H17O+AC8H17O 1.400E+14 -1.610 1.860E+03
        !class16 P.F/100
O2+AC8H17O+AC8H17O=>AC8H17O2+AC8H17O2 0.000E+00 0.000 0.000E+00
AC8H17O=>YC7H15+CH2O 5.689E+24 -3.208 1.914E+04                !class18
YC7H15+CH2O=>AC8H17O 1.000E+11 0.000 1.190E+04
AC8H17O2<=>AC8H16OOH-B 2.500E+10 0.000 2.045E+04
AC8H16OOH-B<=>IC8ETERAB+OH 1.500E+11 0.000 1.425E+04                !class19
reaction1 P.F/2 3.000E+11
AC8H16OOH-BO2<=>AC8H16OOH-B+O2 1.361E+23 -2.357 3.728E+04
AC8H16OOH-BO2<=>IC8KETAB+OH 2.500E+11 0.000 2.100E+04                !class23
reaction PFx10 2.500E+10
IC8KETAB=>IC3H7CHO+TC3H6CHO+OH 1.000E+16 0.000 3.900E+04
        !class 24 reaction
IC3H7CHO+TC3H6CHO+OH=>IC8KETAB 0.000E+00 0.000 0.000E+00

END

THERMO
  300.000  1000.000  5000.000

G70                C  16H  38         G   298.150  5000.000 1000.       1
 3.93197519E+01 9.11470601E-02-3.39721140E-05 5.94437262E-09-3.95796331E-13    2
-6.51665791E+04-1.66160224E+02-2.28147400E+00 1.85127971E-01-9.91782207E-05
3
 1.43398377E-08 3.73230542E-12-5.17449265E+04 5.60024917E+01-4.50429238E+04
4
G30                C  15H  35         G   298.150  5000.000 1000.       1
 3.93197519E+01 9.11470601E-02-3.39721140E-05 5.94437262E-09-3.95796331E-13    2
-6.51665791E+04-1.66160224E+02-2.28147400E+00 1.85127971E-01-9.91782207E-05
3
 1.43398377E-08 3.73230542E-12-5.17449265E+04 5.60024917E+01-4.50429238E+04
4
G50                C  17H  40         G   298.150  5000.000 1000.       1
 3.93197519E+01 9.11470601E-02-3.39721140E-05 5.94437262E-09-3.95796331E-13    2
-6.51665791E+04-1.66160224E+02-2.28147400E+00 1.85127971E-01-9.91782207E-05
3
 1.43398377E-08 3.73230542E-12-5.17449265E+04 5.60024917E+01-4.50429238E+04
4
Diesel             C  14H  34         G   300.00   5000.000 1000.000    1
 3.93197519E+01 9.11470601E-02-3.39721140E-05 5.94437262E-09-3.95796331E-13    2
-6.51665791E+04-1.66160224E+02-2.28147400E+00 1.85127971E-01-9.91782207E-05
3
```

```
 1.43398377E-08 3.73230542E-12-5.17449265E+04 5.60024917E+01-4.50429238E+04
4
C                   C   1               G  0300.00   5000.00  1000.00      1
 0.02602087E+02-0.01787081E-02 0.09087041E-06-0.01149933E-09 0.03310844E-14    2
 0.08542154E+06 0.04195177E+02 0.02498585E+02 0.08085777E-03-0.02697697E-05
3
 0.03040729E-08-0.01106652E-11 0.08545878E+06 0.04753459E+02                   4
H               120186H   1             G  0300.00   5000.00  1000.00      1
 0.02500000E+02 0.00000000E+00 0.00000000E+00 0.00000000E+00 0.00000000E+00
2
 0.02547163E+06-0.04601176E+01 0.02500000E+02 0.00000000E+00 0.00000000E+00
3
 0.00000000E+00 0.00000000E+00 0.02547163E+06-0.04601176E+01                   4
H2              121286H   2             G  0300.00   5000.00  1000.00      1
 0.02991423E+02 0.07000644E-02-0.05633829E-06-0.09231578E-10 0.01582752E-13    2
-0.08350340E+04-0.01355110E+02 0.03298124E+02 0.08249442E-02-0.08143015E-05
3
-0.09475434E-09 0.04134872E-11-0.01012521E+05-0.03294094E+02                   4
O               120186O   1             G  0300.00   5000.00  1000.00      1
 0.02542060E+02-0.02755062E-03-0.03102803E-07 0.04551067E-10-0.04368052E-14
2
 0.02923080E+06 0.04920308E+02 0.02946429E+02-0.01638166E-01 0.02421032E-04
3
-0.01602843E-07 0.03890696E-11 0.02914764E+06 0.02963995E+02                   4
O2              121386O   2             G  0300.00   5000.00  1000.00      1
 0.03697578E+02 0.06135197E-02-0.01258842E-05 0.01775281E-09-0.01136435E-13    2
-0.01233930E+05 0.03189166E+02 0.03212936E+02 0.01127486E-01-0.05756150E-05
3
 0.01313877E-07-0.08768554E-11-0.01005249E+05 0.06034738E+02                   4
OH        7/13/ 0 RUCICH   1O   1    0    0G   300.000  5000.000 1710.000    01
 2.85376040E+00 1.02994334E-03-2.32666477E-07 1.93750704E-11-3.15759847E-16    2
 3.69949720E+03 5.78756825E+00 3.41896226E+00 3.19255801E-04-3.08292717E-07
3
 3.64407494E-10-1.00195479E-13 3.45264448E+03 2.54433372E+00                   4
H2O             20387H   2O   1         G  0300.00   5000.00  1000.00      1
 0.02672146E+02 0.03056293E-01-0.08730260E-05 0.01200996E-08-0.06391618E-13    2
-0.02989921E+06 0.06862817E+02 0.03386842E+02 0.03474982E-01-0.06354696E-04
3
 0.06968581E-07-0.02506588E-10-0.03020811E+06 0.02590233E+02                   4
N2              121286N   2             G  0300.00   5000.00  1000.00      1
 0.02926640E+02 0.01487977E-01-0.05684761E-05 0.01009704E-08-0.06753351E-13    2
-0.09227977E+04 0.05980528E+02 0.03298677E+02 0.01408240E-01-0.03963222E-04
3
 0.05641515E-07-0.02444855E-10-0.01020900E+05 0.03950372E+02                   4
HO2             L 5/89H   1O   2         G   200.000  3500.000  1000.000    1
 4.01721090E+00 2.23982013E-03-6.33658150E-07 1.14246370E-10-1.07908535E-14    2
 1.11856713E+02 3.78510215E+00 4.30179801E+00-4.74912051E-03 2.11582891E-05
3
-2.42763894E-08 9.29225124E-12 2.94808040E+02 3.71666245E+00                   4
H2O2            120186H   2O   2         G  0300.00   5000.00  1000.00      1
 0.04573167E+02 0.04336136E-01-0.01474689E-04 0.02348904E-08-0.01431654E-12    2
```

-0.01800696E+06 0.05011370E+01 0.03388754E+02 0.06569226E-01-0.01485013E-05
3
-0.04625806E-07 0.02471515E-10-0.01766315E+06 0.06785363E+02 4
CO 29/11/04 C 1O 1 0 0G 300.000 5000.000 1429.000 1
3.11216890E+00 1.15948283E-03-3.38480362E-07 4.41403098E-11-2.12862228E-15 2
-1.42718539E+04 5.71725177E+00 3.19036352E+00 8.94419972E-04-3.24927563E-08
3
-1.04599967E-10 2.41965693E-14-1.42869054E+04 5.33277914E+00 4
CO2 29/11/04 C 1O 2 0 0G 300.000 5000.000 1380.000 1
5.18953018E+00 2.06006476E-03-7.33575324E-07 1.17004374E-10-6.91729215E-15 2
-4.93178953E+04-5.18289303E+00 2.57930490E+00 8.24684987E-03-6.42716047E-06
3
2.54637024E-09-4.12030443E-13-4.84162830E+04 8.81141041E+00 4
CH2O 6/29/04 RUSCIC 1H 2O 1 0G 300.000 5000.000 1486.000 01
4.02068394E+00 5.09903417E-03-1.76430480E-06 2.76025879E-10-1.60998042E-14 2
-1.49287258E+04 1.06525547E+00 3.00754197E+00 3.04729496E-03 5.25109246E-06
3
-5.12019281E-09 1.27133795E-12-1.41188397E+04 8.10120233E+00 4
HCO 29/11/04 H 1C 1O 1 0G 300.000 5000.000 1690.000 1
3.44148164E+00 3.52157719E-03-1.24136118E-06 1.97328644E-10-1.16538616E-14 2
3.97409684E+03 6.24593456E+00 3.81049965E+00 8.13269825E-04 3.13164701E-06
3
-2.39478268E-09 5.06894554E-13 4.03859901E+03 4.94843165E+00 4
CH3O 8/ 9/ 4 THERMC 1H 3O 1 0G 300.000 5000.000 1509.000 01
4.64787019E+00 6.90830683E-03-2.34404776E-06 3.61994570E-10-2.09253541E-14 2
-2.99208881E+02-1.57740193E+00 2.23058023E+00 8.53178586E-03 1.02166624E-06
3
-3.41046916E-09 9.94691038E-13 9.45939708E+02 1.28377569E+01 4
CH3O2H 1/14/ 5 THERMC 1H 4O 2 0G 300.000 5000.000 1367.000 21
8.80409289E+00 8.09427218E-03-2.85843274E-06 4.53369754E-10-2.66980707E-14 2
-1.98512174E+04-2.17000591E+01 2.83880024E+00 1.86096249E-02-8.48165412E-06
3
1.00387451E-09 1.71612429E-13-1.74033753E+04 1.16092433E+01 4
CH3O2 1/14/ 5 THERMC 1H 3O 2 0G 300.000 5000.000 1365.000 11
6.34718801E+00 7.92089358E-03-2.76601913E-06 4.35360631E-10-2.54984762E-14 2
-1.83436055E+03-7.42552545E+00 3.80497590E+00 9.80784660E-03-3.90940624E-07
3
-2.23072602E-09 6.43310820E-13-4.55625796E+02 7.81789100E+00 4
CH4 29/11/04 H 4C 1 0 0G 300.000 5000.000 1462.000 1
4.09617653E+00 7.44330845E-03-2.63871900E-06 4.19577604E-10-2.47508050E-14 2
-1.13835704E+04-4.67561383E+00 3.72113020E+00-2.50293289E-03 1.90246534E-05
3
-1.46871253E-08 3.43791152E-12-1.01424099E+04 1.22776596E+00 4
CH3 C 1H 3 0 0G 300.000 5000.000 1389.000 01
3.51281376E+00 5.11412613E-03-1.67632050E-06 2.52495174E-10-1.43302923E-14 2
1.61238027E+04 1.62436112E+00 3.43858162E+00 4.07752664E-03 3.19830994E-07
3
-9.47669390E-10 2.21828166E-13 1.63164018E+04 2.52807406E+00 4
C2H6 8/ 4/ 4 THERMC 2H 6 0 0G 300.000 5000.000 1383.000 11
6.05972630E+00 1.30382837E-02-4.48103942E-06 6.97762095E-10-4.05606353E-14 2

-1.35751226E+04-1.28608001E+01 4.78623203E-02 2.40569127E-02-1.15155912E-05
3
2.48666238E-09-1.78343944E-13-1.10923014E+04 2.06544071E+01 4
CH2CO 121686C 2H 2O 1 G 0300.00 5000.00 1000.00 1
0.06038817E+02 0.05804840E-01-0.01920954E-04 0.02794485E-08-0.01458868E-12 2
-0.08583402E+05-0.07657581E+02 0.02974971E+02 0.01211871E+00-0.02345046E-04
3
-0.06466685E-07 0.03905649E-10-0.07632637E+05 0.08673553E+02 4
CH3COCH2 8/30/ 4 THERMC 3H 5O 1 0G 300.000 5000.000 1388.000 21
1.08892477E+01 1.11540675E-02-3.85516785E-06 6.02834048E-10-3.51533449E-14 2
-1.00741464E+04-3.18043322E+01 1.22337251E+00 3.24546742E-02-2.13542518E-05
3
6.96777735E-09-8.99160299E-13-6.59419324E+03 2.05537233E+01 4
C2H5 8/ 4/ 4 THERMC 2H 5 0 0G 300.000 5000.000 1387.000 11
5.88784390E+00 1.03076793E-02-3.46844396E-06 5.32499257E-10-3.06512651E-14 2
1.15065499E+04-8.49651771E+00 1.32730217E+00 1.76656753E-02-6.14926558E-06
3
-3.01143466E-10 4.38617775E-13 1.34284028E+04 1.71789216E+01 4
C2H4 10/ 4/ 5 THERMC 2H 4 0 0G 300.000 5000.000 1395.000 01
5.22176372E+00 8.96137303E-03-3.04868886E-06 4.71465524E-10-2.72739592E-14 2
3.60389679E+03-7.47789234E+00 2.33879687E-01 1.96334647E-02-1.16833214E-05
3
3.64246453E-09-4.77442715E-13 5.46489338E+03 1.97084228E+01 4
C2H3 10/ 4/ 5 THERMC 2H 3 0 0G 300.000 5000.000 1395.000 01
5.07331248E+00 6.58316278E-03-2.23762924E-06 3.45803379E-10-1.99940490E-14 2
3.37234748E+04-3.39792712E+00 1.25329724E+00 1.56258370E-02-1.07803879E-05
3
4.18054634E-09-7.01360362E-13 3.50734773E+04 1.71341661E+01 4
CH3CHO 8/10/ 4 THERMC 2H 4O 1 0G 300.000 5000.000 1377.000 11
6.98518866E+00 9.67897787E-03-3.31841954E-06 5.16025901E-10-2.99725903E-14 2
-2.39807279E+04-1.27484852E+01 1.77060035E+00 1.84475161E-02-7.24138162E-06
3
2.34364561E-10 3.35543891E-13-2.18078850E+04 1.65023437E+01 4
C2H5CHO 8/10/ 4 THERMC 3H 6O 1 0G 300.000 5000.000 1375.000 21
8.87216223E+00 2.01710762E-02-8.06487647E-06 1.37617784E-09-8.48922325E-14 2
-2.83848527E+04-2.35069163E+01 5.93107530E+00 8.87943855E-03 2.03764325E-05
3
-1.80149348E-08 4.14085655E-12-2.51377751E+04-5.87019974E-01 4
C4H7OOH1-4 4/1/96 THERMC 4H 8O 2 0G 300.000 5000.000 1393.000 41
1.66978343E+01 1.80578399E-02-6.22476839E-06 9.71479434E-10-5.65686551E-14 2
-1.85344720E+04-5.76609547E+01 1.79804670E+00 5.23302551E-02-3.64638246E-05
3
1.31971888E-08-1.97165993E-12-1.32846748E+04 2.25862038E+01 4
C4H7O1-4 4/ 1/96 THERMC 4H 7O 1 0G 300.000 5000.000 1393.000 21
1.31417783E+01 1.64166051E-02-5.56949199E-06 8.60114769E-10-4.97230006E-14 2
1.67967537E+03-4.16160087E+01-2.92647947E-01 4.83149119E-02-3.48133220E-05
3
1.31921468E-08-2.06485553E-12 6.29978883E+03 3.03629978E+01 4
C3H6 10/23/ 5 THERMC 3H 6 0 0G 300.000 5000.000 1388.000 11
8.01595958E+00 1.37023634E-02-4.66249733E-06 7.21254402E-10-4.17370126E-14 2

-1.76749303E+03-2.00160668E+01 3.94615444E-01 2.89107662E-02-1.54886808E-05
3
3.88814209E-09-3.37890352E-13 1.17760132E+03 2.19003736E+01 4
PC4H9 8/ 4/ 4 THERMC 4H 9 0 0G 300.000 5000.000 1391.000 31
1.20779744E+01 1.96264778E-02-6.71302199E-06 1.04206424E-09-6.04469282E-14 2
3.22550473E+03-3.87719384E+01 3.20730933E-01 4.34654454E-02-2.40584970E-05
3
6.28245308E-09-5.80113166E-13 7.71490893E+03 2.57301085E+01 4
C2H5COCH2 4/ 3/ 0 THERMC 4H 7O 1 0G 300.000 5000.000 1383.000 31
1.42098738E+01 1.57866459E-02-5.50529183E-06 8.65870540E-10-5.06913329E-14 2
-1.41284951E+04-4.87132911E+01 1.54013856E+00 4.39486258E-02-2.97002421E-05
3
1.05495313E-08-1.58598769E-12-9.50796505E+03 1.99706641E+01 4
NC3H7CHO 9/27/95 THERMC 4H 8O 1 0G 300.000 5000.000 1378.00 31
1.35988068E+01 1.81652474E-02-6.17844458E-06 9.55980208E-10-5.53442958E-14 2
-3.15845348E+04-4.51790228E+01 1.87415959E+00 4.19240315E-02-2.35148779E-05
3
6.26913673E-09-6.09443908E-13-2.71032194E+04 1.91568574E+01 4
C5H10-1 4/ 7/97 THERMC 5H 10 0 0G 300.000 5000.000 1392.000 31
1.45851539E+01 2.24072471E-02-7.63348025E-06 1.18188966E-09-6.84385139E-14 2
-1.00898205E+04-5.23683936E+01-1.06223481E+00 5.74218294E-02-3.74486890E-05
3
1.27364989E-08-1.79609789E-12-4.46546666E+03 3.22739790E+01 4
C5H9O1-3 4/ 7/97 THERMC 5H 9O 1 0G 300.000 5000.000 1393.000 31
1.86270165E+01 1.85189638E-02-6.21111137E-06 9.52916260E-10-5.48704082E-14 2
-4.97349374E+03-7.09678919E+01-2.22532588E+00 6.97271843E-02-5.42285799E-05
3
2.13591167E-08-3.36511599E-12 1.91826163E+03 3.99711270E+01 4
NC3H7COCH2 2/22/96 THERMC 5H 9O 1 0G 300.000 5000.000 1389.000 31
1.61502419E+01 2.14093466E-02-7.36059614E-06 1.14656816E-09-6.66712722E-14 2
-1.76968561E+04-5.83864884E+01 9.58299271E-01 5.68162532E-02-3.99112781E-05
3
1.52671514E-08-2.49221047E-12-1.23062238E+04 2.34112884E+01 4
NC7H16 7/19/ 0 THERMC 7H 16 0 0G 300.000 5000.000 1391.000 61
2.22148969E+01 3.47675750E-02-1.18407129E-05 1.83298478E-09-1.06130266E-13 2
-3.42760081E+04-9.23040196E+01-1.26836187E+00 8.54355820E-02-5.25346786E-05
3
1.62945721E-08-2.02394925E-12-2.56586565E+04 3.53732912E+01 4
C7H15-2 7/19/ 0 THERMC 7H 15 0 0G 300.000 5000.000 1382.000 61
2.16368842E+01 3.23324804E-02-1.09273807E-05 1.68357060E-09-9.71774091E-14 2
-1.05873616E+04-8.52209653E+01-3.79155767E-02 7.56726570E-02-4.07473634E-05
3
9.32678943E-09-4.92360745E-13-2.35605303E+03 3.37321506E+01 4
C7H15-3 7/19/ 0 THERMC 7H 15 0 0G 300.000 5000.000 1382.000 61
2.16368842E+01 3.23324804E-02-1.09273807E-05 1.68357060E-09-9.71774091E-14 2
-1.05873616E+04-8.52209653E+01-3.79155767E-02 7.56726570E-02-4.07473634E-05
3
9.32678943E-09-4.92360745E-13-2.35605303E+03 3.37321506E+01 4
C7H15O2-2 7/19/ 0 THERMC 7H 15O 2 0G 300.000 5000.000 1390.000 71
2.60535640E+01 3.43831688E-02-1.18713247E-05 1.85450241E-09-1.08052399E-13 2

-3.06842095E+04-1.05407563E+02 3.55252917E-01 9.42381007E-02-6.66955106E-05
3
2.54795583E-08-4.13211105E-12-2.15795254E+04 3.29433435E+01 4
C7H15O2-3 7/19/ 0 THERMC 7H 15O 2 0G 300.000 5000.000 1390.000 71
2.60535640E+01 3.43831688E-02-1.18713247E-05 1.85450241E-09-1.08052399E-13 2
-3.06842095E+04-1.05407563E+02 3.55252917E-01 9.42381007E-02-6.66955106E-05
3
2.54795583E-08-4.13211105E-12-2.15795254E+04 3.29433435E+01 4
C7H14OOH2-4 7/19/0 THERMC 7H 15O 2 0G 300.000 5000.000 1389.000 81
2.74034778E+01 3.27527893E-02-1.12991770E-05 1.76444649E-09-1.02786945E-13 2
-2.48636651E+04-1.10201978E+02 8.49786005E-01 9.25107196E-02-6.25359834E-05
3
2.17880390E-08-3.12720398E-12-1.53640679E+04 3.32997487E+01 4
C7H14OOH3-5 7/19/0 THERMC 7H 15O 2 0G 300.000 5000.000 1389.000 81
2.74034778E+01 3.27527893E-02-1.12991770E-05 1.76444649E-09-1.02786945E-13 2
-2.48636651E+04-1.10201978E+02 8.49786005E-01 9.25107196E-02-6.25359834E-05
3
2.17880390E-08-3.12720398E-12-1.53640679E+04 3.32997487E+01 4
C7H14OOH4-2 7/19/0 THERMC 7H 15O 2 0G 300.000 5000.000 1389.000 81
2.74034778E+01 3.27527893E-02-1.12991770E-05 1.76444649E-09-1.02786945E-13 2
-2.48636651E+04-1.10891460E+02 8.49786005E-01 9.25107196E-02-6.25359834E-05
3
2.17880390E-08-3.12720398E-12-1.53640679E+04 3.26102671E+01 4
C7H14OOH2-4O2 7/19/0 TRMC 7H 15O 4 0G 300.000 5000.000 1390.000 91
3.28358296E+01 3.32767285E-02-1.15833285E-05 1.81958638E-09-1.06434419E-13 2
-4.52873003E+04-1.35975710E+02 1.40912479E+00 1.10720834E-01-8.71178075E-05
3
3.63662749E-08-6.28350689E-12-3.46304788E+04 3.16223383E+01 4
C7H14OOH3-5O2 7/19/0 TRMC 7H 15O 4 0G 300.000 5000.000 1390.000 91
3.28358296E+01 3.32767285E-02-1.15833285E-05 1.81958638E-09-1.06434419E-13 2
-4.52873003E+04-1.35975710E+02 1.40912479E+00 1.10720834E-01-8.71178075E-05
3
3.63662749E-08-6.28350689E-12-3.46304788E+04 3.16223383E+01 4
NC7KET24 7/19/ 0 THERMC 7H 14O 3 0G 300.000 5000.000 1387.000 81
2.88330388E+01 3.20168096E-02-1.11508456E-05 1.75226159E-09-1.02520451E-13 2
-6.20142474E+04-1.17499704E+02 1.52936692E+00 9.58173466E-02-6.96688520E-05
3
2.69540382E-08-4.38728126E-12-5.23839542E+04 2.93851334E+01 4
NC7KET35 7/19/ 0 THERMC 7H 14O 3 0G 300.000 5000.000 1387.000 81
2.88330388E+01 3.20168096E-02-1.11508456E-05 1.75226159E-09-1.02520451E-13 2
-6.20142474E+04-1.17499704E+02 1.52936692E+00 9.58173466E-02-6.96688520E-05
3
2.69540382E-08-4.38728126E-12-5.23839542E+04 2.93851334E+01 4
NC7KET42 7/19/ 0 THERMC 7H 14O 3 0G 300.000 5000.000 1386.000 81
2.86572867E+01 3.21567908E-02-1.11961570E-05 1.75895000E-09-1.02891960E-13 2
-6.20252988E+04-1.16135256E+02 2.32269738E+00 9.45160149E-02-6.99057179E-05
3
2.79772916E-08-4.74244431E-12-5.27586830E+04 2.53458269E+01 4
IC3H7 8/ 4/ 4 THERMC 3H 7 0 0G 300.000 5000.000 1373.000 21
8.14705217E+00 1.58727106E-02-5.44611541E-06 8.47207689E-10-4.92178752E-14 2

6.18073367E+03-1.91980850E+01 1.63417589E+00 2.40171372E-02-4.72808067E-06
3
-3.24354603E-09 1.23539044E-12 9.20752889E+03 1.83848082E+01 4
C3H5-T 10/23/ 5 THERMC 3H 5 0 0G 300.000 5000.000 1382.000 11
7.37492443E+00 1.17510061E-02-4.00021283E-06 6.18947395E-10-3.58215018E-14 2
2.73982108E+04-1.43478655E+01 2.17916644E+00 2.03826623E-02-7.91413834E-06
3
4.76906187E-10 2.70398536E-13 2.96002535E+04 1.48785684E+01 4
IC4H9 8/ 4/ 4 THERMC 4H 9 0 0G 300.000 5000.000 1386.000 31
1.21276930E+01 1.98689494E-02-6.85937004E-06 1.07141528E-09-6.24184609E-14 2
2.11952051E+03-4.08727278E+01-2.21457835E-01 4.63756324E-02-2.88282920E-05
3
9.60200646E-09-1.39021034E-12 6.76153637E+03 2.64801220E+01 4
IC4H8 10/23/ 5 THERMC 4H 8 0 0G 300.000 5000.000 1388.000 21
1.12258330E+01 1.81795798E-02-6.20348592E-06 9.61444458E-10-5.57088057E-14 2
-7.90617899E+03-3.66411888E+01 9.38433173E-01 3.90547287E-02-2.16437148E-05
3
5.87267077E-09-6.14435479E-13-3.95452013E+03 1.98337802E+01 4
IC4H7 10/23/ 5 THERMC 4H 7 0 0G 300.000 5000.000 1393.000 11
1.16382753E+01 1.57681299E-02-5.38538858E-06 8.35172927E-10-4.84141083E-14 2
1.03408230E+04-3.90259890E+01-7.20881697E-04 4.36495730E-02-3.16385877E-05
3
1.23984983E-08-2.04378360E-12 1.43654373E+04 2.33234340E+01 4
IC4H7O 4/ 3/ 0 THERMC 4H 7O 1 0G 300.000 5000.000 1386.000 21
1.33457615E+01 1.61218588E-02-5.44376403E-06 8.38199374E-10-4.83608280E-14 2
6.11443644E+02-4.36818838E+01 1.74700687E+00 4.07783436E-02-2.44750243E-05
3
7.06502958E-09-7.51570589E-13 4.86979233E+03 1.94535999E+01 4
IC3H7CHO 2/22/96 THERMC 4H 8O 1 0G 300.000 5000.000 1391.000 31
1.37501656E+01 1.83126722E-02-6.28572629E-06 9.78250756E-10-5.68538653E-14 2
-3.26936771E+04-4.77270548E+01-2.73021382E-01 4.89696307E-02-3.12770049E-05
3
1.00052945E-08-1.27512074E-12-2.76054737E+04 2.83451139E+01 4
TC3H6CHO 2/22/96 THERMC 4H 7O 1 0G 300.000 5000.000 1389.000 21
1.31013047E+01 1.66391865E-02-5.68457623E-06 8.81808351E-10-5.11290161E-14 2
-1.30638647E+04-4.42705813E+01 1.87052762E+00 4.14869677E-02-2.66815701E-05
3
9.01531610E-09-1.27870633E-12-8.97730744E+03 1.66174178E+01 4
IC4H7OH 4/ 8/97 THERMC 4H 8O 1 0G 300.000 5000.000 1384.000 31
1.35043419E+01 1.78646968E-02-5.99304371E-06 9.18717641E-10-5.28435302E-14 2
-2.58255688E+04-4.44645715E+01 1.69099899E+00 4.27168891E-02-2.49281695E-05
3
7.00961522E-09-7.23262828E-13-2.14512334E+04 1.99500833E+01 4
YC7H15 7/19/ 0 THERMC 7H 15 0 0G 300.000 5000.000 1384.000 61
2.04581471E+01 3.43076361E-02-1.18102635E-05 1.84129611E-09-1.07133806E-13 2
-1.34978774E+04-8.18212264E+01 1.30897106E+00 6.96136442E-02-3.31150057E-05
3
5.82888256E-09 3.54427314E-14-5.78512513E+03 2.45658235E+01 4
IC8H18 7/20/ 0 THERMC 8H 18 0 0G 300.000 5000.000 1396.000 71
2.71373590E+01 3.79004890E-02-1.29437358E-05 2.00760372E-09-1.16400580E-13 2

-4.07958177E+04-1.23277495E+02-4.20868893E+00 1.11440581E-01-7.91346582E-05
3
2.92406242E-08-4.43743191E-12-2.99446875E+04 4.49521701E+01 4
AC8H17 7/20/ 0 THERMC 8H 17 0 0G 300.000 5000.000 1396.000 71
2.67069782E+01 3.57660601E-02-1.22178704E-05 1.89536630E-09-1.09907843E-13 2
-1.57229692E+04-1.17001113E+02-3.41944741E+00 1.06803189E-01-7.65411563E-05
3
2.85341682E-08-4.36478649E-12-5.33514196E+03 4.45471727E+01 4
CC8H17 7/20/ 0 THERMC 8H 17 0 0G 300.000 5000.000 1390.000 71
2.51497158E+01 3.71096845E-02-1.26854483E-05 1.96873429E-09-1.14193894E-13 2
-1.82761790E+04-1.09056834E+02-9.73159697E-02 8.92653724E-02-5.12873814E-05
3
1.37640528E-08-1.27788396E-12-8.81147302E+03 2.89791898E+01 4
DC8H17 7/20/ 0 THERMC 8H 17 0 0G 300.000 5000.000 1396.000 71
2.67069782E+01 3.57660601E-02-1.22178704E-05 1.89536630E-09-1.09907843E-13 2
-1.61255862E+04-1.18098245E+02-3.41944741E+00 1.06803189E-01-7.65411563E-05
3
2.85341682E-08-4.36478649E-12-5.73775897E+03 4.34500414E+01 4
AC8H17O2 7/20/ 0 THERMC 8H 17O 2 0G 300.000 5000.000 1393.000 81
3.02815958E+01 3.78729072E-02-1.30468383E-05 2.03524213E-09-1.18471267E-13 2
-3.48032462E+04-1.31647036E+02-1.78614072E+00 1.14754903E-01-8.50604719E-05
3
3.34040935E-08-5.45173228E-12-2.37742056E+04 4.00275514E+01 4
AC8H17O 7/20/ 0 THERMC 8H 17O 1 0G 300.000 5000.000 1398.000 71
2.88343933E+01 3.63403146E-02-1.23814095E-05 1.91748102E-09-1.11063219E-13 2
-3.29777132E+04-1.26786653E+02-3.80491312E+00 1.15184609E-01-8.57614185E-05
3
3.31877927E-08-5.24475393E-12-2.19418053E+04 4.75187920E+01 4
DC8H17O 7/20/ 0 THERMC 8H 17O 1 0G 300.000 5000.000 1398.000 71
2.88343933E+01 3.63403146E-02-1.23814095E-05 1.91748102E-09-1.11063219E-13 2
-3.29777132E+04-1.27194302E+02-3.80491312E+00 1.15184609E-01-8.57614185E-05
3
3.31877927E-08-5.24475393E-12-2.19418053E+04 4.71111423E+01 4
AC8H16OOH-B 7/20/ 0 THRMC 8H 17O 2 0G 300.000 5000.000 1390.000 91
3.25510943E+01 3.47986732E-02-1.18444590E-05 1.83415878E-09-1.06263255E-13 2
-2.95119890E+04-1.41568260E+02-2.06912730E+00 1.16142139E-01-8.44026727E-05
3
3.10689399E-08-4.59880303E-12-1.76383455E+04 4.40292848E+01 4
IC8ETERAB 8/11/98 THERMC 8H 16O 1 0G 300.000 5000.000 1403.000 51
2.76798014E+01 3.59323006E-02-1.23072657E-05 1.91269208E-09-1.11054254E-13 2
-4.05912134E+04-1.25295695E+02-7.80049041E+00 1.23580877E-01-9.58621529E-05
3
3.83545262E-08-6.21761428E-12-2.88197649E+04 6.34400053E+01 4
AC8H16OOH-BO2 7/20/ 0 TMC 8H 17O 4 0G 300.000 5000.000 1393.000 91
3.68372436E+01 3.70741924E-02-1.28898032E-05 2.02329750E-09-1.18291456E-13 2
-4.93845688E+04-1.61072392E+02-1.29316549E+00 1.32762515E-01-1.07403628E-04
3
4.54644888E-08-7.86976880E-12-3.67109267E+04 4.15232002E+01 4
IC8KETAB 7/20/ 0 THERMC 8H 16O 3 0G 300.000 5000.000 1394.000 91
3.47134000E+01 3.41945225E-02-1.18952719E-05 1.86805496E-09-1.09255878E-13 2

-6.57745821E+04-1.53035860E+02-2.37786754E+00 1.24999274E-01-9.81048338E-05
3
 3.95573283E-08-6.48097453E-12-5.33254847E+04 4.46667297E+01 4
CH2 120186C 1H 2 G 0250.00 4000.00 1000.00 1
 0.03636408E+02 0.01933057E-01-0.01687016E-05-0.01009899E-08 0.01808256E-12 2
 0.04534134E+06 0.02156561E+02 0.03762237E+02 0.01159819E-01 0.02489585E-05
3
 0.08800836E-08-0.07332435E-11 0.04536791E+06 0.01712578E+02 4

END